CARBIDE-FREE NANOSCALE BAINITE

Design and Characterization of a Nanoscale Carbide-Free Bainite Alloy

By JAMES SARAGOSA, B.ENG.

A Thesis Submitted to the Department of Materials Science and Engineering in Partial Fulfillment of the Requirements for the Degree Master of Science

McMaster University MASTER OF SCIENCE (2015) Hamilton, Ontario

TITLE: Design and Characterization of a Carbide-Free Nanoscale Bainite Alloy

AUTHOR: James Saragosa, B.Eng. (McMaster University)

SUPERVISORS: Fateh Fazeli, Gianluigi Botton, Jason Lo

PAGES: xv, 94

Lay Abstract

This project has adopted the science of bainite transformation to develop a suitable alloy and processing method for the fabrication of very strong armour plates at a lower cost compared to commercially available grades. The pilot-scale casting and processing facility at CanmetMATERIALS centre was used to produce full sized, 1ft (304.8mm) by 1ft (304.5mm), prototype armour plates. The plates were subsequently characterized using a variety of techniques to determine interplay between processing parameters, microstructure and the ensuing final performance. The optimized alloy, tailored processing parameters, and characterization information constitute the contribution of the present work to the current state of research.

Abstract

High carbon bainitic steel plates could surpass quench and tempered martensitic counterparts for fabrication of ammunition- and blast-resistant armours. Mechanical properties, microstructure and reaction kinetics of a commercially available carbide-free nanoscale bainite alloy were characterized. Based on the initial characterization and a comprehensive review of the literature a new alloy with lower carbon, higher silicon and cobalt additions was designed and processed into hot-rolled plates (10x10mm and 300x300mm) using CanmetMATERIALS pilot-scale facilities. The heat treated plates achieved strength above 2 GPa with elongation of 14%. Thorough analysis with electron backscattered diffraction revealed that the microstructure consisted of bainitic ferrite laths, islands of retained austenite, areas of mixed martensite-austenite (MA). Transmission electron microscopy confirmed the fine scale of bainitic ferrite and the presence of thin films of retained austenite encompassing bainite laths.

Dilatometric study of the new alloy revealed that forming bainite at higher transformation temperatures, 275°C versus 250°C and 225°C, led to faster overall reaction kinetics and higher final fractions of bainite within 18 hours of isothermal holding. Although it is expected that the fraction of bainite increases at lower temperatures, substantial prolonged holding time is required for completion of the reaction. Microstructural features and particularly bainite lath thickness depended on bainite formation temperature. Ausforming, deformation of austenite at 600°C for 25-45% strain prior to decomposition to bainite, however led to a decrease in reaction rate and final fraction of bainite.

Tensile testing of austempered specimens showed that higher transformation temperature yielded a stronger microstructure, which was attributed to the formation of thinner bainitic ferrite laths. Higher transformation temperatures led to an increase in ductility. Tensile testing of the ausformed specimens showed a reduction in both strength and ductility. A negative correlation was seen between the amount of MA areas in the microstructure and total elongation.

Acknowledgements

First and foremost I would like to thank my supervisors Fateh Fazeli, Jason Lo, and Dr. Gianluigi Botton for their academic guidance and for providing me with an exciting and engaging project.

My project has involved a large number and variety of experiments which were only feasible thanks to the help of scientists and technicians at McMaster University and CanmetMATERIALS: I would like to thank Victoria Jarvis for conducting the XRD experiments and coming up with the two austenite model, Chris Butcher for his help with EBSD and for electropolishing my XRD samples, Marta Aniolek for running the dilatometer experiments, Carmen Andrei and Xiang Wang running the TEM, Colin Scott and Babak Shalchi Amrikhiz for doing the EELS carbon measurements, Jian Li for running the EBSD microscope, Renata Zivadil for bestowing a great deal of metallography knowledge and advice unto me, the casting and rolling teams at CanmetMATERIALS for producing the designed alloy, Jonathan McKinley and JP Talon for their sage advice, and finally all of my colleagues for their help and support.

Table of Contents

List of Figures

List of Equations

List of Tables

List of Abbreviations and Symbols

A%-Total Elongation in percent

Bs-Bainite Start Temperature

CI-Confidence Index

CVN-Charpy V-Notch

EBSD- Electron Backscattered Diffraction

EDM-Electrical Discharge Machining

EELS-Electron Energy Loss Spectroscopy

HHA-High Hardness Armour

IQ-Image Quality

LAV-Light Armoured Vehicle

MA-Martensite Austenite

Ms-Martensite Start Temperature

OES-Optical Emission Spectroscopy

RHA-Rolled Homogenized Armour

SEM-Scanning Electron Microscopy

T_0-T zero

TEM-Transmission Electron Microscopy

UHA-Ultra High Hardness Armour

α-Ferrite (or Bainitic Ferrite)

γ-Austenite

Declaration of Academic Achievement

EELS

Dr. Colin Scott and Dr. Babak Shalchi Amrikhiz developed the EELS method used to locally measure carbon content and did all the measurements in the present work. My responsibility was to explain the measurements.

XRD

Victoria Jarvis did the majority of the data analysis calculating phase fractions and lattice parameter, and also came up with the two austenite phase analysis model in an attempt to differentiate between thin films and blocks of retained austenite. I was responsible for calculating the amount of carbon in retained austenite from the lattice parameter and explaining all of the results from XRD.

1 Introduction

1.1. Background

The LAV (light armoured vehicle) 3 III, shown in Figure 1, is Canada's main combat vehicle and its protection capabilities must be kept up to date [1]. The current work is part of a larger project to enhance the armour on the LAV III by adding on composite plates. The specific role of the material being researched here is to act as add-on or appliqué armour. As indicated in Figure 2 add-on armour is placed outside of the welded steel hull of a vehicle. In this case the plates will be used as the outer most layer to absorb projectile energy and throw the projectile off course before making contact with the next layer.

Figure 1-LAV III-Canada's light armoured vehicle [1]

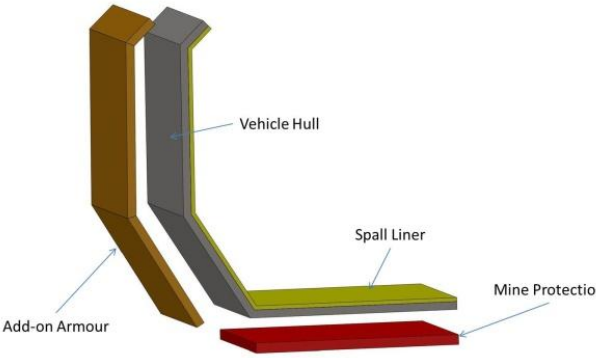

Figure 2-Schematic diagram of LAV armour layout [2]

Bainite was originally discovered by Davenport and Bain in the 1920's during experiments where austenite was isothermally treated just above the temperature martensite formation was expected [3]. It was noted as being tougher than tempered martensite, but still having the same hardness [3]. Research into this particular type of bainite done by Bhadeshia and his colleagues begun with the continuous cooling from an austenite to a homogenizing temperature with alloys containing 2% Mn or 3.5% Ni [4]. They then moved their research away from the nickel additions, in an attempt to reduce cost. They went on to making manganese containing alloys which were isothermally transformed over the course of days, and then adding small amounts of cobalt and aluminum to accelerate the bainite transformation [5]. The resulting microstructure demonstrated tensile strength beyond 2GPa and introduced as hard bainite or super bainite [6, 7].

Super bainite is a mixed microstructure which consists of fine bainitic ferrite plates whose thickness is in the scale of tens of nanometers, separated by thin films of retained austenite which are supersaturated with carbon, it can also contain small islands blocky retained austenite and the aggregate is free of carbides. The nanoscale of the structure is of particular importance because strength of these structures is inversely related to thickness of the bainitic ferrite plates. The austenite in the mixture is responsible for the ductility of the alloy and also contributes to work hardening via transformation induced plasticity (TRIP) mechanism.

Super bainite production begins by reheating the part to a suitable temperature for enough time to transform its structure to austenite. It is then typically quenched to a temperature at which the austenite can transform to bainite, a few tens of degrees above martensite start temperature. As the part is held at this bainite isothermal transformation temperature longer, more bainitic ferrite is formed. Once a desired mix of bainitic ferrite and remaining austenite is obtained the part is then quenched to room temperature. The austenite is stabilized due to carbon enrichment and can be retained.

Super bainite is attractive as armour material due to its combination of high strength and hardness, as well as ductility and impact energy. Conventional steel armours such as rolled homogenized armour (RHA) standard, MIL-A-12560 requires a hardness of 500HV with a charpy impact value of 21 J, values which many bainitic alloys in the literature surpass. Tata steel provides a commercial bainitic alloy which boasts hardness values of 570 BHN (617 HV), sufficient enough to qualify it for the Ultra-high-hardness armour (UHA) category, see MIL-DTL-32332 [8], as does the cobalt-aluminum alloy from Bhadeshia and his colleague's work [6]. Moreover, the high volume fraction of retained austenite and lack of carbide particles brings about high toughness and ductility which is hardly demonstrated by quenched and tempered armour steel.

The current rolled homogenized armour is formed by severely quenching the steel followed by tempering. The severe quench step needs to be performed very carefully to avoid the formation of any cracks which would permanently compromise a part's mechanical/ballistic performance. The rolled homogenized armours currently available typically contain nickel which drives the price of the product up. The milder quench and relatively cheaper alloying systems associated with super bainite production also make it attractive alternative to currently available products.

Originally the goal of this project was to design and create an alloy similar to Tata steel's, then create one that is superior with respect to mechanical properties, processing, and/or alloy composition price. However due to Tata's

poor ductility perhaps the MARS 600 quenched and tempered alloy from Arcellor Mittal would serve as a better industrial benchmark, see Table 1.

Table 1-Mechanical properties of Tata-Pavise bainite, and Mars 600 martensite

		Hardness	UTS (MPa)	YS (MPa)	A%	CVN (J) (20°C)	CV(J) (-40°C)
Mars 600	Typical Value	600 HB (630/650 HV 30kg)	2100	1550	10	13	11
	Minimum Value	≥ 578 HB	≥ 2000	≥1300	≥7	-	≥8
Tata-Pavise		> 570 HB	>2000	1300	5	2.00	1.39

1.2. Current Gap in Research

With regards to the current state of research into super bainite, while there has been a great deal of work, it only seems to cover a couple of alloying systems most of which are either in the range of 0.4 or 0.8% carbon. This project will contribute by providing detailed characterization of at least one new alloy having a 0.7% carbon content. There is also not a great deal of research that has tensile results for ausformed bainitic steels which this project has provided.

1.3. Approach

The project was carried out by performing a literature review to understand the interplay between alloying elements, thermal and mechanical processing, and final mechanical properties. Based on the review an alloy was suggested. After the casting and shaping of the alloy thermomechanical simulations carried out in a dilatometer to determine the reaction kinetics of the alloy and characterize the resultant microstructures. The most promising thermomechanical processing cycles were then carried out on tensile bars and CVN impact specimens to gauge the resulting mechanical properties. Finally the highest performing heat treating parameters were carried out on fullsized 1'(304.8mm) by 1' and 4inch by 4"(101.6mm) ballistic samples.

1.4. Project Objectives

1. Develop proper method and use CanmetMATERIALS' pilot scale processing facilities to fabricate full sized, 1ft (304.8mm) x 1ft (304.5mm), prototype superbainitic armour plates
2. Understand kinetics of bainite transformation and interplay between process parameters and microstructure evolution to select ideal heat treatment parameters (including deformation)
3. Determine static and ballistic performance of prototype plate

2 Literature Review

2.1. Super Bainite Microstructure and Processing

2.1.1. Bainite Transformation

The transformation of austenite to bainitic ferrite has been discussed as a shear or diffusional transformation. Figure 3 shows the free energy curves for ferrite and austenite at a given temperature T_1. According to the displacive approach bainitic ferrite, with a carbon concentration indicated by Ae1, will transform from austenite. As bainitic ferrite forms it partitions carbon into the surrounding austenite. Transformation occurs until retained austenite reaches the concentration indicated by T_0. The T_0 curve is made up of the points where ferrite and austenite have both the same chemical composition and free energy (i.e. the point at which the ferrite and austenite free energy curves intersect at a given temperature. The T_0' curve is T_0 modified to also account for the strain energy associated with austenite transforming to bainite [9]. Bainite will form below the T_0' curve once the growth and nucleation criterion (shown below) have been met [9].

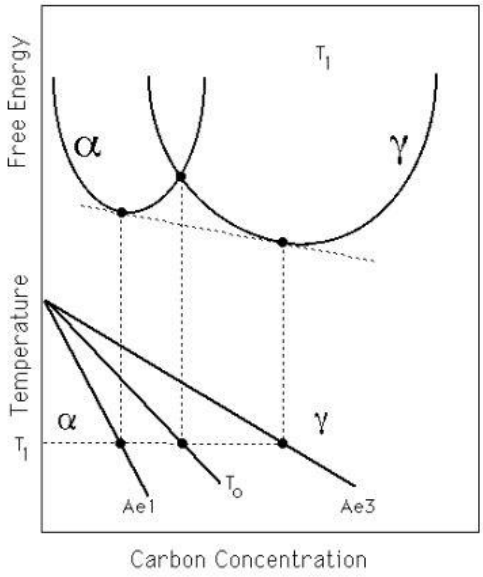

Figure 3-T_0 curve, Bainite formation is not favored above the T_0 curve [10]

Growth

$$\Delta G^{\gamma\rightarrow\alpha} < -G_{SB}$$

where:

G_{SB}≈400J mol^{-1} which is the strain energy of bainite [9]

$\Delta G^{\gamma\rightarrow\alpha}$ is the driving force for growth [11]

Nucleation

$\Delta G_m < G_N$

where:

ΔG_m is the Gibbs free energy change caused by nucleation of bainite

G_N is a function based on the displacive nature of bainite nucleation [5].

G_N=3.45463 T_h-3499.4 J mol^{-1}, where T_h is the highest temperature for an alloy at which a displacive reaction will occur [12].

Bainitic ferrite will continue to grow and nucleate at a given temperature until the carbon content in the retained austenite reaches levels beyond the T_0' curve. The carbon composition in austenite can be calculated using:

Equation 1-Carbon balance in between bainitic ferrite and austenite.

$$x_\gamma = \bar{x} + V_B \frac{(x-s)}{(1-V_B)} \text{ ...[11],}$$

where s = amount of carbon in solid solution of ferrite, and x̄ denotes carbon concentration of the alloy

2.1.2. Microstructure

The "super bainite" microstructure is relatively simple, it is composed of fine plates of bainitic ferrite and retained austenite[6]. Retained austenite is present in two forms: 1-thin films that form between ferrite plates and 2-as blocks [6]. The microstructure does not contain carbides which is a consequence of appropriate additions of Si [6]. The nanoscale of the bainitic ferrite - retained austenite composite microstructure is the main source of its excellent strength and toughness [7].

Ferrite plates

Due to the shear nature of ferrite formation in the bainite transformation, plates of bainitic ferrite have both a high dislocation density [6], and a high fraction of carbon (up to 0.35% mass has been observed) [6]. A correlation exists between the dislocation density and carbon content [13, 14], and it has even been suggested that the excess carbon segregates onto the dislocations [6]. The dislocation density in the bainitic ferrite is another mechanism credited with strengthening the microstructure which is defined by Equation 2 [6].

Equation 2-Contribution of dislocation density in bainite to strength

$$\Delta\sigma \approx 7.34 \times 10^{-6}(\rho)^{0.5} \text{ MPa...[7]}$$

Where ρ is dislocation density given in m^{-2}.

The second mechanism that contributes to the ferrite's strengthening is its thickness which is defined by Equation 3 [6].

Equation 3-Contribution of bainite lath thickness to strength

$$\Delta\sigma \approx 115\ (L^{-1}) \text{ MPa...[5]}$$

where mean linear intercept (in micrometers) ≈ 2*plate thickness [5]. Therefore to increase the strength of the bainite, thinner ferrite plates are desirable. It has been determined that there are three factors that contribute to ferrite plate thickness:

1. strength of the parent austenite [15]
2. free energy accompanying the austenite→ ferrite transformation ($\Delta G^{\gamma\rightarrow\alpha}$) [15]
3. transformation temperature (although this is a smaller contribution) [15]

Although transformation temperature is noted as having a smaller contribution to plate thickness it has the secondary effect of influencing the strength of austenite and transformation energy. This translates into ferrite plates being thicker at higher transformation temperatures [6].

Figure 4 shows the strengthening contribution of dislocation density and plate boundaries for different transformation temperatures. Alloy compositions can be seen in Table 2. It should also be noted from Figure 4 that a decrease in plate thickness and increase in dislocation density occur by lowering the treatment temperature.

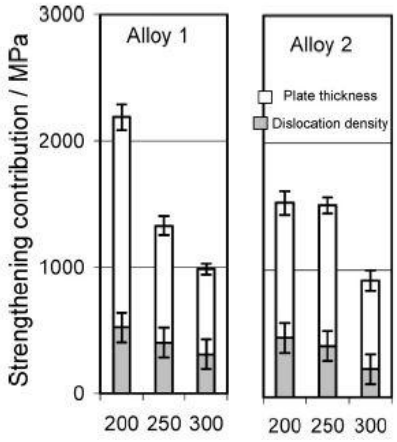

Figure 4-Strength contributions and effect of isothermal treatment Temperature. Alloy 1-0.80C-1.59Si-2.01Mn-0.24Mo-1Cr-1.51Co, Alloy 2-0.79C-1.56Si-1.98Mn-0.24Mo-1.01Cr-1.51Co-1.01 [13]

Table 2-Alloys that compliment Figure 4 taken from [6, 13]

Alloy	C	Si	Mn	Mo	Cr	Co	Al	P	S
1	0.80	1.59	2.01	0.24	1	1.51	-	0.002	0.002
2	0.79	1.56	1.98	0.24	1.01	1.51	1.01	0.002	0.002

The fraction of bainitic ferrite is another microstructural features that controls the final mechanical properties. There are two ways to increase the total fraction of bainitic ferrite:

1. The overall carbon concentration can be reduced, which increases the equilibrium fraction of bainite and the amount of reaction it takes for the parent austenite to enrich with sufficient carbon for transformation to become unfavourable [11].
2. Certain substitution alloying elements can be added shifting the T_0' curve to higher carbon concentrations [11].

Retained austenite

Retained austenite is the softest phase in bainite composite structure [6], and it is credited with having the greatest contributions to toughness, ductility and elongation [13]. As mentioned before retained austenite is present as both thin films separating ferrite plates and as blocky regions. Besides its inherent softness retained austenite also contributes to ductility and work hardening by transforming to martensite when strained, i.e. TRIP mechanism [6, 13]. The strain induced transformation happens above the martensite start temperature

(M_s) and below the temperature referred to as M_d [6]. M_d is defined as the temperature above which strain induced transformations are not possible [6]. M_s and M_d therefore represent the stability range of austenite. Stability is dependent on:

1. Temperature [6]
2. Austenite chemistry-C, Mn, Si and Al have large influences on mechanical stability and M_d and M_s, especially Carbon [6]
3. Shape-thin films of austenite are constrained by surrounding ferrite grains which impedes their transformation to martensite [6]

A higher M_d indicates lower austenite stability and therefore faster and larger transformation [6]. This was however, viewed as having a negative effect on ductility [6]. One study found that thin films of retained austenite are too stable to capitalize on the TRIP mechanism due to carbon super-saturation and shape [6]. However it is also widely accepted that large blocky austenite has negative effects on toughness [6]. But blocks do contain less carbon, and as a result are less stable [6]. Table 3 shows the effects of isothermal transformation temperature on retained austenite carbon content, stability and morphology for two alloys. It can be seen that blocky and total austenite content increase with increasing treatment temperature. Retained austenite stability also decreases as treatment temperature increases. On the other hand at the lowest treatment temperature retained austenite exists mainly as thin films and is highly stable, which agrees with the above theory.

Table 3-Austenite information determined via XRD for alloys from Table 2, Md is the temperature above which austenite will no longer transform to martensite [6]

Alloy	Isothermal transformation T (°C)	C_γ (wt. %)	$V_{\gamma\text{-total}}$	$V_{\gamma Film}$	$V_{\gamma Blocky}$	M_s (°C)	M_d (°C)
1	200	1.1	0.13	0.129	0.0001	-10	391
	250	1.4	0.21	0.12	0.09	-35	301
	300	1.49	0.25	0.11	0.14	-40	271
2	200	1.47	0.17	0.123	0.04	16	321
	250	1.7	0.21	0.12	0.09	-10	251
	300	1.9	0.37	0.09	0.28	-27	221

Carbides

As previously mentioned, thanks to the use of silicon, carbide precipitation is generally avoided in the formation of this microstructure [15]. Carbides are known to cause failure by void formation and cleavage fracture [6] which is why it is desirable to avoid their formation. While it is generally accepted that no carbides will form an atom probe study did manage to identify F-C carbides in ferrite plates [16]. Due to the high dislocation density in bainitic ferrite the fine carbides were not visible during TEM characterization [16]. The study found that carbides were present in high dislocation density areas and determined that they were likely a result of long treatment times [16]. The APT study was done on a **0.79C-1.5Si-1.89Mn-0.98Cr-0.24Mo-1.06Al-1.58Co** wt% alloy which was austenitized at 1100°C for 30 minutes (PAG=60μm), then isothermally treated at 200°C for 10 days in a salt bath furnace [16]. Results from the APT study are shown in Table 4.

Table 4-Composition results from APT study, Iron is balance. Taken from [16]

		C	Si	Mn	Al	Co	Cr
Steel composition		3.48	2.85	1.9	2.083	1.42	1.0
Fe-C carbides	Fe_3C	25±0.08	2.5±0.2	1.14±0.2	1.99±0.1	0.9±0.1	0.8±0.04
	$Fe_{2.4}C$ (ε)	30±1	2.2±0.2	1.0±0.1	1.98±0.2	0.9±0.1	0.7±0.1
	$Fe_{32}C_4$	10±1.5	2.3±0.2	2.2±0.1	2±0.1	1.2±0.1	0.8±0.05
Bainitic Ferrite	BF/Fe-C	0.3±0.05	4.5±0.5	1.3±0.5	2.4±0.5	0.9±0.02	1.4±0.2
	BF	0.7±0.1	4.8±0.2	1.4±0.2	2.9±0.2	0.9±0.1	1.3±0.1
Retained Austenite	RA low C	1.9±0.5	3.7±0.1	1.4±0.2	2.7±0.3	0.8±0.1	1.7±0.3
	RA high C	6±1	2.9±0.7	1.9±0.4	3.2±0.5	1.1±0.1	2±0.1

2.1.3. Alloying Elements

Appropriate carbon content is important for both processing and performance. As mentioned in the previous section carbon fraction heavily influences retained austenite stability. It is also used to keep both the bainite start (B_s) and M_s temperatures low, and achieve faster bainite transformation rates [7]. In the literature high carbon alloys (≥0.8 wt% C) were isothermally treated in the 200-300°C range [6, 13, 15], whereas lower C alloys were treated in the 340-420°C range [11]. Consider that since a small scale microstructure is desirable for both strength and toughness it is then desirable to form bainite at the lowest temperature possible [6, 15]. As such, higher carbon contents indirectly influence the final strength by lowering the reaction temperature range for bainite.

Silicon does not dissolve in cementite, therefore its presence impedes cementite precipitation during cooling [15]. It has been suggested that at least 1.5 wt% Si is required to avoid carbide formation [15], which is interesting considering that the Tata steel contains only ≈0.75wt% Si.

Manganese and chromium are added mainly for hardenability [7]. They also contribute to lowering the B_S (albeit to a lesser extent than carbon) by stabilizing austenite relative to ferrite [15]. The balance of Cr to Mn is also important, if the Mn content is lower, the Cr content must be raised to maintain a similar B_S and V_B [11].

In a ted study, in which specimens were annealed intercritically to obtain an equal volume mix of ferrite and austenite before isothermal treatment the effects of Si and Mn were examined more closely, see Table 5 for alloys [17]. Some of their findings may be relevant:

1. By increasing Mn content the optimum cooling rate to obtain retained austenite is lowered and the optimum holding temperature is increased. While the stability of the retained austenite was not affected, its fraction was increased [17].
2. Increasing the amount of Si added increases the stability of the retained austenite which increased the product of tensile strength and total elongation [17].
3. When more Si and Mn was added, isothermal treatment time had to be increased to achieve maximum total elongation [17].
4. While adding large amounts of Si and Mn increases the amount of retained austenite, the lower carbon content still equates to lower stability and as a result the combination of strength and ductility does not improve [17].

Table 5-Alloy compositions for intercritical annealing study, isothermal bainite transformation temperatures ranged from 350-400°C [17]

Alloy	C	Si	Mn	P	S
A	0.201	1.240	0.950	0.0040	0.0063
B	0.200	1.560	0.951	0.0030	0.0057
C	0.199	2.100	0.940	0.0030	0.0058
D	0.202	1.210	1.550	0.0050	0.0062
E	0.195	1.210	1.550	0.0050	0.0058
F	0.202	0.810	1.870	0.0080	0.0065
G	0.201	1.240	1.800	0.0030	0.0062
H	0.202	1.640	1.834	0.0030	0.0062

Adding cobalt and or aluminum in quantities of less than 2wt% accelerate the austenite to bainite reaction [5, 15] . It has also been noted that using both Co and Al together had the best contribution to improved bainite transformation kinetics [15]. These additions accelerate the transformation by increasing the free energy change between austenite and ferrite (which is the driving force) [5, 7]. Accelerating the transformation also has some interesting effects on the microstructure and hardness which can be seen in Table 7. Higher fractions of bainite are present in the alloys with Co and Al [11], which also means that there are fewer areas of detrimental blocky austenite present [5]. Furthermore the bainite formed from alloys 2 and 3 have smaller bainite plates, and higher corresponding hardness values. Besides the improvements to the microstructure alloys 2 and 3 also transformed much faster than alloy 1 as shown in Table 7 and Figure 5.

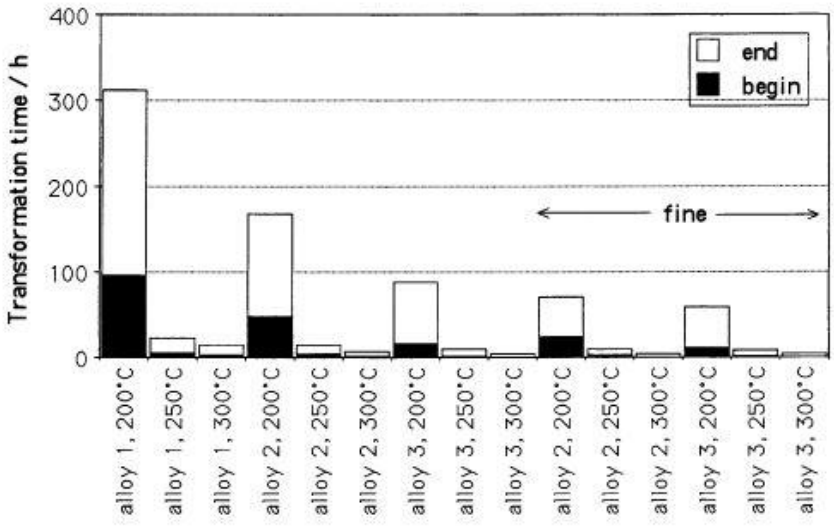

Figure 5-Reaction times at three isothermal treatment temperatures for various alloys. The sections labeled as fine have been austenitized at 900°C for 30 minutes whereas the other specimens were austenitized at 1000°C for 15 minutes [4]

It should also be noted that for alloys with higher concentrations of cobalt more chromium is required to achieve the same time before displacive reaction begins (t_{disp}), see Figure 6 and final volume fraction of bainite (V_b) [6].

Table 6-Alloy compositions for study on acceleration of bainite transformation [5]

Alloy	C	Si	Mn	Mo	Cr	V	Co	Al
1	0.98	1.46	1.89	0.26	1.26	0.09	-	-
2	0.83	1.57	1.98	0.24	1.02	-	1.54	-
3	0.78	1.49	1.95	0.24	0.97	-	1.60	0.99

Table 7-Isothermal treatment parameters, and bainite properties. Where (fine) is indicated the austenite grain size was refined by austenitizing at 900°C for 30 minutes as opposed to 1000°C for 15 minutes [5].

Alloy	Isothermal T(°C)	Time (h)	Thickness (nm)	Error (nm)	V_B	Hardness (HV 20)
1	300	240	124	4	0.55	420
	250	600	55	1.9	0.63	550
	200	363	35	1.3	0.69	619
2 (fine)	300	10	64	3.1	0.75	500
	250	14	49	3.2	0.79	589
	200	72	30	1.6	0.87	660
2	300	24	106	10	0.67	490
	250	24	38	2.5	0.76	640
	200	216	38	2	0.79	690
3 (fine)	300	8	52	3.7	0.63	500
	250	10	41	1.9	0.79	565
	200	72	45	3.3	0.83	650
3	300	8	57	4	0.66	490
	250	24	45	3.3	0.77	640
	200	216	40	3.6	0.78	650

The purpose of molybdenum is to reduce phosphorus embrittlement and increase hardenability [11]. Molybdenum additions also shift T_0' to lower C_γ, so it should be added sparingly [4].

Nickel can be added to increase both the tensile strength and toughness without detracting from the ductility [11]. The nickel content has to be balanced against the chromium (needs to be lowered with Ni addition) content to retain the same t_{disp} and V_b (at a given Temperature) [11]. Caution also has to be taken when nickel is added with other substitutional alloying elements such as Co and Al, since too many substitutional elements may end up slowing the transformation down enough for appreciable amounts of martensite to form [11]. Nickel is also noted as being an expensive alloying element [11].

2.1.4. Processing Considerations

The effect of processing factors on microstructure and final properties that need to be considered are austenitization treatment and time, cooling rate, and isothermal treatment temperature and holding time. Figure 5 demonstrates that austenitizing at a lower temperature of 900°C resulted in quicker reactions than samples austenitized at 1000°C. Figure 5 also shows that reactions begin and end quicker at higher isothermal holding temperatures. Samples that are treated at higher temperatures generally contain more retained austenite and have coarser plates of ferrite [6]. However samples treated at lower temperatures tend to have retained austenite limited to thin films [6]. As will be discussed later, specimens treated at higher temperatures tend to have greater total elongations, whereas lower treatment temperatures correlate to higher strength but less elongation[6].

Treatment time, temperature and cooling rate must also be tailored to the alloy system. Where the high carbon alloys can be isothermally treated in the 200-300°C range as in Table 7, lower carbon alloys have to be treated closer to the 350-420°C range as seen in Figure 6. Treatment temperature will always have to be above the Ms temperature, to avoid martensite formation, and below the Bs temperature. The cooling rate from austenitization to isothermal treatment temperature also has to be fast enough to avoid the nose of the diffusion transformation curve. The following calculations can be used to determine the shortest time required for diffusive and shear transformations:

Equation 4-Equation for minimum time to reach the bainite nose (displacive)

$$t_{disp\text{-}TTT}=\exp[(243200/RT)-135+20\log(T)-5\log\Delta G_m]...[11]$$

Equation 5-Equation for minimum time to reach the ferrite/pearlite nose (diffusional)

$$t_{dif\text{-}TTT}=\exp[(603100/RT)-190.5+20\log(T)-4\log\Delta G_m]...[11]$$

"where, ΔG_m is the available driving force for nucleation as a function of the activity of carbon in ferrite and austenite"[11].

It is also important to note in this section that cooling the bulk of material from austenitization temperature (usually 1200°C) care must be taken to avoid martensite formation. Proper cooling is also required, since high carbon

martensite cracks easily, which would leave permanent large scale defects in the material [5, 7].

Table 8-Variation in Bs and Ms for 3 alloy systems [5]

Alloy	C	Si	Mn	Mo	Cr	V	Co	Al	Ms (°C)	Bs (°C)
1	0.98	1.46	1.89	0.26	1.26	0.09	-	-	125	335
2	0.83	1.57	1.98	0.24	1.02	-	1.54	-	120	360
3	0.78	1.49	1.95	0.24	0.97	-	1.60	0.99	155	385

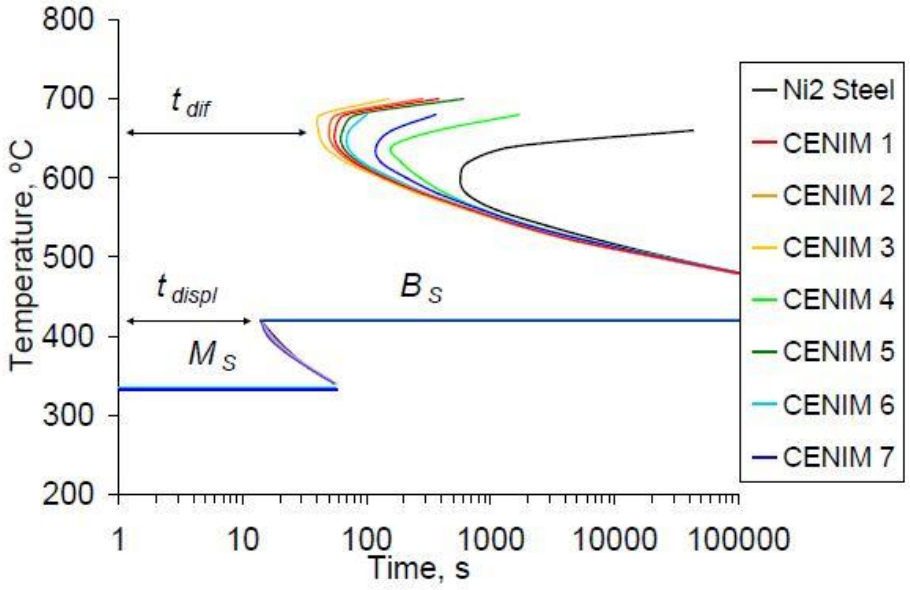

Figure 6-TTT diagram for 0.30 wt% C alloys[11]

2.2. Mechanical Properties

Obtaining the optimized mechanical properties requires the correct alloy composition and appropriate heat treatment and processing conditions. With respect to processing conditions, samples treated at higher isothermal temperatures tend to retain more austenite and as a result have higher total elongations and lower strengths [6]. Fracture toughness also increases with increasing isothermal treatment temperature as illustrated in Figure 7. The product of ultimate tensile strength and total elongation, which can serve as a rough indication of energy absorption also seems to increase with increased isothermal temperature as seen in Table 28 in Appendix 1.

With regards to the effects of elemental composition on final mechanical properties, Table 28 in Appendix 1 provides a brief summary of the literature. The best performing alloy with respect to strength and ductility is from [18] and is relatively simple, it does however take 2 weeks at the isothermal temperature to produce and only compression data was available for it. The next best performer is the Al+Co alloy from [6] which requires only a couple hours to produce. Finally it is also worth noting that at the cost of strength, alloy 1 transformed at 300°C absorbs the most energy during tensile deformation, which can be seen in Figure 8.

Figure 8 also illustrates that bainite deformation curves generally do not have a distinct yield point, and as a result the 0.2% offset yield stress is often used to define them[19]. Another important feature of this specific type of bainite's deformation curve is that the majority of plastic deformation is uniform elongation, and only small amounts of necking are expected [7]. It is also shown that the different strength-deformation behaviours achieved from different treatment temperatures can have very different work hardening profiles [6].

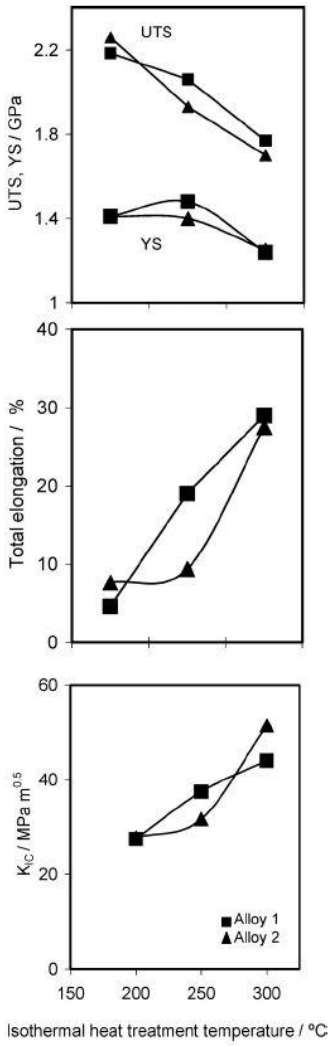

Figure 7-Effect of isothermal transformation temperature on mechanical properties: Alloy 1=0.83C-1.57Si-1.98Mn-0.24Mo-1.02Cr-1.54Co, Alloy 2 = 0.78C-1.49Si-1.95Mn-0.24Mo-1.60Co-0.99Al [13]

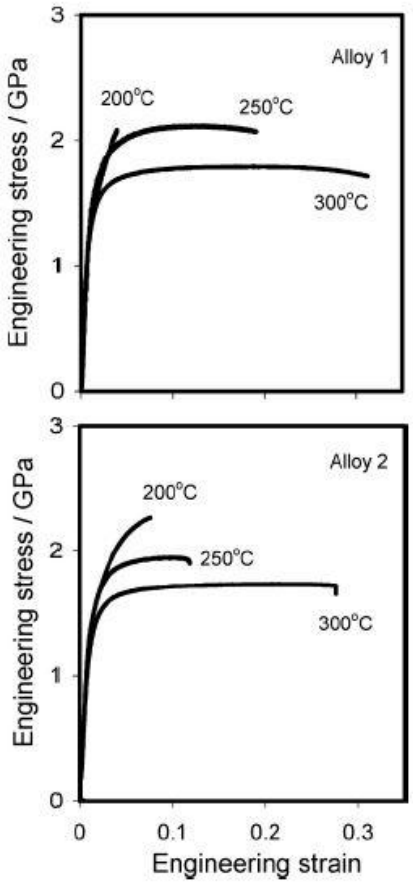

Figure 8-effect of isothermal transformation time on tensile deformation. Alloy 1=0.83C-1.57Si-1.98Mn-0.24Mo-1.02Cr-1.54Co, Alloy 2 = 0.78C-1.49-1.95Mn-0.24Mo-1.60Co-0.99Al [5]

2.3. Discussion and Recommendations

From the literature examined it can be concluded that to achieve the strongest microstructure possible for a given alloy, heat treatment temperature should be as low as possible (as close to Ms as possible). For most high carbon alloys (approximately 0.8% C) this will be approximately 200°C. If ductility and high energy absorption are desired then the highest possible temperature (near

Bs) is the best for treatment and between these two temperatures varying balances of strength and ductility can be achieved.

As far as improving upon the Tata alloy design, the most obvious discrepancy with qualified alloys for hard bainite is Tata's insufficient silicon content which at 0.75 wt% Si, is roughly half the of the recommended 1.5wt% Si typical in the literature. High tendency of carbide precipitation could explain the brittle performance of the Tata alloy i.e. the low advertised elongation values. For alternative new cast alloy, higher than 1.5wt%Si is strongly recommended.

The carbon content of the alloy serves multiple functions. Carbon content has a large effect on the Ms temperature and consequently has an influence on the lowest possible bainite transformation temperature that can be used [20]. High carbon alloys have lower Ms temperatures and can therefore be transformed to bainite at lower temperatures, forming thinner, more dislocation rich and therefore stronger bainite plates. The Tata alloy's Ms temperature is calculated in Table 9 using various empirical formulae to be between 140°C and 200°C. However, despite its low Ms the Tata alloy is still transformed at an isothermal temperature of 250°C to achieve ideal properties. The literature examined in this report does suggest that transforming at 250°C provides a good balance of both strength and ductility, but this begs the question: Is such a high carbon concentration (0.8 wt. %C) needed if the ideal transformation temperature is so much higher than the Ms? Table 9 also shows the results of empirical calculations for lower amounts of carbon, according to which as little as 0.65 wt.%C can be present in the alloy to still safely transform to bainite at 250°C without the risk of forming martensite.

Lowering the carbon concentration should have two positive effects on the final product. First, it should result in faster transformation and shorter isothermal holding times. As bainitic ferrite is formed, carbon must diffuse out of it creating a higher carbon concentration in front of the interface. Lower carbon increases the driving force for bainite formation. Furthermore, lower carbon content results in a smaller carbon pile up and thus requires less time for diffusion away into the remaining austenite; therefore accelerating overall transformation. Second, it should also create a higher final fraction of ferrite in the microstructure. Lower alloy carbon content pushes back the relative time at which the carbon concentration in the retained austenite reaches the critical value at T_0, which marks the point at which the transformation stops. Since ferrite is the stronger phase, having a higher final fraction of it should result in a stronger final product as well.

Higher carbon content also increases the stability of retained austenite which is essential for fully leveraging the TRIP effect of this microstructure. This

brings up another question: will altering the alloy's total carbon concentration influence the stability of the retained austenite? If the bainite transformation is allowed to proceed to completion it will be halted as a result of the carbon concentration of retained austenite reaching the critical value of T_0, which depends on transformation temperature not the alloy's carbon content. Therefore if the reaction is allowed to proceed to completion the final carbon concentration in the retained austenite should be the same at a given transformation temperature regardless of the alloy's carbon content. However, as mentioned before, the transformation time will vary. In the case of the Tata alloy, it is transformed for 6 hours, which according to dilatometry is not enough time for the reaction to reach completion. Their brochure claims that holding at 250°C for 6 hours leaves a microstructure composed of 70% bainitic ferrite and 30% austenite. In this case there is still enough carbon to stabilize the austenite at room temperature. However, if a lower carbon alloy is going to be made, care will have to be taken to make sure that there is enough carbon in the retained austenite to stabilize it.

Table 9-Prediction of Martensite and Bainite start Temperatures using empirical calculations based on composition. Note that these calculations do not account for Si, Co, or Al

	Investigator	C	Mn	Cr	Ni	Mo	M_s(°C)	B_s(°C)
Tata Steel	Steven and Haynes [21]	0.8	1.4	1	0	0.3	-	393
	Steven and Haynes [20]	0.8	1.4	1	0	0.3	158	-
	Andrews (linear) [20]	0.8	1.4	1	0	0.3	143	-
	Andrews (product) [20]	0.8	1.4	1	0	0.3	201	-
0.7 Carbon	Steven and Haynes [21]	0.7	1.4	1	0	0.3	-	
	Steven and Haynes [20]	0.7	1.4	1	0	0.3	206	-
	Andrews (linear) [20]	0.7	1.4	1	0	0.3	185	-
	Andrews (product) [20]	0.7	1.4	1	0	0.3	222	-
0.65 Carbon	Steven and Haynes [21]	0.65	1.4	1	0	0.3	-	433
	Steven and Haynes [20]	0.65	1.4	1	0	0.3	230	-
	Andrews (linear) [20]	0.65	1.4	1	0	0.3	207	-
	Andrews (product) [20]	0.65	1.4	1	0	0.3	235	-
0.6 Carbon	Steven and Haynes [21]	0.6	1.4	1	0	0.3	-	447
	Steven and Haynes [20]	0.6	1.4	1	0	0.3	253	-
	Andrews (linear) [20]	0.6	1.4	1	0	0.3	228	-
	Andrews (product) [20]	0.6	1.4	1	0	0.3	249	-

Additions of cobalt and or aluminum accelerate the transformation by increasing the free energy change between austenite and ferrite [5, 7]. This leads to lower necessary transformation hold times, thinner bainitic ferrite plates as well as a higher final fraction of ferrite, and therefore a harder final structure. When reviewing mechanical performance of the Co+Al alloy produced at 200°C performed similarly to the Mars 600 product. When produced at 250°C it loses some strength but gains much more ductility and energy absorption. Because of the positive effects cobalt and aluminum on both mechanical properties and transformation speed it is recommended that they are added to the alloy as well. It has been recommended that they are used in quantities less than 2 wt% [5, 15].

It may also be beneficial to add nickel to the system to increase its strength, then treat at a lower temperature to increase ductility. However, adding too many substitutional elements could slow down the bainite transformation making martensite formation more likely, or increasing treatment times [11]. Care would have to be taken to avoid that scenario. It is not recommended that nickel be included in the alloy because it is expensive, and altering the carbon content will provide enough variation to study for now. Nickel's effects would be something interesting to investigate in the future if another alloy is made.

3 Experimental Procedure

3.1. Tata Pavise Plates

The first material in the current work examined is Tata's Pavise plate, a commercially available superbainite plate intended for use as appliqué armour. The plates are a steel alloy with a nominal composition of Fe- 0.8C-0.72Si-1.4Mn-1.0Cr-0.3Mo (wt.%). Tata steel heat treated the plates by austenitization at 900°C for half an hour followed by quenching to 250°C and isothermal holding for 6h to form bainite. The inventory of as received Tata plates (in the heat treated state) purchased is shown in Figure 9.

(A) 1 Unperforated
49 cm x 49 cm x 8.5mm

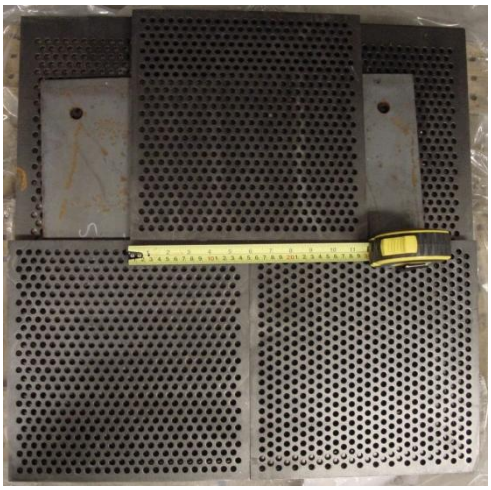

(B) 3 Perforated
30cm x 30cm x 1cm

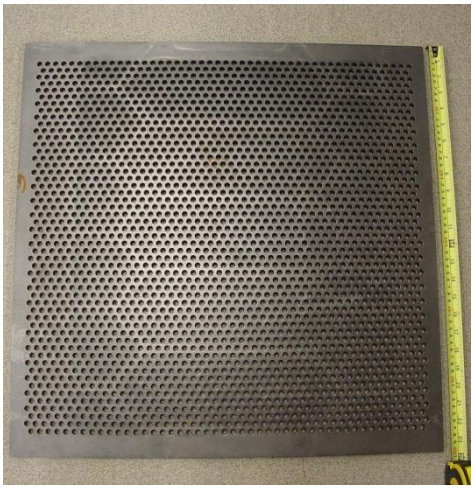

(C) 1 Perforated
60 cm x 60 cm x 1cm

Figure 9-As received plates of Tata's Pavise carbide-free bainite alloy

The Tata plates are only available with perforations, the unperforated plate was a custom order. Perforation reduces the weight of the plate, makes it easier to heat treat without forming cracks. Perforations also make it more difficult for cracks to propagate throughout the length of the plate.

3.2. CMAT Alloy

The second material in this study was designed and produced completely at CanmetMATERIALS and is endearingly referred to as the CMAT alloy. It has a composition of Fe-0.74C-1.92Si-2.17Mn-0.57Cr-0.24Mo-1.51Co (wt.%).

3.2.1. Casting of CMAT Alloy

The CMAT alloy was designed based on preliminary experimental assessments of the Tata alloy and literature. It was made with an increased level of silicon, lower carbon, as well as cobalt. Casting was done in a vacuum induction furnace, 135kg of the alloy was melted and poured into 3 ingots with a cross section of 3.75”(95.25mm) by 8”(203.2mm). A sample was cut from each ingot to confirm the chemistry using OES and LECO methods. (Casting and chemical analysis were done by the CanmetMATERIALS Casting team)

3.2.2. Rolling and Forging

To breakdown the cast microstructure and to mitigate compositional heterogeneity the ingots were subjected to hot deformation either by forging or rolling. Forging, using open die tooling and a hydraulic press, as shown in Figure 10, was done on rectangular prisms with dimensions 3”(76.2mm)x3” (76.2mm)x3.75”(95.25mm) which were cut from the ingots and hot forged into disks with a diameter of 7”(177.8mm) and thickness of 0.8”(20.32mm) according to the schedule shown in Figure 11.

(A) **(B)**

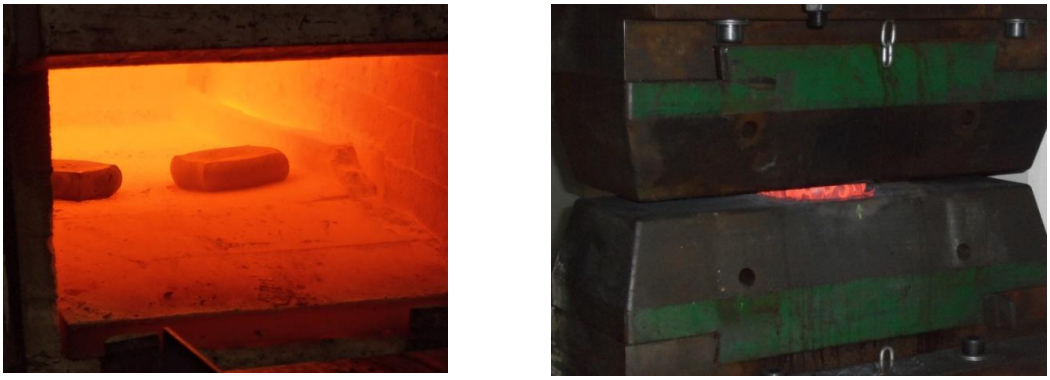

Figure 10-A:forged CMAT alloy disks being reheated to 1150°C between passes. B:hot disk being forged

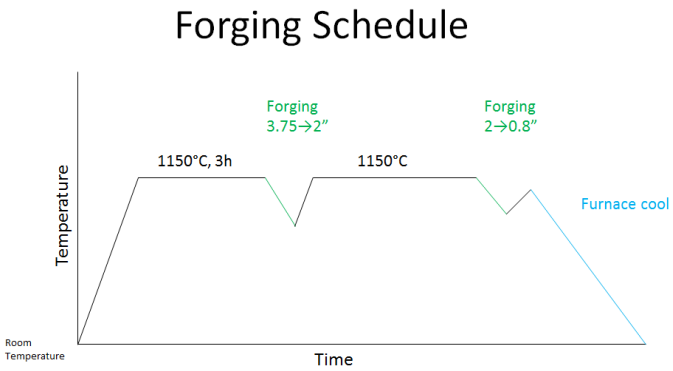

Figure 11-Hot forging schedule for CMAT alloy

Hot rolling was used to produce full sized plates. Sheets of 11mm and 20mm thickness and approximately 8”(203.32mm) width were hot rolled from the CMAT alloy. To produce 1'(304.8mm)x1'(304.8mm) ballistic test plates the initial slabs had to be cross rolled, see Figure 12. (Forging and Rolling were done by the metal forming team at CanmetMATERIALS.)

3.2.3. Heat Treatment

Slightly oversized rectangular outlines of subsized tensile and Charpy V-notch impact samples were heat treated. The gauge sections were then machined after heat treatment to avoid any warping due to heating and cooling cycles in the final tensile and CVN specimens. Tata samples were taken from un-heat treated plates. CMAT specimens were taken from the hot forged disks as described previoulsy. Tensile and Charpy specimens were heat treated using an open atmosphere furnace to austenitize at 900°C for one hour then quenched into a salt bath at the transformation temperature of either 250°C or 275°C for either 6 or 12 hours.

The salt bath used for tensile and Charpy specimens was a Lindberg pit furnace with a steel crucible, just over 4”(101.6mm) inner diameter containing molten salts. A thermocouple was placed into the salt bath to track its temperature throughout the experiment. Temperature fluctuations of ±10°C were noted, including when the sample was first quenched in the bath from 900°C. Round tensile specimens were also cut from the CMAT alloy hot forged disks and heat treated following the same procedure.

The 4”(101.6mm) x4”(101.6mm) plates were cut from the 8”(203.2mm) wide 11mm rolled piece. The 1’(304.8mm)x1’(304.8mm) plates were cut from the cross-rolled piece. Plates were ground down to a thickness of 11mm. A larger salt bath was needed to be used to heat treat the plates to accommodate their geometry and thermal mass, it is shown in Figure 13.

Figure 12-CMAT alloy plates produced with respective heat treatments written on them

Ausforming was carried out on small slabs of CMAT alloy that would be small enough to make 2 subsized tensile samples out of after deformation. Specimens had thermocouples embedded to track temperature. The same salt bath and homogenizing furnace that were used to heat treat the other tensile samples were used in this experiment as well. A 1200 ton Macrodyne hydraulic press was also used to deform the sample. Samples were austenitized at 900°C for an hour then placed on the press and allowed to cool to 600°C at which point they were deformed, and transferred immediately to placed in the salt bath for bainite transformation.

(A) **(B)**

Figure 13-Equipment used to heat treat CMAT alloy. A: Pyradia carburizing furnace. B: Park thermal salt bath.

3.3. Characterization

3.3.1. Chemical Spectroscopy

Carbon, sulphur, oxygen and nitrogen concentrations were determined using LECO analyzers. The LECO machine destroys the sample, and measures the chemistry through the bulk of the samples. The rest of the element concentrations were determined using a Baird optical emission spectrometer (OES). The Baird OES measures chemistry at the surface of a given sample thus proper sectioning is required.

3.3.2. Dilatometry Study

A Bahr DIL805 dilatometer, see Figure 14, was used to physically simulate the heat treatment of the commercial Tata Pavise plate and alternative heat treatments similar to it, while collecting phase transformation data. This was conducted for both the Tata and CMAT alloys. For ausforming and some austempering experiments rod shaped specimens 5mm in diameter and 10 mm in length were used. For a few austempering experiments hollow rod specimens of diameter 4mm, wall thickness 0.7mm and length 8mm were used. A dilatometer detects phase transformations by measuring changes in length with respect to time and temperature during simulation.

Samples for the Tata alloy were taken from the heat treated solid plate purchased. Samples from the CMAT alloy were taken from the hot forged disks.

Following reheating the samples were cooled from the austenitizing temperature at different rates to generate a continuous cooling transformation (CCT) diagram and to determine the critical cooling rates. The second step was to repeat the austempering thermal cycle for various bainite transformation temperatures (225, 250, and 275°C) and transformation times (1, 6, 12, and 18 hours). Finally ausforming experiments were performed where samples were quenched from the austenitization temperature to 600°C then deformed and quenched again to the bainite transformation temperature. Ausforming experiments were done for different amounts of deformation (25, 35, and 45%) as well as various transformation temperatures and times. (Marta Aniolek operated the dilatometer for all experiments.)

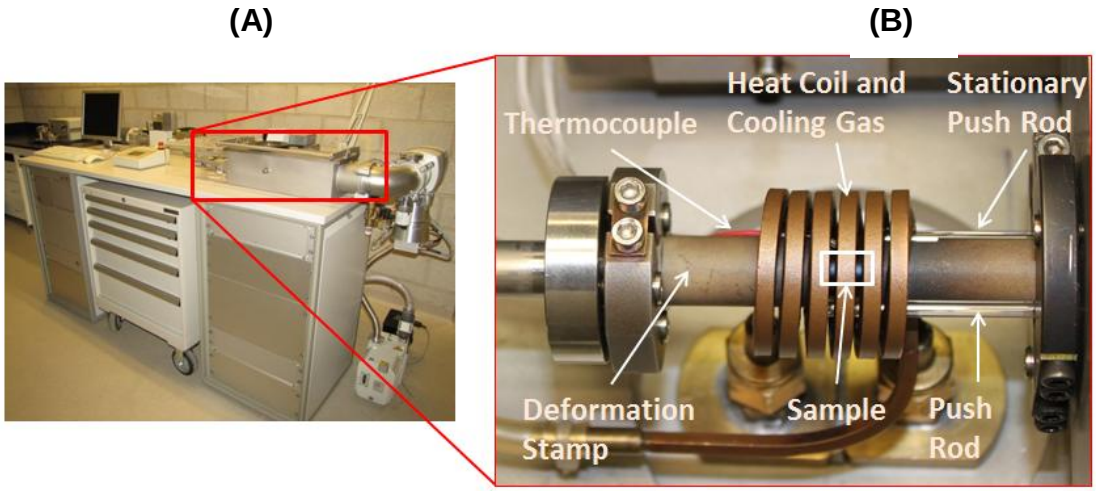

Figure 14-A:Dilatometer. B:Interior chamber of the dilatometer.

3.3.3. Optical Images and Metallographic Preparation

An Olympus PMG3 light microscope was used to initially characterize the microstructures that resulted from heat treatments. Samples were cold mounted in epoxy, ground and polished using the procedures outlined in Table 10 and Table 11, then etched in a 2%Nitric acid-98%Ethanol solution to reveal the microstructure.

Table 10-Metallography sample preparation procedure for austempered samples

Step	Plane Grinding 1	Plane Grinding 2	Fine Grinding	Polishing 1	Polishing 2	Chemical Polish
Surface	Piano 120 grit	Piano 220 grit	Allegro	DAC	NAP	OP Chem
Abrasive	-	-	9 µm	3 µm	1 µm	OPS
Lubricant	Water	Water	Blue	Blue	Blue	-
Rpm	150-300	150	150	150	150	150
Force (N)	150	150	20 (switch to single sample holder)	20	20	15-20
Time (min)	To depth/flat	5-10	10	5-8		10 on machine

Table 11-Metalography sample preparation procedure for ausformed samples

Step	Plane Grinding 1	Plane Grinding 2	Fine Grinding	Polishing 1	Polishing 2	Chemical Polish
Surface	Piano 120 grit	Piano 220 grit	Allegro	DAC	NAP	OP Chem
Abrasive	-	-	9 µm	3 µm	1 µm	OPS
Lubricant	Water	Water	Blue	Blue	Blue	-
Rpm	150-300	150	150	150	150	150
Force (N)	150	150	15 (switch to single sample holder)	10	10	10
Time (min)	To depth/flat	5-10	10	5-8		10 on machine 5-10 by hand

3.3.4. Electron Backscattered Diffraction (EBSD)

The examined Tata samples were extracted from the solid heat treated plate purchased from Tata steel. Samples for the CMAT alloy analysis were cut from the ends of tested tensile specimens. The examined face was cut at approximately half the depth of the tensile sample. Samples were ground and polished following the same steps as outlined in Table 10 and Table 11 with an additional 10 minutes of chemical polishing done by hand. It should be noted that having the flattest possible sample provides the best EBSD data. Furthermore, Samples that looked slightly etched or overpolished after chem polish usually performed the best. Epoxy mounts were coated (sample surface remained uncoated) with carbon paint to avoid charging and attached to a stand with copper tape. The sample stand was mounted onto a holder in the SEM which tilts the sample 70°.

A FEI Nova NanoSEM 650 scanning electron microscope with an EDAX TSL EBSD detector was used to collect data. The best results were obtained using the following microscope parameters: beam energy of 15keV, spot size of 5, working distance of 12mm. Specific EBSD parameters used were 4x4 binning,

a step size of 40nm, and a scan area/window of 50x50μm. The TSL acquisition software was set up to scan for the austenite and ferrite phases. Since ferrite and martensite both have body centered lattice cells that differ only slightly along the c-axis it is difficult to differentiate between the two. In this case they will both be identified by EBSD as ferrite then differentiated later based on morphology, image quality and confidence interval. The software stores data based on the position, crystal structure and orientation, image quality, and confidence index of a given point being scanned. After scanning this information was compiled in TSL's OIM analysis software to generate various maps and data. (Jian Li, Renata Zavadil and Chris Butcher operated the SEM for all EBSD scans.)

3.3.5. Scanning Electron Microscopy (SEM)

The NanoSEM was also used to characterize the as received Tata microstructure and to examine it for carbides. The sample was prepared according to the same steps for optical microscopy sample preparation. (Renata Zavadil operated the SEM.)

3.3.6. Transmission Electron Microscopy (TEM)

A JEOL JEM 2010F 200kV TEM was used to observe the microstructure of the CMAT alloy at high magnifications. It was used to examine the presence of thin films of austenite that encompass ferrite laths and to search for carbides.

TEM samples were taken from tensile specimen ends using the same cross section that was examined with optical microscopy and EBSD. Samples were prepared by cutting an 800μm strip from the tensile bar then punching 3mm diameter disks out of it. The disks were then ground with emery cloth to a height of 80μm and a 1200 grit surface finish. Samples were then polished and dimpled using 6μm and 3μm diamond paste followed by an OPS solution. Finally samples were perforated using an ion mill. (Carmen Andrei operated the TEM and Xiang Wang provided invaluable expertise with regards to analysis of the microstructure.)

3.3.7. X-Ray Diffraction (XRD)

XRD was used to measure phase fraction of retained austenite (FCC), and combined fractions of bainitic ferrite (BCC), martensite (BCT). It was also used to seek evidence of carbides. The unit cell parameter of retained austenite was also measured. This will correlate to the amount of carbon in the austenite lattice. A higher carbon concentration increases the lattice parameters of retained austenite shifting it to a lower 2theta value. An equation developed by Dyson and Holmes is used to calculate the carbon composition based on lattice parameter [22].

XRD samples were taken from the ends of used tensile specimens. The cross-section examined was perpendicular to the fracture surfaces and covers the through thickness of the plate. Samples were mounted in epoxy, ground and polished using the same steps as in the optical sample preparation method outlined in Table 10 and Table 11. An electrical connection was then made by drilling a stainless steel screw through the epoxy mount until it contacted the bottom of the specimen. The sample was then electropolished to remove any cold work that may have been introduced during the grinding and polishing which may have caused less stable retained austenite to transform to martensite (therefore throwing off phase fraction measurements). A solution of 6.2mL perchloric acid, 70mL ethanol, 10.0 mL butyl cellosolve and 13.7 mL distilled water was used for electropolishing [23]. Electropolishing left a pitted surface on the sample with parent austenite boundaries appearing to etch less than the rest of the microstructure, from optical inspection. (Chris Butcher did the electropolishing.)

XRD measurements were done with a Bruker D8 advance powder diffractometer. The machine has an area detector which makes scanning faster than a traditional point detector. A cobalt radiation source was used, as copper radiation makes steel samples fluoresce. Initially samples were tested by rotating the sample parallel to its face in an effort to de-texturize the data. Later the samples were rocked about the sample's X-axis as well to further de-texture the data.

Martensite has a body centered tetragonal unit cell whereas bainitic ferrite has a body centered cubic cell. The difference is manifested in martensite being a fraction of an angstrom longer in the c-axis, a difference which is difficult to measure with X-ray diffraction. Therefore XRD results labeled as ferrite or martensite are both added into one component which represents the fraction of body centered iron in a given specimen.

The diffraction patterns were combined and loaded into EVA. Another program called Topaz was then used to perform Rietveld refinement. Topaz is a modeling software which integrates the intensity curves by refining a number of variables simultaneously, variables which can be selected. The phases were selected: martensite, ferrite and austenite. Furthermore, by examining the diffraction patterns a preferred orientation in the (111)γ,(002)γ, (110)M, (011)M bands was noticed. The preferred orientation was accounted for in Topaz. (Victoria Jarvis did all of the XRD experiments and obtained the phase fractions and austenite lattice parameters)

3.3.8. Mechanical Properties

Hardness measurements were done using either a Vickers hardness(HV) machine or a Rockwell hardness (HRC) tester. Microhardness (HV_{500g}) measurements were done on the Tata alloy dilatometer specimens.

Tensile testing was done in an MTS-312.41 frame with a 500kN load cell. An Instron-262-604, 25mm gauge clamp-on extensometer was used to measure sample elongation throughout testing. Plate type and subsized tensile samples whose dimensions can be seen in Figure 15 were machined from the heat treated Tata plate. Subsized samples were also taken from the un-heat treated Tata plate and then treated in house. Subsized flat and round CMAT alloy specimens were taken from the hot forged disks. All specimens were machined with a wire EDM avoid introducing heat into the sample which could have affected the microstructure. Mechanical grinding was also used to get all samples down to final thickness.

E8/E8M – 13a

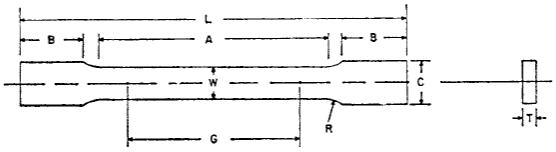

Dimensions			
	Standard Specimens		Subsize Specimen
	Plate-Type, 40 mm [1.500 in.] Wide	Sheet-Type, 12.5 mm [0.500 in.] Wide	6 mm [0.250 in.] Wide
	mm [in.]	mm [in.]	mm [in.]
G—Gauge length (Note 1 and Note 2)	200.0 ± 0.2 [8.00 ± 0.01]	50.0 ± 0.1 [2.000 ± 0.005]	25.0 ± 0.1 [1.000 ± 0.003]
W—Width (Note 3 and Note 4)	40.0 ± 2.0 [1.500 ± 0.125, -0.250]	12.5 ± 0.2 [0.500 ± 0.010]	6.0 ± 0.1 [0.250 ± 0.005]
T—Thickness (Note 5)		thickness of material	
R—Radius of fillet, min (Note 6)	25 [1]	12.5 [0.500]	6 [0.250]
L—Overall length, min (Note 2, Note 7, and Note 8)	450 [18]	200 [8]	100 [4]
A—Length of reduced section, min	225 [9]	57 [2.25]	32 [1.25]
B—Length of grip section, min (Note 9)	75 [3]	50 [2]	30 [1.25]
C—Width of grip section, approximate (Note 4 and Note 9)	50 [2]	20 [0.750]	10 [0.375]

Figure 15-Schematic of tensile testing specimen [24]

Charpy v-notched (CVN) impact testing was performed to measure the energy absorption (toughness) of the alloys. Sample dimensions can be seen in Figure 16. Tata samples were taken from the as heat treated purchased plate. Since the plate was only 8mm thick subsized CVN samples had to be used, having a height of 7.5mm. Sample orientation was selected in such a way that crack propagation would be on the same plane as in the tensile tests. Full sized Tata samples were also machined from un-heat treated plates then treated in house. CMAT alloy CVN specimens were machined from the hot forged disks. All machining of CVN specimens was done using a wire EDM due to the material's high hardness.

Samples from each different heat treatment were tested at room temperature. Some samples were also tested at -40°C since this test temperature was specified in the military standards [8, 25, 26]. Samples were cooled in an ethanol bath at -40°C to get them to the temperature then tested immediately. (Jie Liang operated the tensile and CVN testing machines.)

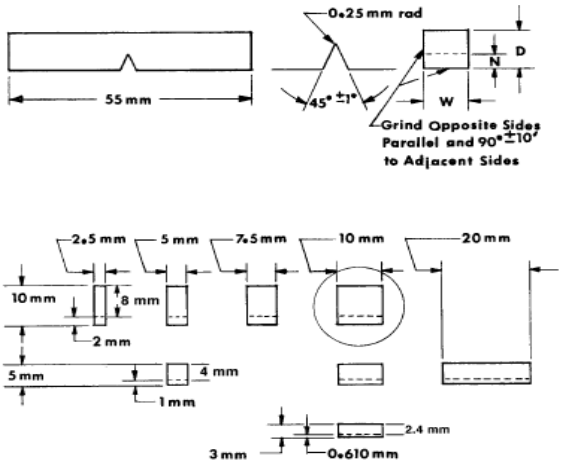

Figure 16-schematic diagram of v-notched Charpy impact test specimens[27]

3.3.9. Non-Destructive Testing-Liquid Penetrant

The liquid penetrant test reveals cracks in a part, in this case the heat treated perforated and un-perforated Tata plates. A dye that fluoresces when exposed to ultraviolet (UV) light is applied to the entire surface of the plate. It is given time to infiltrate any cracks and the excess is wiped off. The UV light is then turned on and any cracks can then be seen. (Jason Ripski did the liquid penetrant test.)

3.3.10. EELS-Local Measurement of Carbon Content

A proper EELS technique to measure local carbon content in TEM is currently being developed and optimized at CanmetMATERIALS. This technique was used on the TEM samples to measure the carbon content in individual laths of bainite and thin films of austenite. (Colin Scott and Babak Shalchi Amrikhiz did the EELS measurements and subsequent data analysis to determine carbon concentrations)

4 Results

4.1. Characterization of As-Received Tata Plates

4.1.1. Liquid Penetrant Test

The liquid penetrant test revealed cracks throughout the purchased heat treated unperforated Tata plate as shown in Figure 17. This technique does not provide quantitative data about crack depth but by visual insepction cracks appeared to be roughly 500µm deep. Furthermore, it can be seen that the cracks pass through the regions from which the tensile specimens were taken. The test was also performed on the heat treated perforated plate and no cracks were observed.

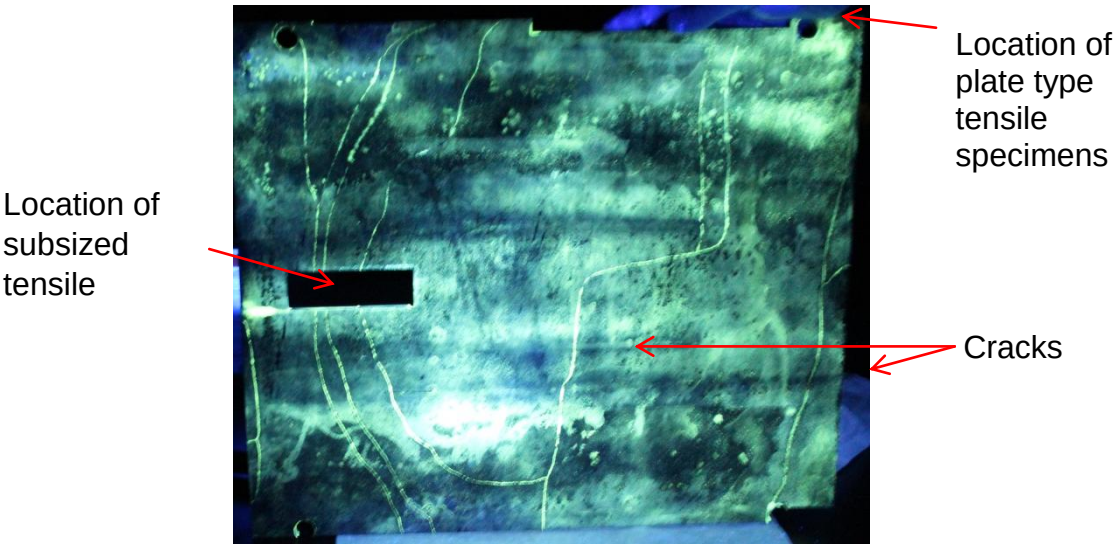

Figure 17-Photograph of the purchased heat treated Tata plate after dye infiltration.

4.1.2. Optical Microscopy of the Heat Treated Tata Plate

Initial optical microscopy of the Tata heat treated plate in Figure 18 shows a decarburized layer on the surface of the plate, as well as the core bainite structure which appears to be banded. Figure 19 shows a higher magnification image of the bulk microstructure in which small white islands of blocky retained austenite and dark laths of bainitic ferrite/martensite are present. As a result of decarburization the surface layer has less stable austenite with a higher Ms temperature. It is therefore likely that the surface layer is mostly comprised of hard, brittle untempered martensite.

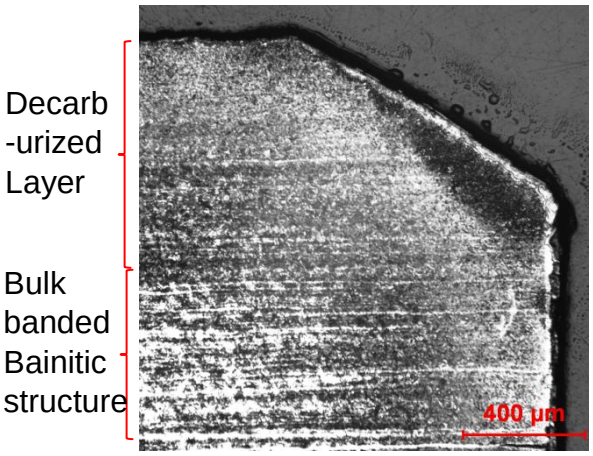

Figure 18-Optical micrograph of the corner of the heat treated Tata plate. Etched with 2% Nital

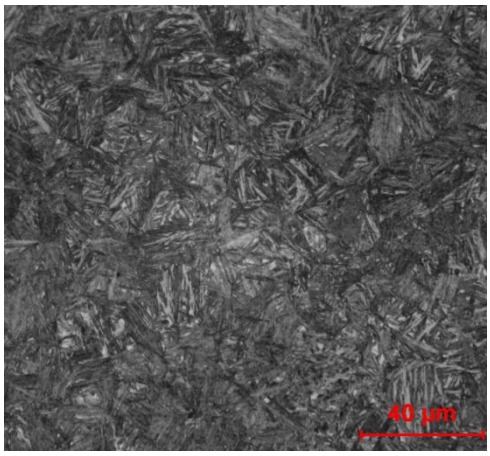

Figure 19-Bulk microstructure of the heat treated Tata plate. Etched with 2% Nital

4.1.3. Scanning Electron Microscopy (SEM) of Tata Plate

SEM of the bulk bainitic structure of the plate, see Figure 19, clearly shows the very fine scale of the microstructure. Blocky austenite and bainitic ferrite laths are labeled. Bainite laths were arranged in a few packets within each prior austenite grain. Blocky retained austenite segments were entrapped between adjacent packets.

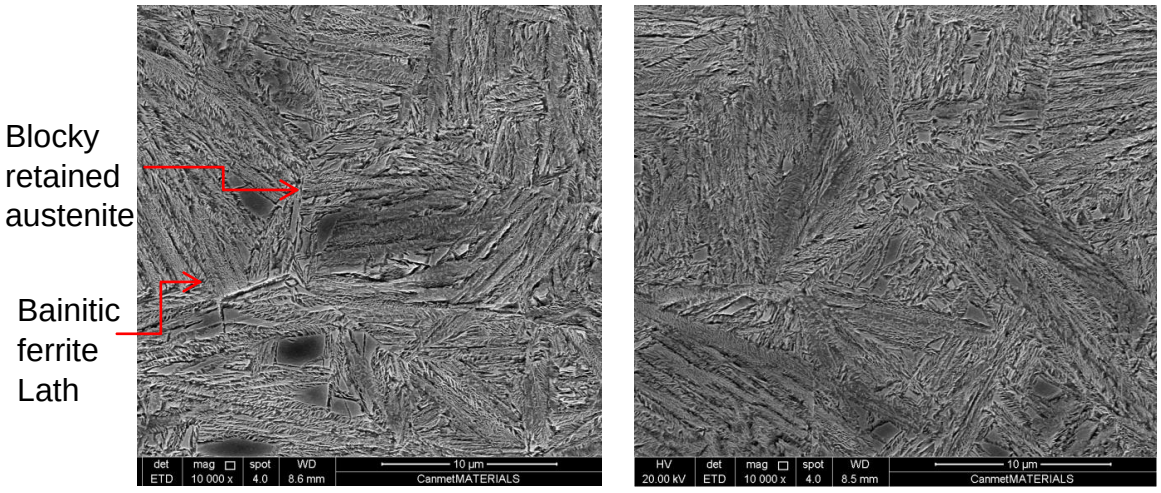

Figure 20-SEM of perforated and heat treated Tata plate

4.2. Optical Microscopy

4.2.1. Optical Microscopy of Tata Alloy

Micrographs of Tata alloy dilatometer samples that have been ausformed are shown in Figure 21. Dark laths of bainitic ferrite are present with bright areas being islands of retained austenite or martensite-austenite with a more grey tint. A band, the whiter region, can be seen passing from left to right through the middle of the micrograph shown in Figure 21 D. The bands are likely a result of manganese that segregated during the solidification of the cast ingots. Segregated areas where then stretching during forming, and were present in the dilatometer samples before they were ausformed.

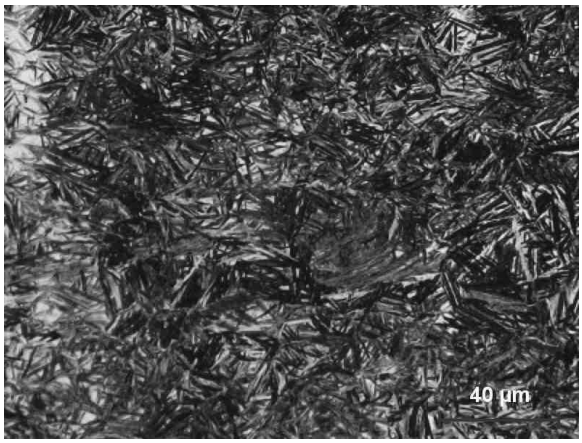

(A) Tata-250°C-6h-25% deformation 500x magnification, etched with 2% nital

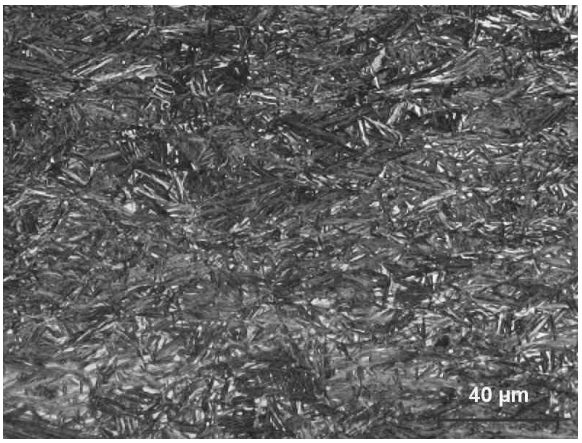

(B) Tata-250°C-6h-45% deformation 500x magnification, etched with 2% nital

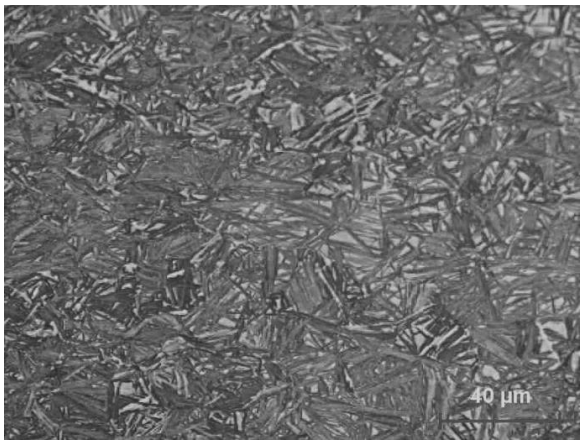

(C) Tata-275°C-6h-25% deformation 500x magnification, etched with 2% nital

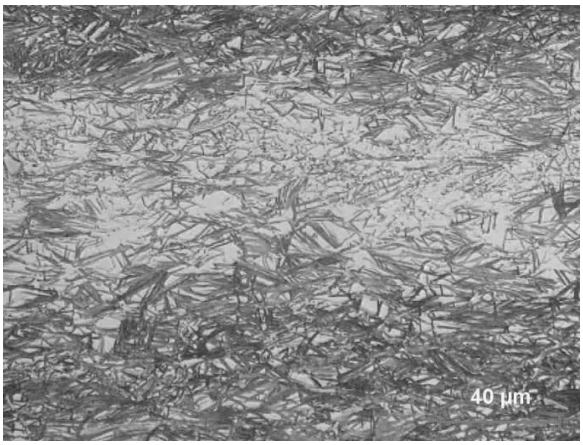

(D) Tata-275°C-6h-45% deformation 500x magnification, etched with 2% nital

Figure 21-Tata alloy, ausformed dilatometer samples

4.2.2. Optical Microscopy of CMAT Alloy

The micrographs of the samples cooled from the austenitization temperature (900°C) to room temperature are shown in Figure 22. According to the dilatometer data no bainite was formed during cooling, the microstructures should therefore be composed of martensite and some retained austenite.

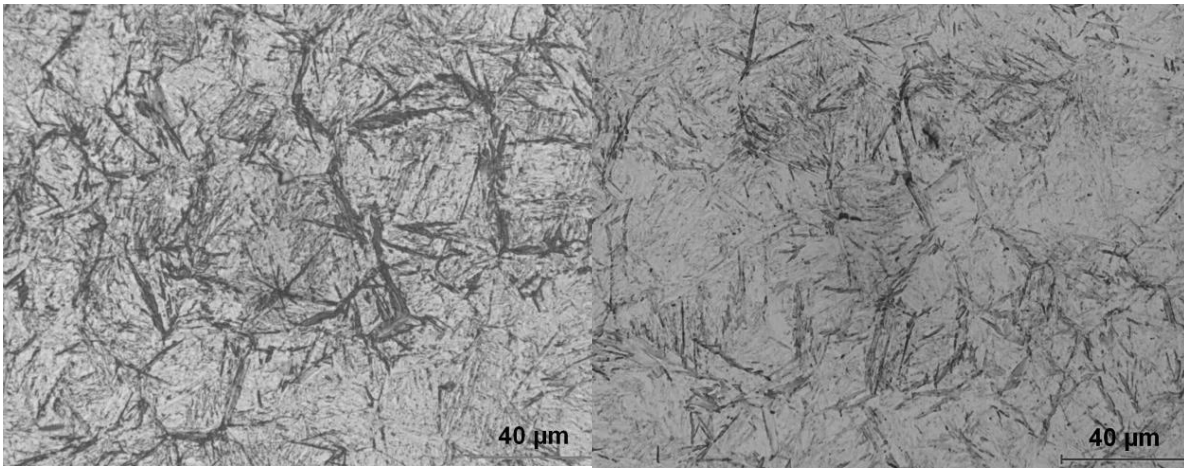

Figure 22-CMAT alloy CCT specimens. Left: 5°C/s cooling rate. Right: 10°C/s cooing rate.

The microstructures of the austempered CMAT alloy round tensile specimens are shown in Figure 23. The specimen treated at 250°C for 6 hours should, according to the dilatometer results, contain an appreciable amount of martensite. It is difficult to see which areas are martensitic using optical microscopy, but according to the EBSD micrographs martensite mixed with retained austenite should be present in the white islands that would be identified as just retained austenite in all three of the other micrographs. Packets of bainitic ferrite laths within prior austenite grains can be seen for all the conditions. Discrete blocky austenite islands are more readily visible for treatment at 275°C.

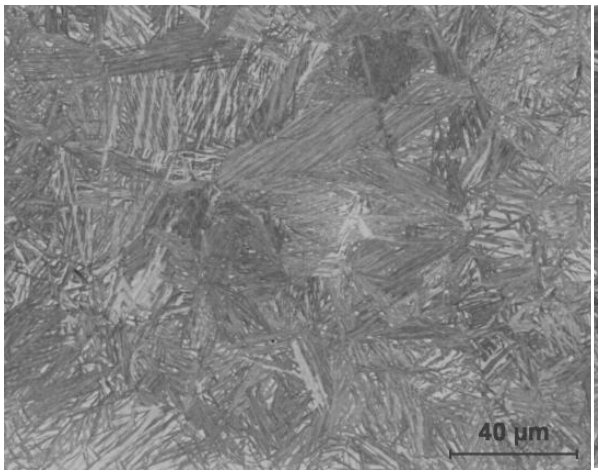

(A) CMAT-250°C-6h
500x magnification, etched with 2% nital

(B) CMAT-250°C-12h
500x magnification, etched with 2% nital

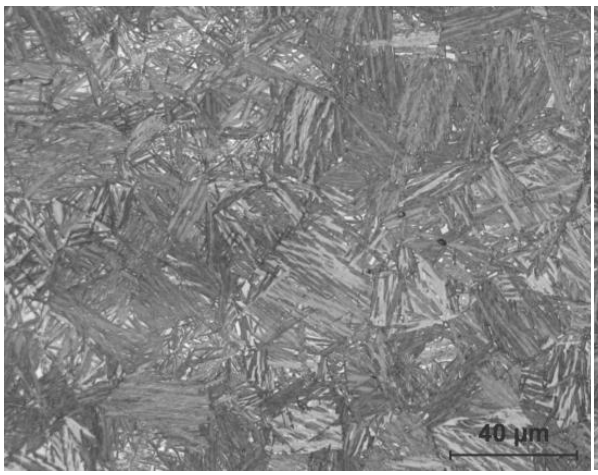

(C) CMAT-275°C-6h
500x magnification, etched with 2% nital

(D) CMAT-275°C-12h
500x magnification, etched with 2% nital

Figure 23-CMAT alloy, austempered, round tensile specimens

Figure 24 shows the microstructures of variously ausformed CMAT alloy specimens. The specimens deformed at 600°C then treated at 250°C for 6 hours (Figure 24 A and C) appear to be much more refined than their austempered counterpart. The specimen deformed 45% and treated at 250°C for 1 hour contains almost no bainite, and it is composed mainly of martensite laths and martensite-retained austenite regions.

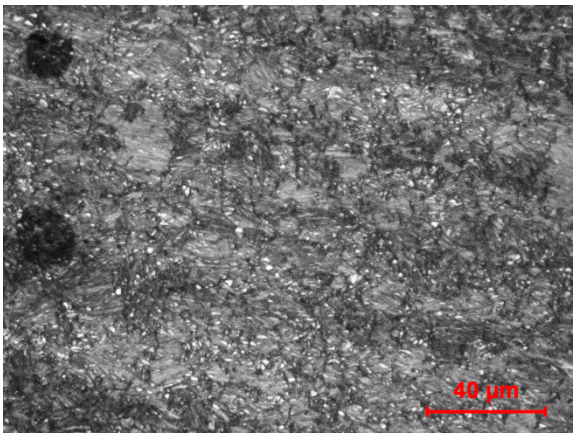

(A) CMAT-250°C-6h-25%deformation 500x magnification, etched with 2% nital

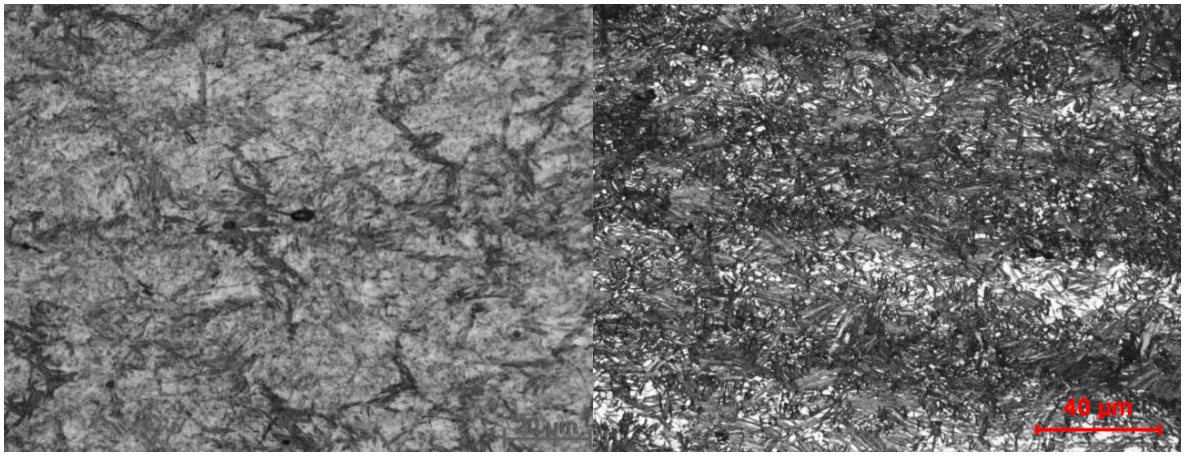

(B) CMAT-250°C-1h-45%deformation etched with 2% nital

(C) CMAT-250°C-6h-45%deformation 500x magnification, etched with 2% nital, note the bands visible in across the micrograph

Figure 24-CMAT alloy, ausformed specimens

4.3. Dilatometry

The dilatometer data can be examined for change of length over time as shown in Figure 25 or elongation over temperature as seen in Figure 26. In both cases the segments showing bainite and martensite transformations are labeled. In Figure 25 following the reheating and cooling segment to isothermal holding segment, a noticeable incubation period (lack of expansion) is obvious prior to the bainite reaction (which is associated with expansion). The holding was not

sufficient to complete the transformation. Note that in length change vs. temperature curves such as Figure 26 linear elongation represents only thermal expansion or contraction whereas curvature shows a phase transformation. During cooling from the reheating temperature (900°C), no signature of any austenite decomposition is seen confirming that 10°C/s was adequate to suppress ferrite/pearlite formation. Furthermore, after 5 hours of isothermal bainite formation (vertical segment) and upon cooling to room temperature, a significant fraction of the remaining austenite transformed to martensite.

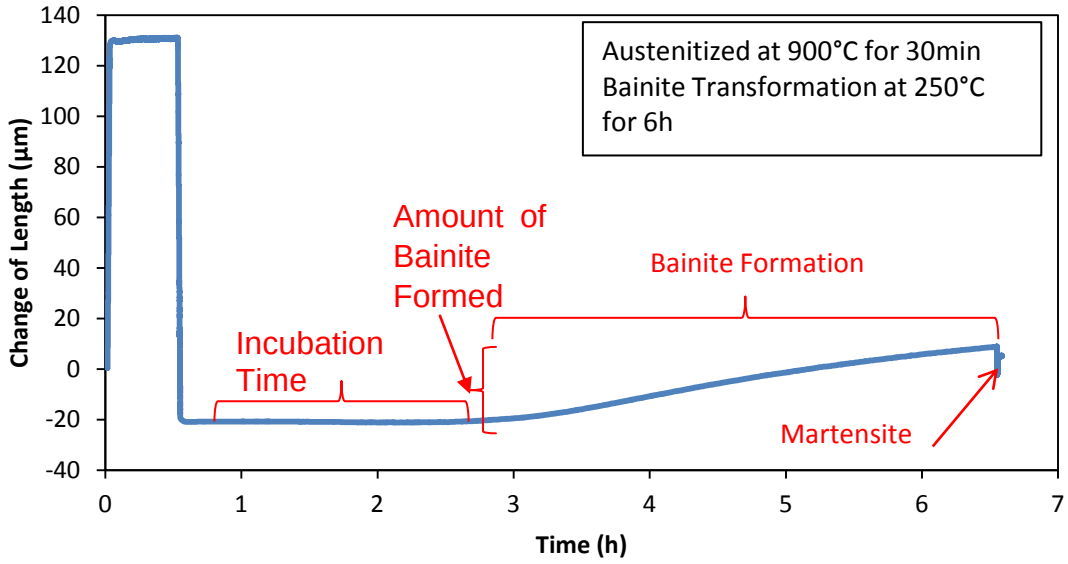

Figure 25-Change in length vs. time curve for CMAT alloy sample transformed to bainite at 250°C for 6 hours

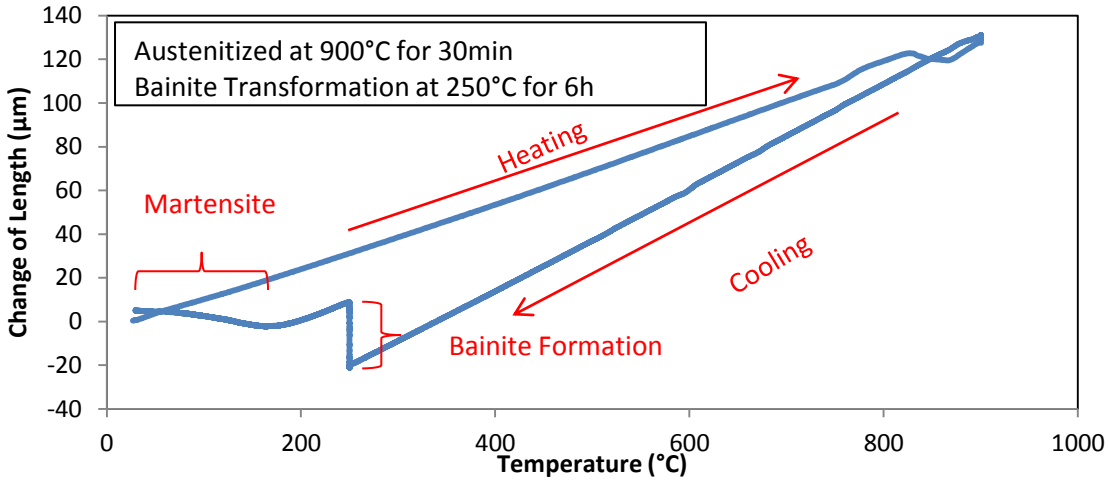

Figure 26-Change in length vs. temperature curve for CMAT alloy sample transformed to bainite at 250°C for 6 hours

4.3.1. Dilatometer Study of Tata Alloy

Initially for the dilatometer study hollow cylindrical samples were used for the continuous cooling and austempering experiments and solid cylindrical samples were going to be used for ausforming. Experiments done comparing the two sample geometry are shown in Figure 27. The results are close, with hollow samples transforming slightly faster, but it was decided that only solid specimens would be used for all experiments for more accurate and consistent comparison.

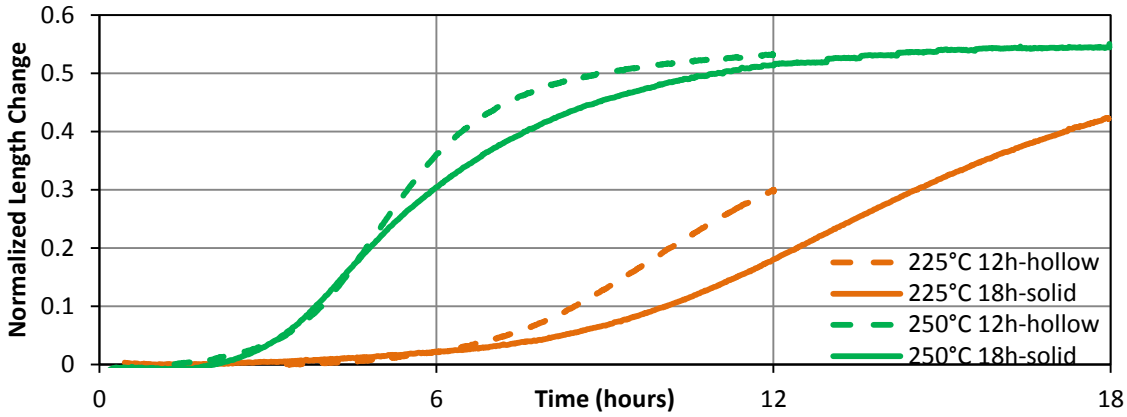

Figure 27-Tata alloy austempering isothermal bainite transformation profiles comparing hollow to solid samples

The isothermal bainite transformation of the austempering dilatometer experiments are shown in Figure 28 for the Tata specimens. Higher transformation temperatures led to shorter incubation times. A similar fraction of bainite was formed by treating at 275°C and 250°C after 18 hours noting that the reaction at 250°C was not complete yet. A smaller amount of bainite formed when treating at 225°C however the reaction has not finished after 18 hours. The rate of reaction can be further analyzed by Figure 29 which plots the first derivative of curves shown in Figure 27. It can be seen in Figure 29 that higher transformation temperatures also correspond to higher peak rates of reaction which occur sooner.

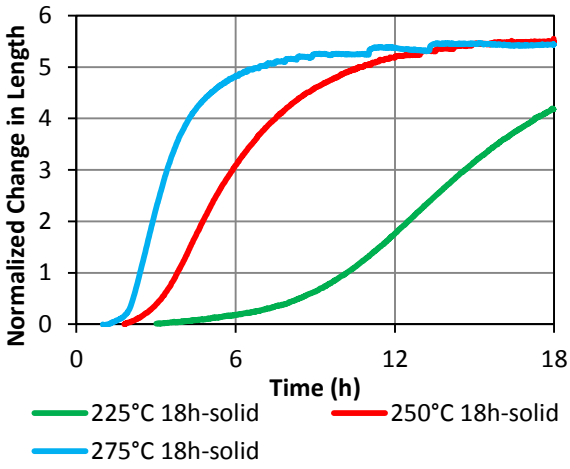

Figure 28-Austempered isothermal bainite transformation kinetics for Tata alloy. Austenitization was done at 900°C for 30min

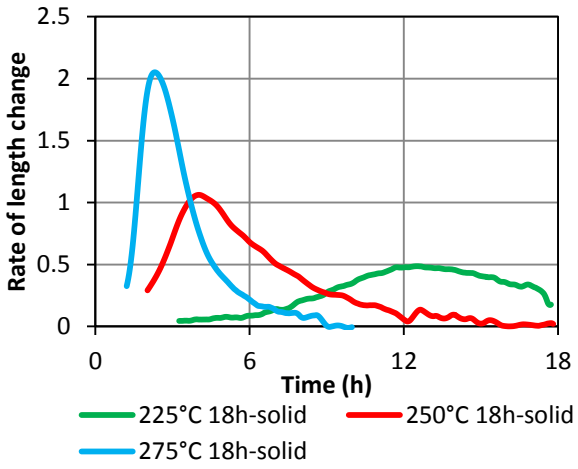

Figure 29-Ausformed isothermal bainite transformation for Tata alloy

The ausforming experiments for specimens transformed at 250°C are shown in Figure 30. A deformation of 25% decreased incubation time and increased reaction rate earlier than in the austempered counterpart. Furthermore, although almost the same fraction of bainite was formed after 6 hours of holding with 25% deformation compared to the strain free sample, the reaction tended to slow down earlier in the deformed specimens. Applying 45% deformation caused reaction to occur immediately upon reaching the transformation temperature without incubation, with a large fraction formed. However, the reaction rate dropped off quickly in this case and further bainite formation was ceased.

The results of ausforming followed by transformation at 275°C are shown in Figure 31. A deformation of 25% decreased the incubation time but had overall slower reaction kinetics and a lower final fraction of bainite formed. Similar behavior was seen with 45% deformation with even slower reaction kinetics and a lower final fraction of bainite.

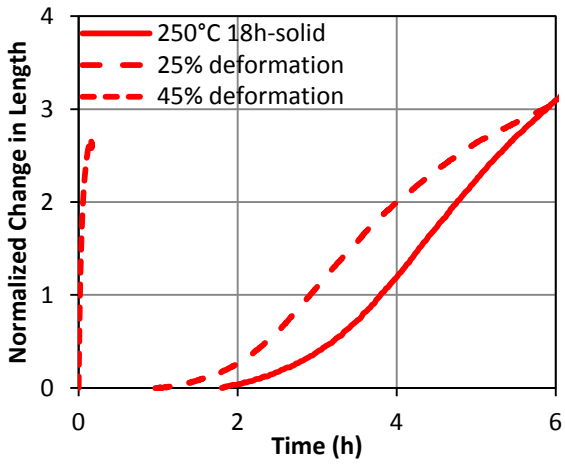

Figure 30-Various degrees of ausforming with transformation done at 250°C and deformation applied at 600°C for Tata alloy

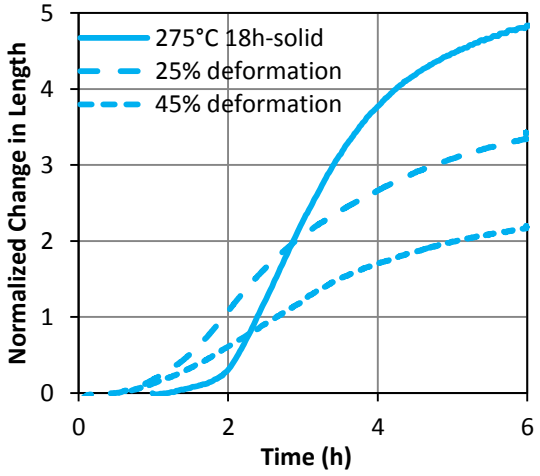

Figure 31-Various degrees of ausforming with transformation done at 250°C and deformation applied at 600°C for Tata alloy

4.3.2. Dilatometer Study of CMAT Alloy

The isothermal transformation profiles of the CMAT alloy for various transformation temperatures are shown in Figure 32. Higher transformation temperatures led to shorter incubation times and higher final fractions of bainite formed within the 18 hour time allotted. There is a greater difference in final fraction between 250°C and 275°C than was observed in the Tata alloy.

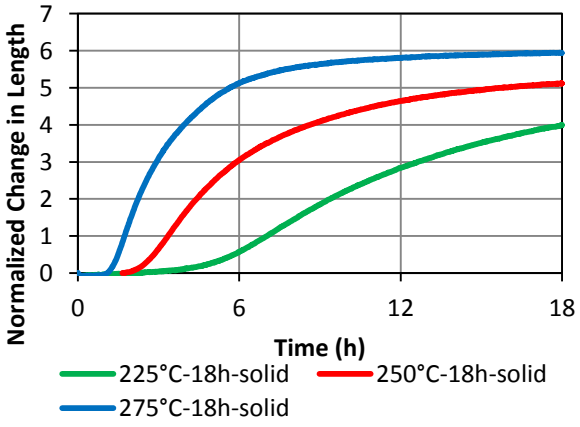

Figure 32-Austempered isothermal bainite transformation kinetics for CMAT alloy. Austenitization was done at 900°C for 30min

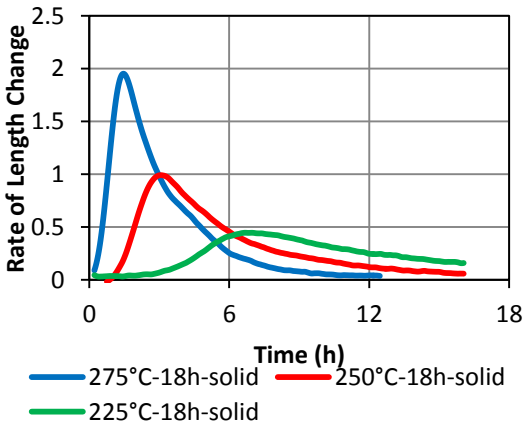

Figure 33-Austempered isothermal bainite transformation rate for CMAT alloy

Figure 33 shows the corresponding transformation rates. Higher transformation temperatures had higher transformation rates which occurred

sooner. The trend is the same as in the Tata alloy. At 275°C the bainite transformation looks complete after 18 hours judging by the plateau in the reaction rate. However at 250°C and 225°C the transformation has not completed after only 18 hours.

The results of bainite transformation at 250°C after deformation are shown in Figure 34. The smaller deformation of 25% had little effect on incubation time and decreased the final fraction of bainite formed when compared to the undeformed counterpart. It also slightly decreased the peak transformation rate as well, see Figure 35. A deformation of 45% greatly reduced incubation time, it is almost instantaneous and increased the maximum transformation rate. However, after approximately 30 minutes transformation halted, leading to an overall lower final fraction.

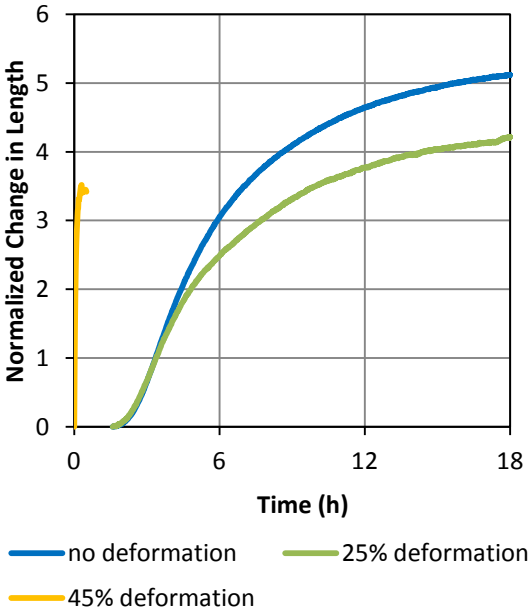

Figure 34-Ausformed isothermal bainite transformation kinetics at 250°C for CMAT alloy. Austenitization at 900°C for 30 mins. Deformation at 600°C.

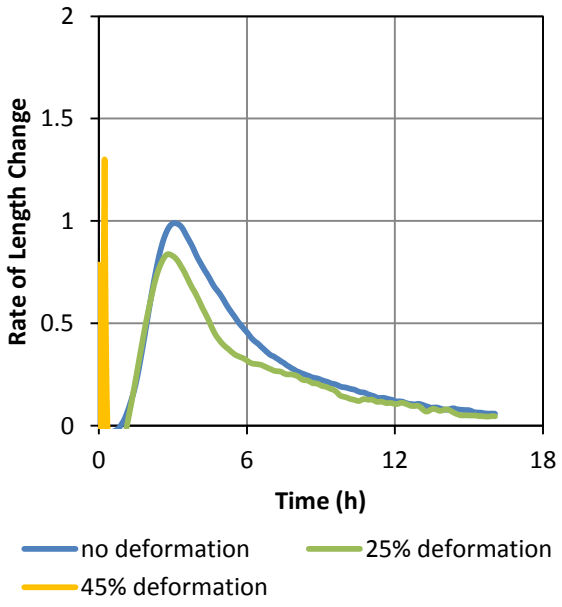

Figure 35-Ausformed isothermal bainite rate of transformation for 250°C

When transforming at a higher transformation temperature, 275°C, the incubation time was slightly decreased when deformed 25% and slightly increased when deformed 35%, as shown in Figure 36. Furthermore, higher amounts of deformation resulted in decreasing final fractions of bainite. Figure 37

shows that increasing amounts of deformation lead to a decrease in maximum rate of transformation.

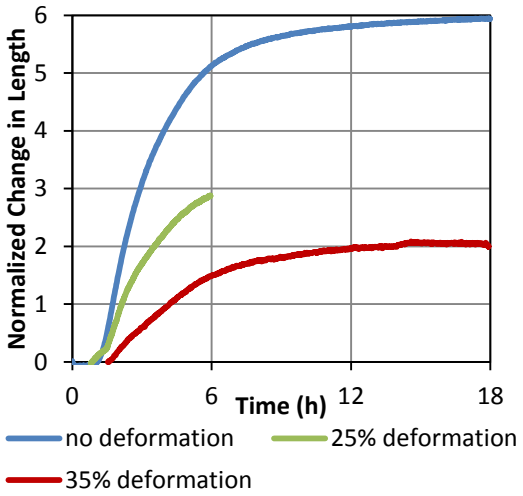

Figure 36-Ausformed isothermal bainite transformation kinetics at 275°C for CMAT alloy. Austenitization at 900°C for 30 mins. Deformation at 600°C.

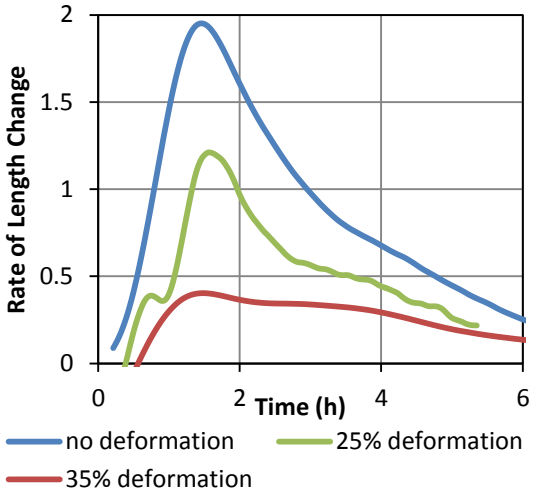

Figure 37- Ausformed isothermal bainite rate of transformation for 275°C

The dilatation curves were analyzed following isothermal bainite formation and upon cooling to room temperature for both ausforming and austempering specimens, see Figure 38. The length change during cooling indicates whether the remaining austenite transforms to martensite or not. There is no indication of martensite formation for the sample transformed at 275°C and very little for the sample transformed at 250°C for 12 hours (straight dilatation line). Transforming at 250°C for 6 hours led to more martensite formation and a higher Ms temperature. It can also be seen that increasing the amount of deformation when transforming at 250°C for 6 hours lowers the Ms temperature.

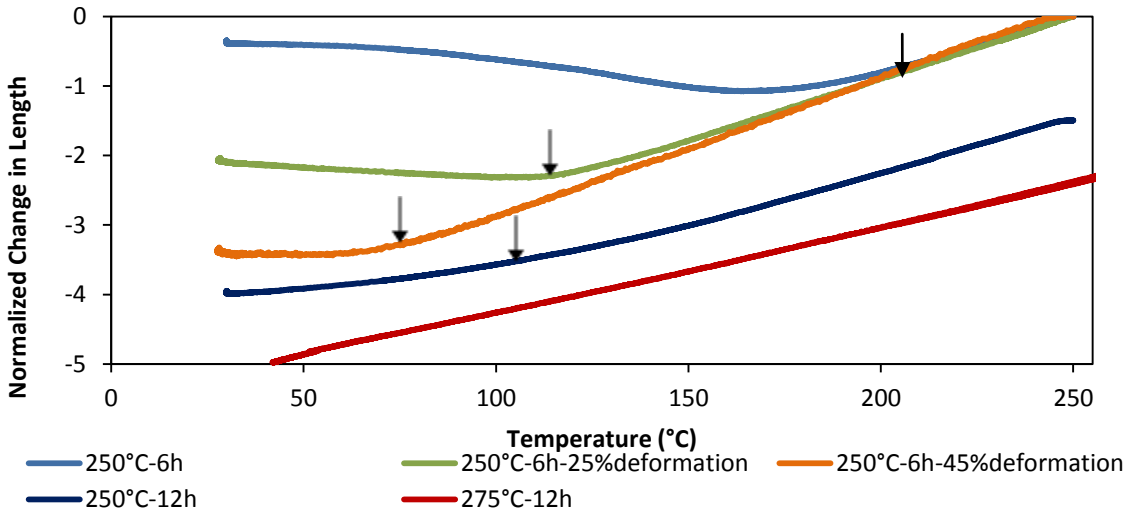

Figure 38-Length change of remaining austenite upon cooling from isothermal holding for CMAT alloy. The cooling rate is 10°C/s. The curves have been offset along the y-axis for ease of interpretation. Ms points are marked with arrows.

4.4. Electron Backscattered Diffraction (EBSD)

In general, the EBSD micrographs clearly show that at higher temperature (275°C vs. 250°C) bainite forms as thicker laths. Furthermore, prior deformation of austenite at 600°C leads to smaller, and typically shorter, laths of bainite compared to bainite formed by austempering with transformation at the same temperature and time. At higher transformation temperature larger areas of blocky retained austenite are observed regardless of the initial state of austenite, it being deformed or undeformed. There is also a difference in blocky retained austenite morphology for samples transformed at 250°C. The microstructure transformed for 12 hours seems to have more uniform areas of blocky retained austenite, whereas the sample transformed for only 6 hours has more regions of spotty austenite.

Spotty areas that exist as lines between bainite laths are likely signal from thin film austenite that is too thin (10-20nm) to be precisely measured by EBSD, since the area of the interaction beam is approximately 50nm in diameter.

It is important to have a general understanding of how TSL acquisition software identifies points to generate EBSD data. It uses a voting system to identify points from Kikuchi band patterns. Triple points between bands on the Kikuchi pattern are located and the angles between them are measured and compared to a Miller index database [28]. A “vote” is a solution from the Miller index database decided for one triplet and the solution with the most votes wins [28]. The confidence index is calculation is shown in Equation 6. It is based on the amount of votes for the most popular and second most popular solutions from

Equation 6**,** where V_1 and V_2 are the number of votes for the first and second most popular solutions respectively and V_{IDEAL} is the maximum possible amount of votes [28]. Confidence intervals with a value greater than 0.1 are considered to be indexed with a 95% success rate, however from zero to 0.1 there is a much lower chance of accurate indexing [28]. Therefore a point with a confidence index above 0.1 is relatively reliable, and a point with a confidence index below 0.1 is questionable.

Equation 6-Calculation for Confidence Index(CI)

$$CI = \frac{V_1 - V_2}{V_{IDEAL}}$$

While lower image quality can be associated with more strains or dislocation in the structure, as it would be with martensite vs. bainite [29], low confidence index suggests that the specimen is not well prepared and that good identification was not possible. When examining the maps of the ausformed specimens it should be noted that they had significantly lower average confidence indices than the austempered maps. Furthermore it is difficult to differentiate between martensite and bainite based on the expectation that martensite has the lower image quality, because most low images quality areas are located in low confidence areas.

The EBSD images for the as received Tata Pavise plate are shown in Figure 39. In image quality maps bright areas correspond to high image quality and dark areas are spots with low image quality. In orientation maps colour is assigned based on crystallographic orientation. In phase maps austenite is red and bainite and martensite are green. The images show bainite laths and very fine austenite islands as well as MA areas.

Tata-As received material

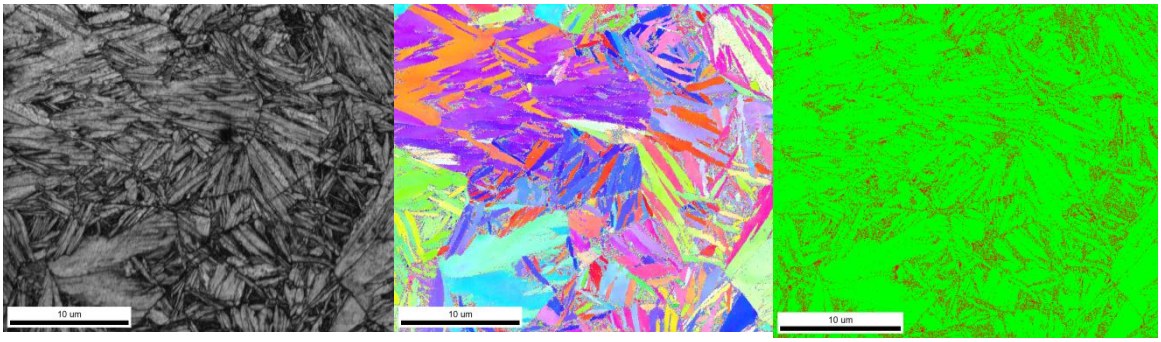

Image quality map Orientation map Phase identification map

Figure 39-EBSD maps of the as received Tata Pavise plate

The EBSD images of the CMAT alloy with the same heat treatment as the Tata Pavise plate (austenitized at 900°C for 30 minutes then transformed to bainite at 250°C for 6 hours is shown in Figure 40. The images show bainite laths of similar thickness to the Tata plate and similar MA areas. However the CMAT alloy also has larger islands of retained austenite. The CMAT specimen treated at the same temperature but for 12 hours also has bainite laths with similar thickness but lacks spotty MA regions and also has more and larger retained austenite islands.

CMAT-250°C-6h

Average Confidence Index =0.32

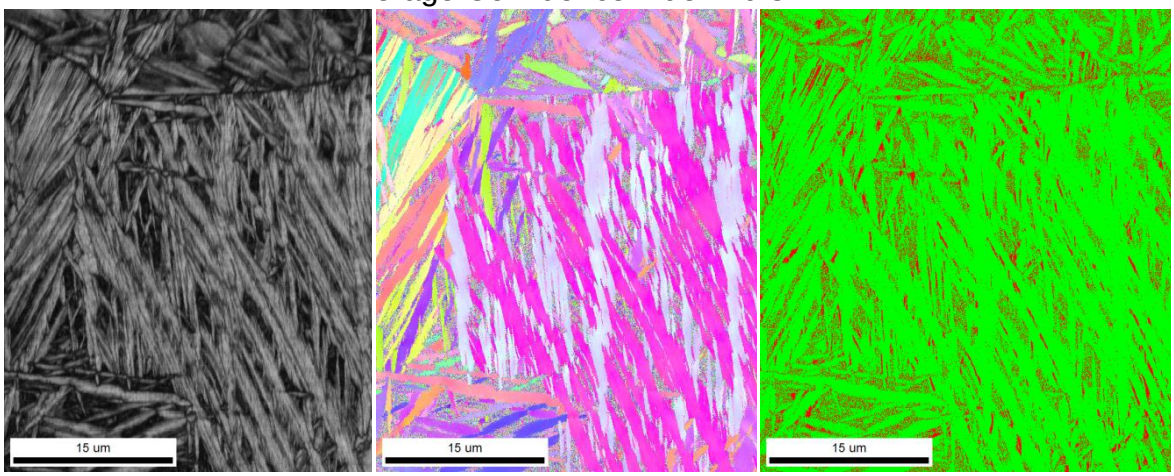

Image quality map Orientation map Phase identification map

CMAT-250°C-12h

Average Confidence Index =0.51

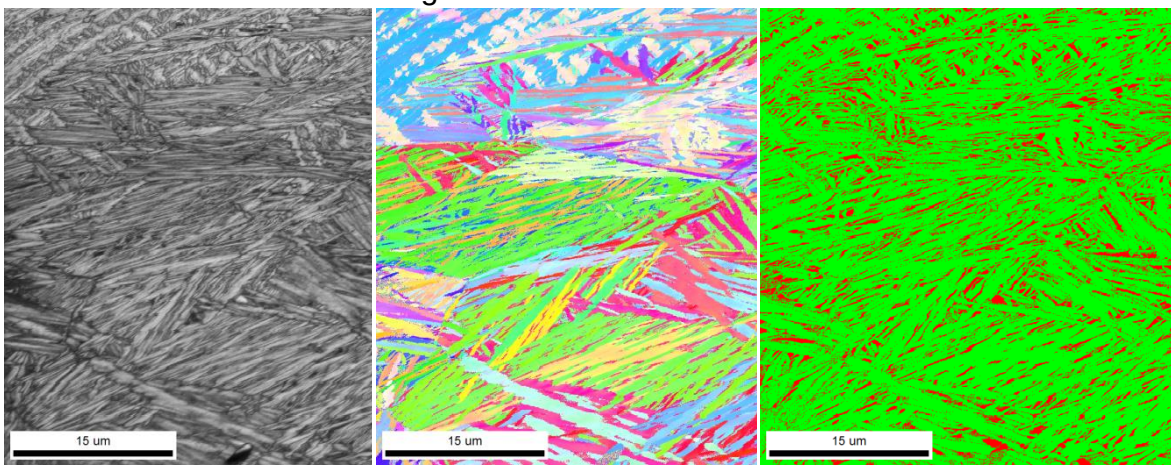

Image quality map Orientation map Phase identification map

Figure 40-EBSD images of austempered CMAT alloy transformed to bainite at 250°C

Figure 41 shows the microstructures of specimens transformed to bainite at the higher temperature, 275°C. Both transformation times yielded coarser bainite laths than is seen in the specimens transformed at lower temperature. They also have larger islands of retained austenite. Some signs of lath coalescence and overall coarsening of lath structures can be seen for 12 hour holding at 275°C compared to 6 hours.

CMAT-275°C-6h

Average Confidence Index = 0.49

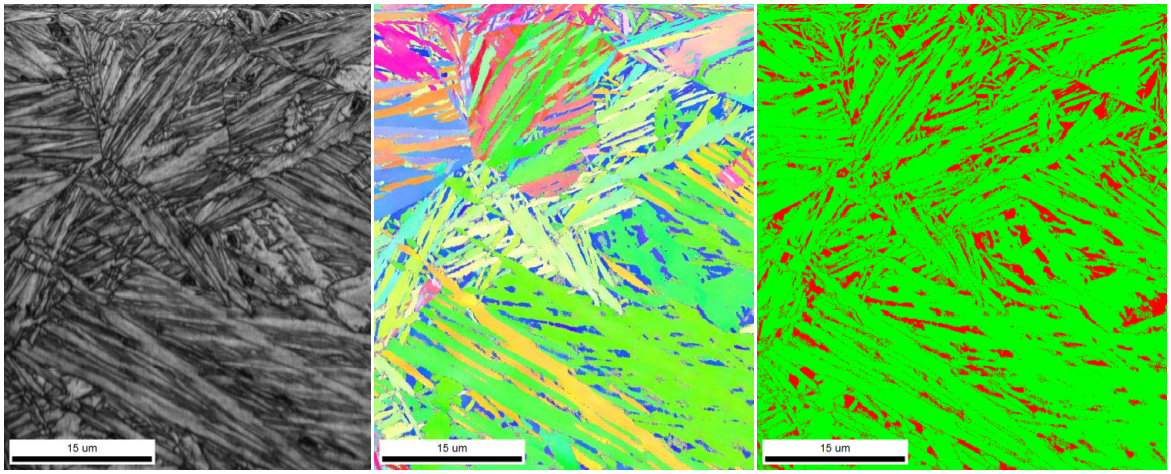

Image quality map Orientation map Phase identification map

CMAT-275°C-12h

Average Confidence Index = 0.34

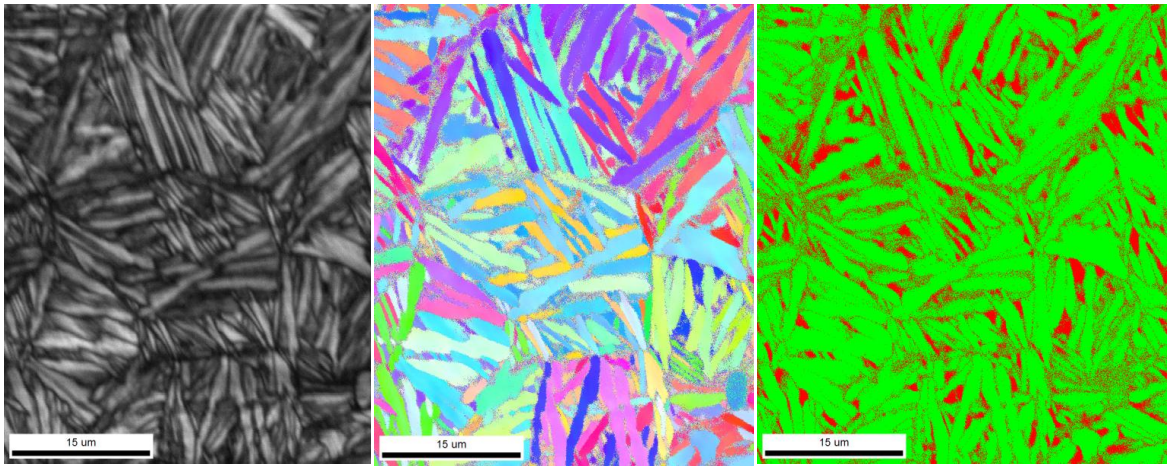

Image quality map Orientation map Phase identification map

Figure 41-EBSD images of austempered CMAT alloy transformed to bainite at 275°C

Micrographs of CMAT specimens that were ausformed by deforming 25% at 600°C then subsequently transforming to bainite are shown in Figure 42. The bainite laths appear to be thinner and shorter than their undeformed counterparts treated at the same temperature. Furthermore, the ausformed microstructures appear to have a greater amount of MA areas and fewer bainite laths.

CMAT-250°C-25%deformation-6h

Average Confidence Index = 0.13

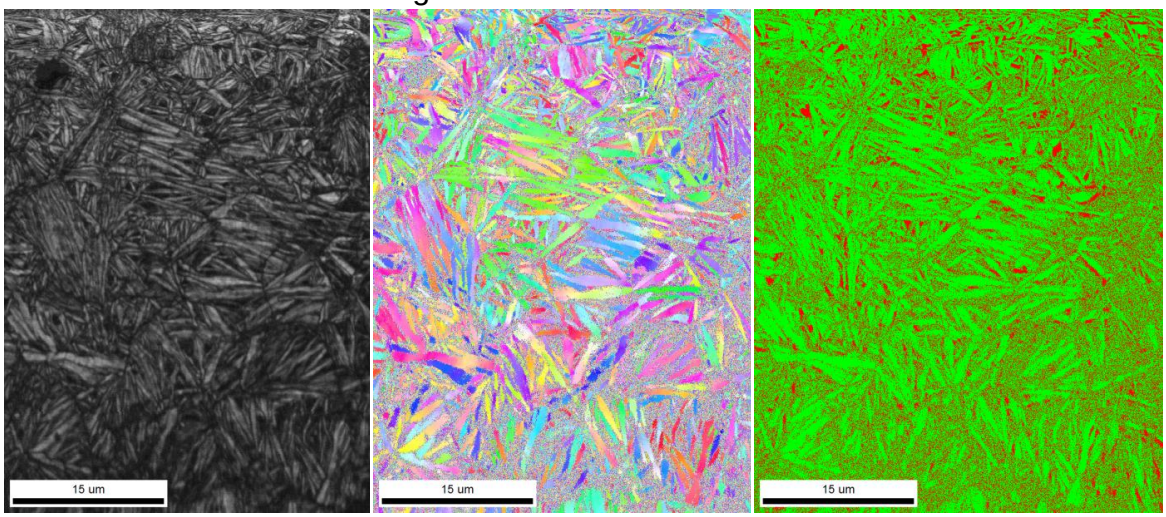

Image quality map Orientation map Phase identification map

CMAT-250°C-25%deformation-12h

Average Confidence Index = 0.05

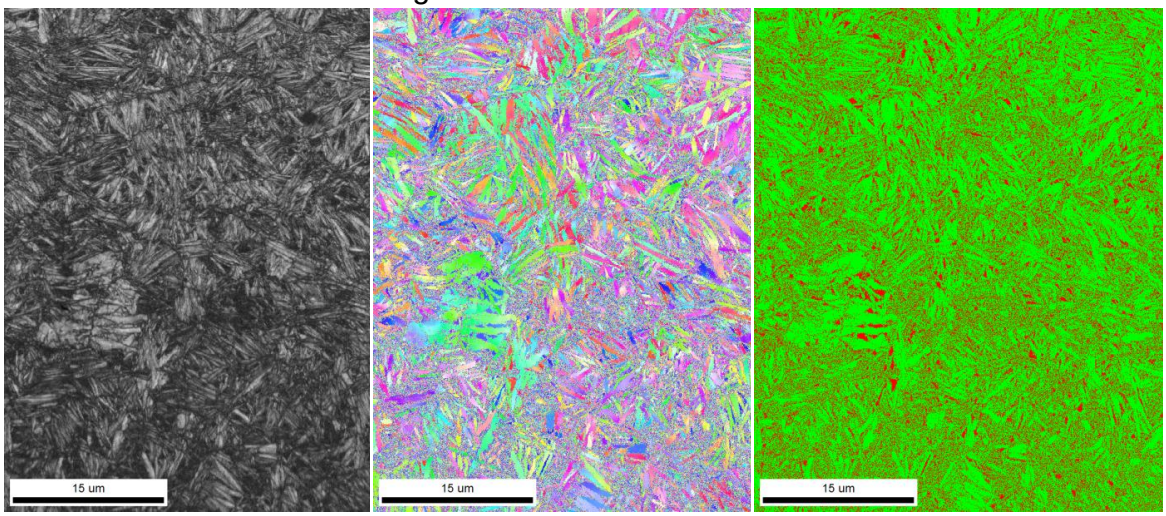

Image quality map Orientation map Phase identification map

Figure 42-EBSD images of ausformed CMAT alloy, deformed 25% at 600°C, transformed to bainite at 250°C

The ausformed specimens deformed 45% then transformed at 250°C are shown in Figure 43. For the specimen treated for 6 hours bainite laths appear to be even thinner and shorter than the 25% deformation specimens. Furthermore there are even more MA areas and fewer bainite laths. The specimen deformed 45% then transformed for only an hour has only a small amount of bainite laths in it, which are incredibly short. The majority of the microstructure seems to be composed of MA areas. Larger fractions of MA in the ausformed specimens are also reflected by the lower confidence indices of their EBSD scans.

CMAT-250°C-45%deformation-1h

Average Confidence Index = 0.09

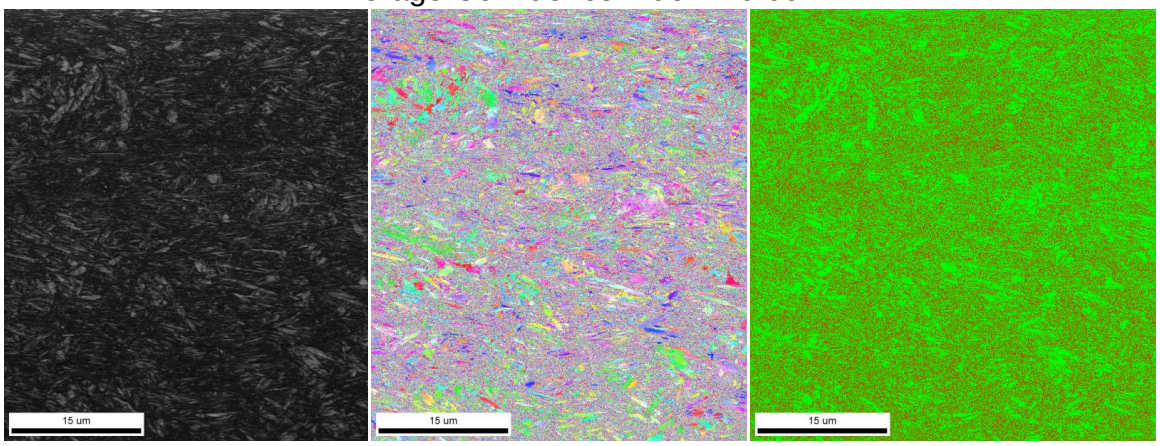

Image quality map Orientation map Phase identification map

CMAT-250°C-45%deformation-6h

Average Confidence Index = 0. 17

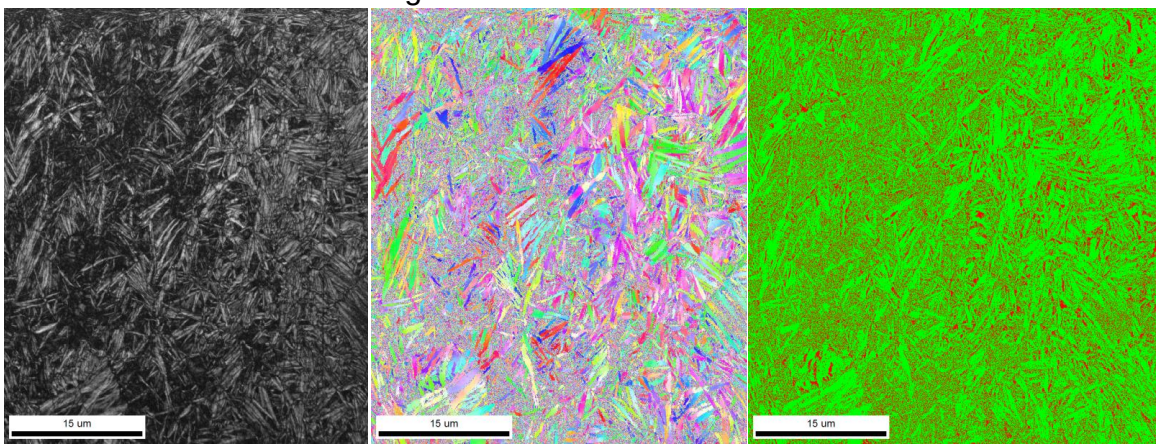

Image quality map Orientation map Phase identification map

Figure 43-EBSD images of ausformed CMAT alloy, deformed 45% at 600°C, transformed to bainite at 250°C

4.4. TEM

The TEM images in Figure 44 show the incredibly fine scale of the bainitic ferrite laths and retained austenite thin films. The microstructure consists of aggregates of high dislocation density ferrite laths separated by very thin layers of retained austenite. The dark field image of the sample austempered at 250°C shows the distribution of thin film retained austenite between ferrite laths. It is also important to note that no evidence of carbides was seen during the TEM analysis. Bainite laths formed at 250°C are thinner than 100nm. Furthermore, deformation at 600°C prior to bainite transformation has clearly promoted the refinement of lath dimensions and structures.

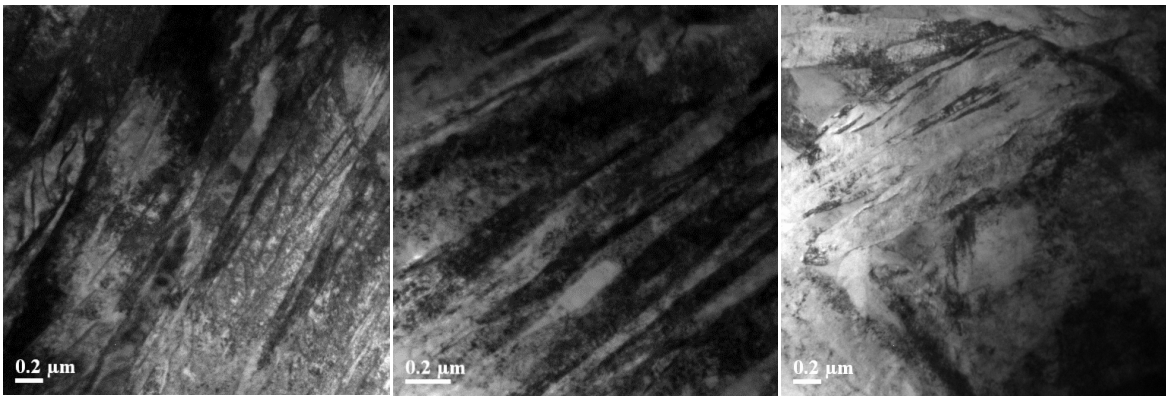

(A) Austempered 250°C

(B) Ausformed 250°C-25%deformation

(C) Austempered 275°C

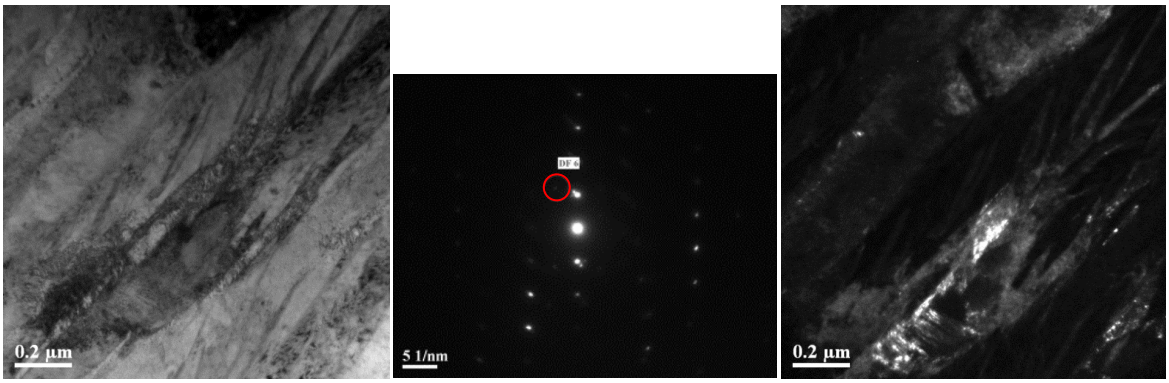

(D) Austempered 250°C Bright Field Image

(E) Austempered 250°C Diffraction pattern from area in **D**

(F) Austempered 250°C Dark field image from diffraction spot shown in **E**

Figure 44-TEM images of austempered and ausformed CMAT alloy structure

4.5. Carbon Concentration Measurements from Electron Energy Loss Spectroscopy (EELS)

Selected areas were subjected to EELS analysis as illustrated in Figure 45. The results of the EELS analysis are shown in Table 12 and averages in Table 13. Austenite clearly contains the most amount of carbon, but bainitic ferrite also has a large amount. It is also worth noting that the area average carbon is very close to the nominal 0.74% carbon value that the alloy contains in the case of the specimen transformed at 250°C.

Table 12-EELS measurement of CMAT alloy transformed to bainite at 250°C for 12hours

	C/Fe ratio	C/Fe (at)	C %wt	Comments
AREA1	0.096	0.067	1.51	200 nm martensite+austenite -1
AREA1	0.059	0.041	0.93	200 nm martensite+austenite -2
AREA2	0.086	0.060	1.36	200 nm austenite+ferrite
AREA3	0.019	0.013	0.30	50 nm bainitic ferrite (thin)
AREA4	0.030	0.021	0.48	50 nm bainitic ferrite
AREA5	0.199	0.139	3.14	20 nm austenite lath
AREA5	0.195	0.136	3.07	20 nm austenite lath
AREA6	0.028	0.019	0.44	20 nm bainitic ferrite
AREA7	0.184	0.129	2.90	20 nm austenite lath
AREA8	0.029	0.020	0.45	50 nm bainitic ferrite
AREA9	0.161	0.113	2.54	50 nm austenite lath
AREA10	0.024	0.017	0.38	50 nm bainitic ferrite
AREA11	0.059	0.041	0.93	500nm martensite?
AREA12	0.042	0.029	0.67	500nm ferrite + austenite average
AREA13	0.023	0.016	0.36	20nm bainitic ferrite -1
AREA13	0.014	0.009	0.22	20nm bainitic ferrite -2

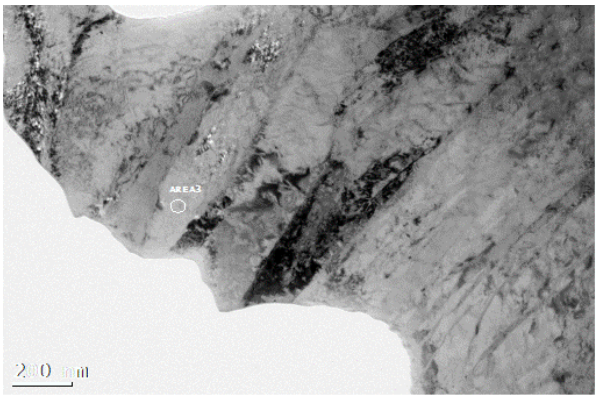

Figure 45-TEM image of CMAT specimen transformed to bainite at 250°C for 12h. The marked area shows were EELS data was taken from.

The phases of areas characterized with EELS were first identified by diffraction pattern as shown in Figure 46. The corresponding carbon measurement for area 4 can be seen in Table 12.

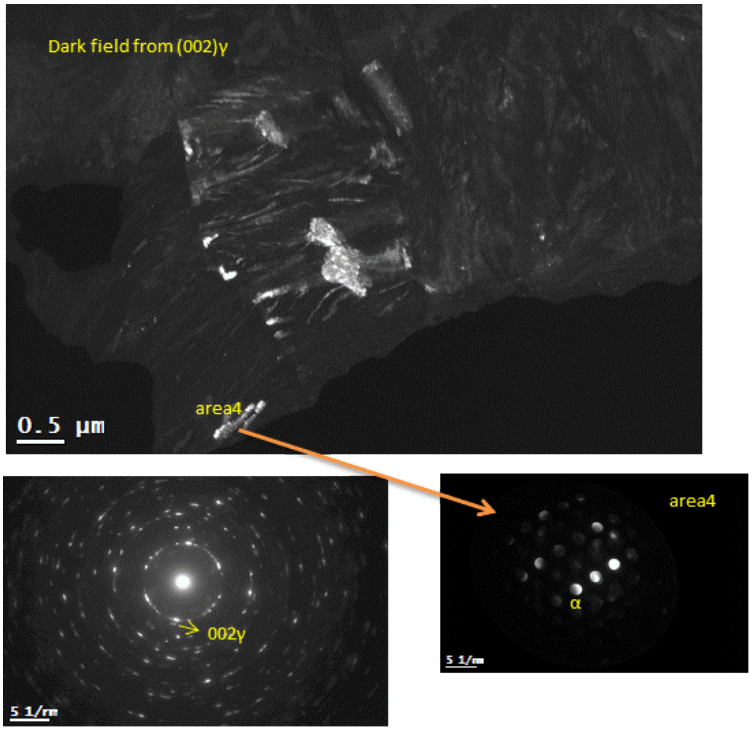

Figure 46-Dark field image of CMAT alloy specimen transformed to bainite at 250°C for 12h from (002)γ reflection, and subsequent diffraction pattern identifing area 4 as bainite.

Table 13 shows the average carbon concentrations of each phase. It is interesting to note that bainite formed at the lower transformation temperature has a higher fraction of carbon.

Table 13-Average of EELS analysis of CMAT alloy

Bainite Transformation Parameters	Phase	Number of points	Average %wt. C
250°C-12h	Austenite	4	1.97
	Bainitic ferrite	6	0.28
	Area averages	5	0.73
275°C-12h	Austenite	2	2.07
	Bainitic ferrite	3	0.14
	Area averages	1	0.47

4.6. X-Ray Diffraction (XRD)

An example of the 2D diffraction patterns is shown in Figure 47. Inspection of the diffraction patterns reveals preferred orientations of the (111)γ, (002)γ, (110)M, (011)M planes. This can be seen by noting which diffraction lines have areas variation in brightness across them, which is indicative of texture. The corresponding plot of intensity as a function of 2θ is shown in Figure 48. Integration of the peaks allows for calculation of the phase fractions.

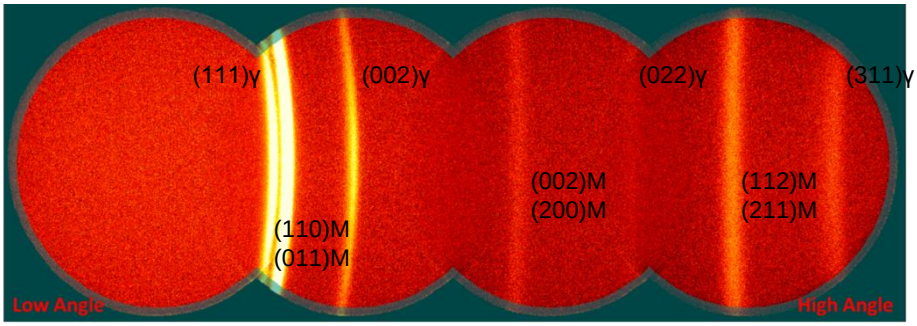

Figure 47-Combination of diffraction patterns from the CMAT sample deformed 25% at 600°C then transformed at 250°C for 6 hours. The image has been rotated 180° so that peaks correspond with the intensity plot in Figure 48 below.

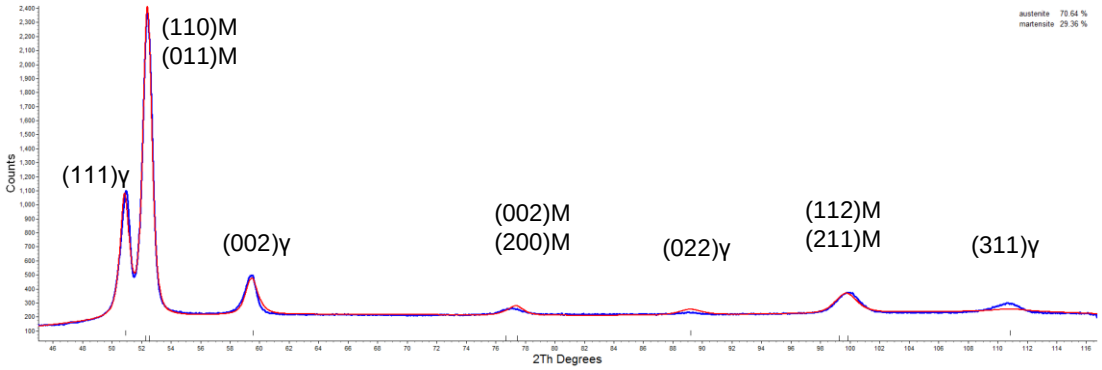

Figure 48-Intensity vs. 2Theta plot generated in EVA from the XRD pattern shown in Figure 47. Blue line corresponds to measured values and the red line shows the fitting simulation values.

The results of the Tata sample scans, see Table 14 are in line with what the Tata Steel brochure promises which is up to 30% retained austenite [30].

Table 14-XRD measurements of Tata Pavise plate

Sample	% Austenite	% Body Centered
TATA-AR 1	24.9	75.1
TATA-AR 2	26.3	73.7

The results of the XRD on the CMAT alloy are presented in Table 15. It can be seen that the austempered samples transformed for 12 hours have less retained austenite than their 6 hour counterparts. It can also be seen that the ausformed specimens have more retained austenite than their un-deformed counterparts.

Table 15-XRD results for CMAT alloy after various heat treatments

Specimen	Austenite wt%	Austenite unit Cell parameter(Å)
CMAT-250C-6h	30.24	3.6045(2)
CMAT-250C-12h	23.65	3.6142(2)
CMAT-275C-6h	28.29	3.6177(2)
CMAT-275C-12h	24.34	3.6181(2)
CMAT-250C-6h-0.25%	31.1	3.614(2)
CMAT-250C-6h-0.45%	34.7	3.6079(1)
CMAT-250C-12h-0.25%	34.1	3.6081(1)
CMAT-250C-1h-0.45%	26.2	3.5905(1)

As mentioned earlier there are two morphologies of retained austenite: thin films and blocky islands. While the two morphologies share a face centered cubic unit cell they should have significantly different carbon compositions and therefore different lattice parameters due to dilatation from the extra carbon. Thin films which should have a higher carbon content and more dilated unit cell, should have its peaks shifted to lower 2theta values. It is worth considering that there will also be some variation between carbon composition and lattice size, due to variation in grain size, within the thin films and blocky islands. However there should be a much greater average difference between the overall morphologies.

In order to separate the fraction of retained austenite measured from XRD the modeling software was set to refine for two separate austenite phases, similar to the work of Podder et al. [31]. Figure 49 shows the two sets of austenite as refined in the modeling software (EVA). The dark purple curve represents the model fitting to the red experimental values. The two austenite phase model leads to much better fitting of the model to the measurements, see the (022) and (311)γ peaks when compared to the one austenite model in Figure 48. It should also be noted that the blue peaks, which represent the thin film austenite, are shifted to lower 2theta values which is due to their higher concentration of carbon and increased lattice parameter.

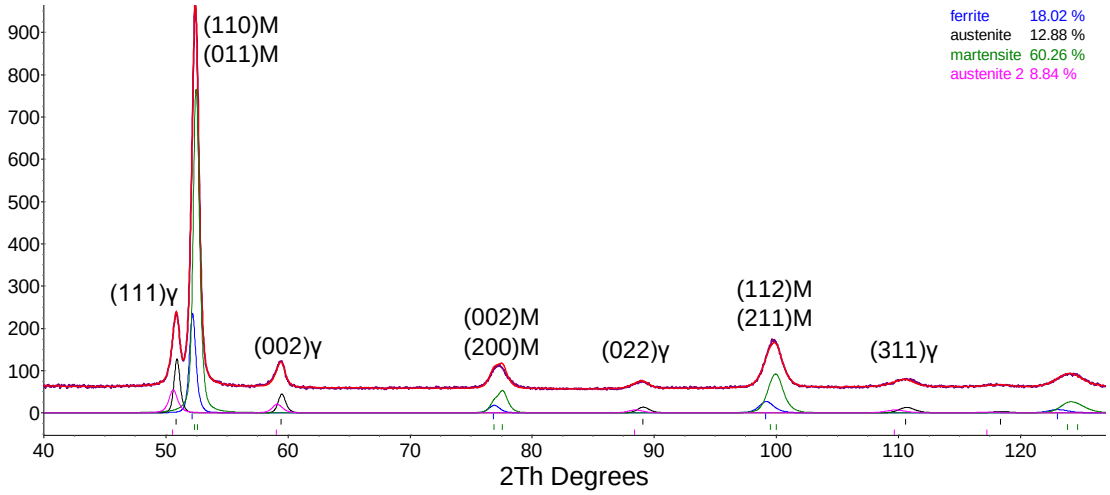

Figure 49-Intensity vs. 2Theta plot generated in EVA from XRD patterns for the sample transformed at 250°C for 12 hours.

The results of the 2 austenite phase refinement model are summarized below in Table 16 and allow the modeling software to fit the simulated curves to the experimental ones more accurately.

Table 16-XRD results from CMAT alloy, 2 austenite phase models.

Specimen	Blocky Austenite wt%	Austenite unit Cell parameter (Å)	Thin Film Austenite wt%	Austenite unit Cell parameter (Å)	Total wt% Austenite
250C-6h	12.5	3.5968(3)	13.32	3.6204(8)	25.82
250C-12h	12.88	3.6083(6)	8.84	3.629(2)	21.72
275C-6h	20.01	3.6145(3)	4.81	3.640(3)	24.82
275C-12h	13.14	3.6155(4)	11.68	3.627(2)	24.82
250C-6h-0.25%	20.2	3.6091(5)	8.6	3.636(3)	28.8
250C-6h-0.45%	19.1	3.5997(4)	12.0	3.626(1)	31.1
250C-12h-0.25%	17.0	3.6006(3)	14.0	3.629(1)	31
250C-1h-0.45%	16.3	3.5827(5)	4.2	3.5932(5)	20.5

Because martensite and bainitic ferrite both have a body centered unit cell similar in size, using XRD to measure fractions of the two can be difficult. However, since both martensite and bainite formation are measured by dilatometer, the transformation data can be used to determine the relative amounts of both phases. The assumption is made that martensite formation stops when the dilatometer stops recording, approximately 30°C. It also does not take into account the change in thermal contraction due to the decreasing fraction of austenite as martensite forms. Figure 50 shows the fraction of austenite as measured with XRD and the fraction of face centered steel divided into martensite and bainite based on the dilatometer data.

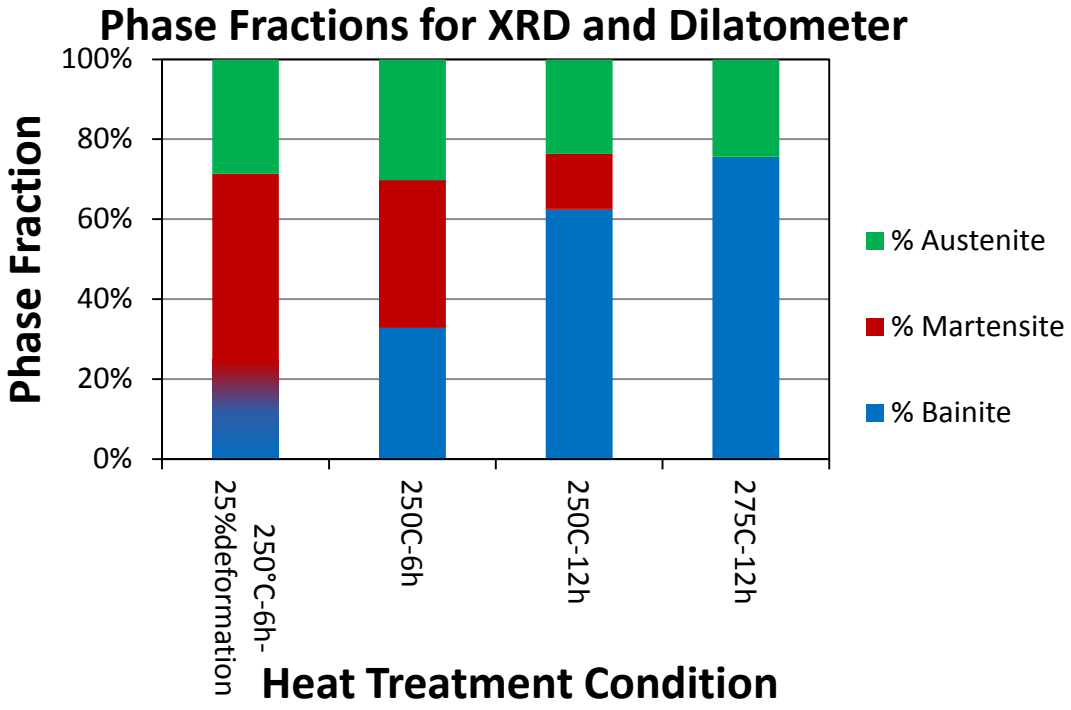

Figure 50-Austenite fraction determined with XRD and bainite and martensite fractions calculated from dilatometer data

4.7. Mechanical Testing

The preliminary tensile data for the as received heat treated unperforated Tata plate is shown in Figure 51 and listed in Table 17. It is evident from Table 17 that after failure at approximately 1.1 GPa and 1% elongation, that the material did not perform as well as advertised. Charpy impact properties of the Tata plate are shown in Table 18. The CVN toughness value was very low and the fracture was completely brittle. There was no CVN data provided by the manufacturer to compare to.

Table 17 also lists all equipment used for the tensile testing. During the second tensile test the machine could not produce enough force to break the specimen. Therefore the sample was removed and placed into a machine that could pull with more force. Due to machine calibration a different strain gauge also had to be used. The data from both parts of tensile test 2 were combined in Figure 51.

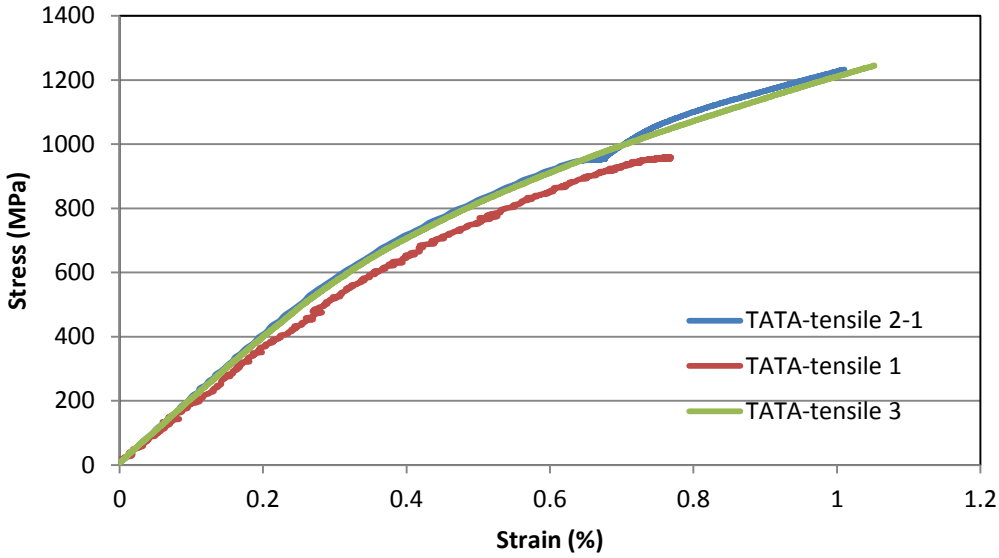

Figure 51-Initial tensile testing of unperforated as-received heat treated Tata plate. Specimens were subsized.

Table 17-Accompanying tensile data from Figure 51, and list of equipment used for each test. Advertised properties for Tata Pavise plate are also included for comparison.

Sample	Yield strength (MPa)	Ultimate tensile strength (MPa)	Total elongation (ε_T %)	Equipment
1	934	960	0.77	MTS-Opticalvideo extensometer MTS-Landmark 310 frame – 100kN
2	-	1233	1	**Started** with: MTS-Optical video extensometer MTS-Landmark 310 frame – 100kN **Finished** with: Instron-262-604, 25mm gauge, Clamp-on extensometer MTS-312.41 frame – 500kN
3	997	1246	1.1	Instron-262-604, 25mm gauge, Clamp-on extensometer MTS-312.41 frame – 500kN
Tata	1300	>2000	5	Advertised Properties

Table 18-CVN properties of the purchased heat treated Tata plate. These values are for subsized samples. The impact energy is 75% of a full sized sample.

Test Temperature	Average Charpy impact energy (J)
Room T	2.00
-40°C	1.39

The tensile data for Tata alloy samples treated in-house at CanmetMATERIALS can be seen in Figure 52 and Table 19. The values for the samples treated with the same thermal cycle as the as-received heat treated Tata plate (6 hours transforming at 250°C) show better performance than the tests on the as-received heat treated material and also better strength than advertised. Furthermore, Tata specimens treated at the higher transformation temperature of 275°C had a slight drop in strength but did have better elongation. Interestingly the CVN data, see Table 20, does not show an appreciable difference in energy absorption across the two transformation temperatures. However the re-treated samples' CVN values do show improvement over the as received values shown in Table 18.

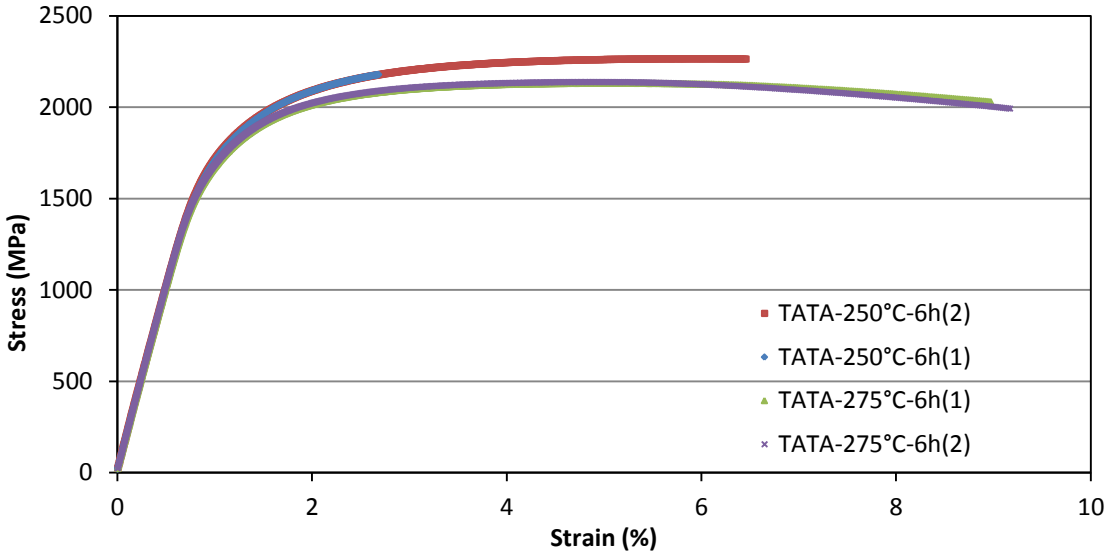

Figure 52-Tensile data for Tata alloy samples heat treated at CanmetMATERIALS

Table 19-Summary of data from Figure 52

Sample Id	YS	UTS	elongation
TATA-250°C-6h-1	1746	2178	2.6
TATA-250°C-6h-2	1747	2264	6.6
TATA-275°C-5.5h-1	1691	2131	9.1
TATA-275°C-5.5h-2	1702	2137	9.1

Table 20-CVN data for Tata alloy samples treated at CanmetMATERIALS

Sample ID	Temperature	CVN (J)
TATA-250°C-6h-1	Room T	5.7
TATA-250°C-6h-2	Room T	4.3
TATA-275°C-5.5h-1	Room T	5.2
TATA-275°C-5.5h-2	Room T	5.5

Figure 53 shows the hardness of the Tata alloy with respect to ausforming time and temperature. There seems to be a trend between lower transformation temperature and higher hardness. Furthermore, increasing the duration of transformation time from 6 to 12 hours also seems to increase the hardness slightly, which is likely a result of having more bainitic ferrite in the final microstructure. The exception to these trends is the sample treated at 225°C for 6 hours. It can be seen from the dilatometer curve that after 6 hours at 225°C very little bainitic ferrite has formed which means that the rest of the microstructure is likely martensite upon quenching to room temperature which is much harder.

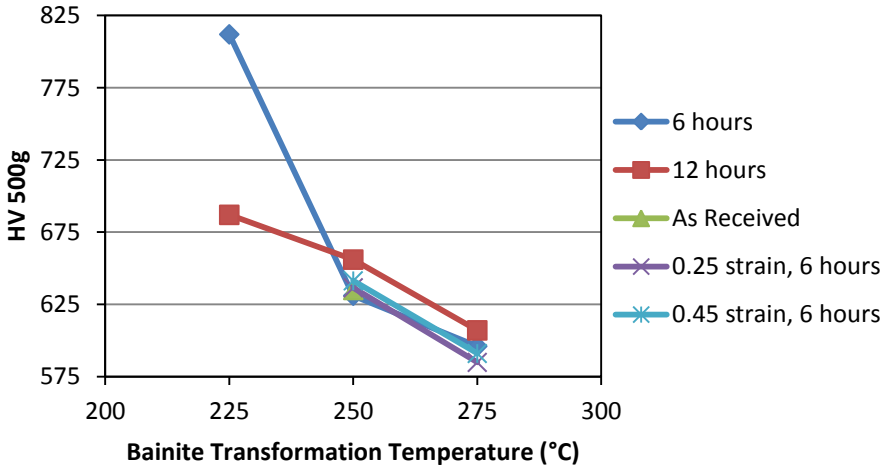

Figure 53-Variation in hardness as an effect of austempering and ausforming conditions studied with dilatometry for Tata alloy

Figure 54 and Table 21 show the tensile properties for various heat treatments on the CMAT alloy. In general treatment at lower temperature led to higher strength and lower ductility. The specimen treated at 225°C was the strongest and the specimen treated at 275°C had the best elongation values. Furthermore specimens treated at the same temperature but for longer times typically had higher values of total elongation. The combination of 2000MPa strength and 15% total elongation for the specimen treated for 12 hours at 250°C showed overall excellent performance.

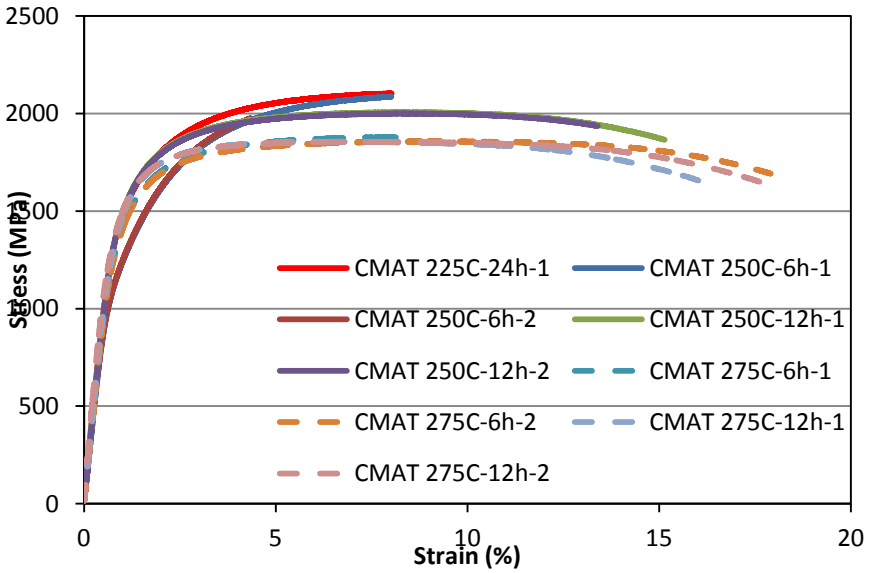

Figure 54-Tensile data for round CMAT alloy specimens

Table 21-Summary of tests from Figure 54

Sample ID	Max Elongation (%)	UTS (MPa)
CMAT 225C-24h-1	8.0	2102
CMAT 250C-6h-1	8.0	2086
CMAT 250C-6h-2	4.3	1975
CMAT 250C-12h-1	15.1	2005
CMAT 250C-12h-2	13.4	1999
CMAT 275C-6h-1	8.1	1878
CMAT 275C-6h-2	17.9	1856
CMAT 275C-12h-1	16.4	1854
CMAT 275C-12h-2	17.8	1855

The fracture surfaces, as seen in Figure 55, suggest that fracture was mostly brittle. However, some thin ductile areas are also present as seen in the higher magnification image. They are likely thin films of retained austenite. Overall it is hard to find the signatures of ductile fracture and dimple formation; cleavage facets prevail on the fracture surface. No attempts have been made to correlate the size of the cleavage face with microstrucutral features; e.g. bainite packet size. It is also worth noting that the tensile properties of the rectangular subsized CMAT specimens, as shown in Figure 56 and Table 23 are comparable to those of their round counterparts.

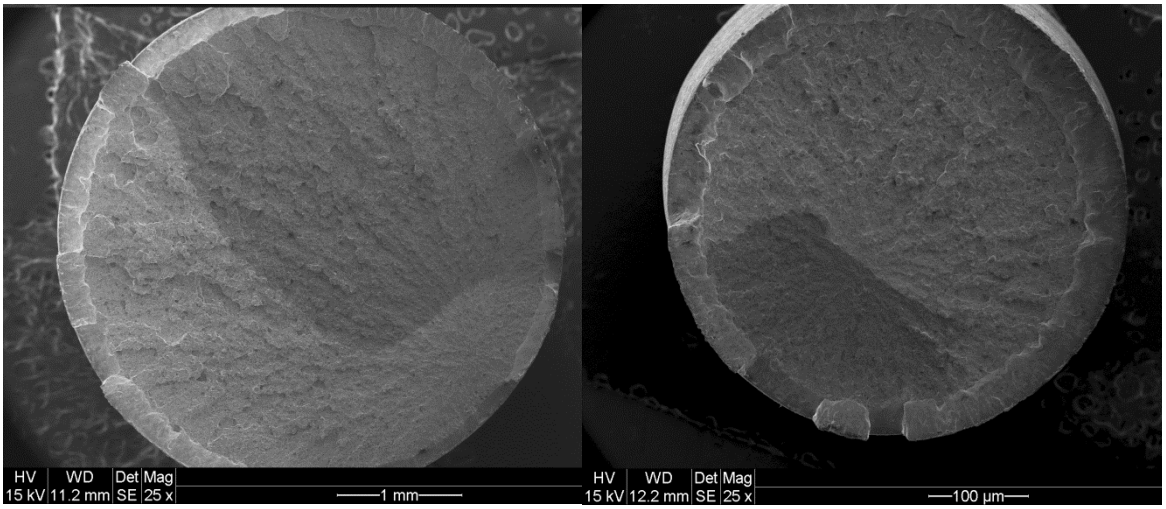

CMAT-250°C-6h **CMAT-250°C-12h**

CMAT-275°C-12h **CMAT-275°C-12h**

Figure 55-SEM micrographs of fracture surfaces of round tensile samples

To confirm that tensile specimen shape did not have a major effect on strength values subsized rectangular tensile samples were also made from ausformed CMAT alloy. The data is presented in Figure 56 and summarized in Table 22. The results are similar to the round tensile data confirming that shape did not significantly affect the tensile values. This was to confirm that the edges of the flat tensile bars did not promote premature failure.

The tensile properties of the ausformed CMAT specimens are presented in Figure 57 and Table 23. For the specimen deformed 25% and treated at 250°C for 6 hours there was not a large change in mechanical properties. However all other ausformed samples have lower strength and total elongations than their undeformed counterparts.

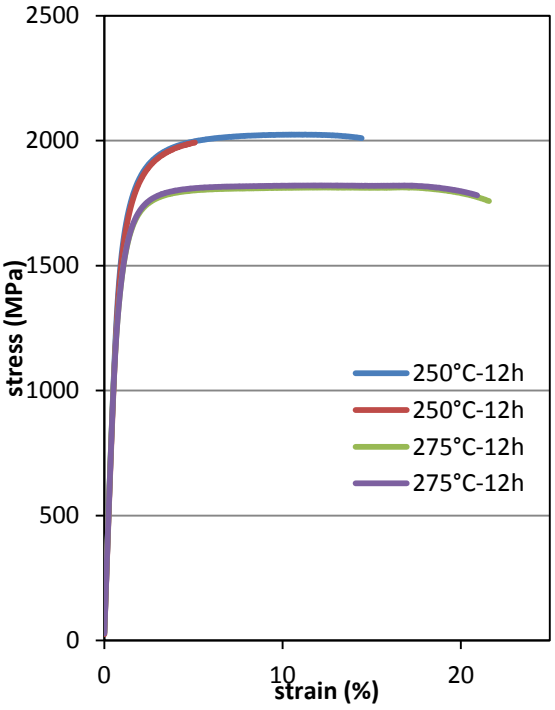

Figure 56-Flow curves for rectangular austempered CMAT alloy samples

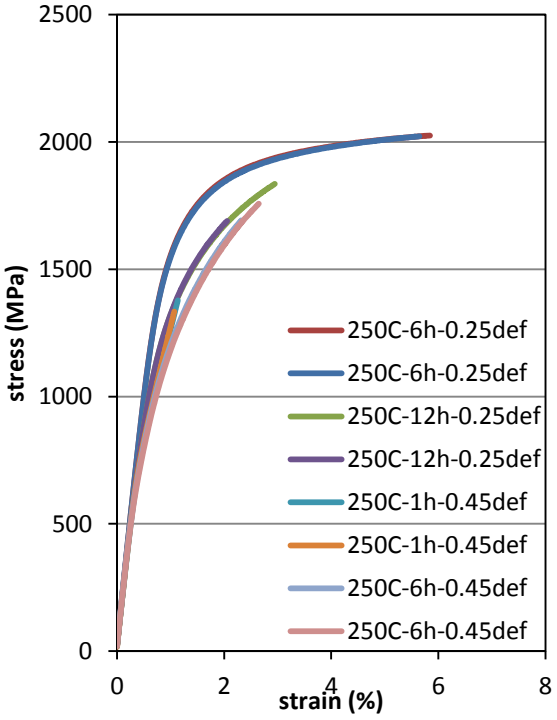

Figure 57-Flow curves from rectangular ausformed CMAT alloy samples

Table 22-Summary of tensile results from rectangular austempered CMAT alloy specimens

Sample Id	YS (MPa)	UTS (MPa)	Elongation (%)
250°C-12h-1	1533	2024	14.5
250°C-12h-2	1511	1933	5.4
275°C-12h-1	1383	1814	21.1
275°C-12h-2	1385	1821	20.9

Table 23-Summary of tensile results from rectangular ausformed CMAT alloy specimens

Sample Id	YS (MPa)	UTS (MPa)	Elongation (%)
250°C-6h-0.25def-1	1522	2026	6.4
250°C-6h-0.25def-2	1514	2023	6.1
250°C-12h-0.25def-1	1192	1835	NA
250°C-12h-0.25def-2	1186	1690	2.2
250°C-1h-0.45def-1	1028	1377	1.3
250°C-1h-0.45def-2	1025	1334	1.3
250°C-6h-0.45def-1	1010	1692	2.4
250°C-6h-0.45def-1	977	1757	2.6

The CVN data for the CMAT alloy is presented in Table 24. It shows that the CMAT alloy has higher impact energy absorption than the Tata alloy. However the CMAT samples were treated for 12 hours, whereas the Tata specimens were only treated for 6 hours.

Table 24-CVN data of CMAT alloy

Sample ID	Temperature	CVN (J)
CMAT-250C-12h-1	r	7.2
CMAT-250C-12h-2	r	6.8
CMAT-250C-12h-3	-40	3.6
CMAT-275C-12h-1	r	11.9
CMAT-275C-12h-2	r	8.7
CMAT-275C-12h-3	r	11.1

5 Discussion

5.1. Banite Reaction Kinetics

5.1.1. Austempering

As seen in the dilatometer bainite transformation curves shown in section R3 higher bainite transformation temperatures resulted in shorter incubation times and higher bainite transformation rate. These trends are common throughout the literature [5, 6, 18, 32, 33, 34]. Incubation time is dictated by how long it takes a noticeable amount of nuclei to form. Both diffusional and displacive approaches can be adopted to describe the trend of incubation time with undercooling below Bs (bainite start temperature). For instance, Bhadeshia proposed Equation 7, which can be rearranged to solve for nucleation start time as shown in Equation 8, where z, Q', and C_4 are constants that need to be determined experimentally, p is a linear correlation coefficient which also needs to be varied based on experimental data, T is the transformation temperature, and ΔF_m is the maximum possible chemical driving force (also written as ΔG_m), and R is the gas constant [35].

Equation 7-Bhadeshia's bainite transformation start time equation

$$ln\left|\frac{(\Delta F_m)^p \tau}{T^z}\right| = \frac{Q\prime}{RT} + C_4 ...[35]$$

Equation 8-Bhadeshia's bainite transformation start time equation rearranged to solve for incubation time

$$\tau = \frac{T^z}{(\Delta F_m)^p} exp\left[\frac{Q\prime}{RT} + C_4\right]$$

The experimental use of Equation 7 is not perfect since it does not account for other possible nucleation mechanisms which may occur simultaneously, but it does predict the expected C-curve shape, where τ is initially longer closer to Bs, decreasing gradually as undercooling increases due to higher driving force, and then increasing subsequently with higher undercoolings until the Ms temperature, as seen in Figure 59 [35]. The trend is also seen in the current work where lower transformation temperatures had longer incubation times. No increase in incubation time at higher transformation temperature was observed, likely because the highest temperature used, 275°C, is still relatively below the nose of the transformation C-curve.

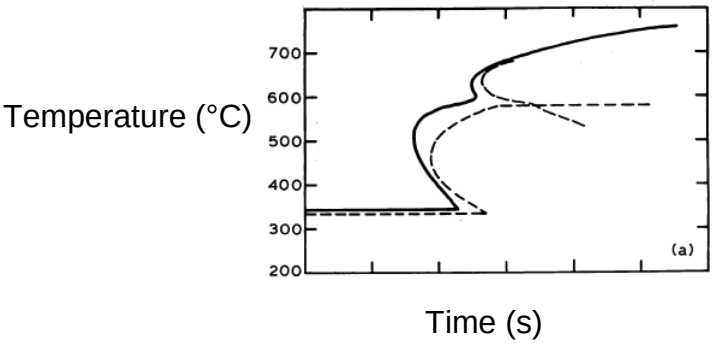

Figure 58-TTT curve. Dashed line shows calculated values, solid line shows experimental[35]

Fraction/extent of Transformation

The maximum fraction of bainitic ferrite that can be formed is theoretically dictated by thermodynamics which can be represented by a phase diagram as illustrated by Figure 59. It shows the paraequilibrium phase boundaries which in this case represents the compositions at which only carbon has equal chemical potential in both involved phases [19]. The T_0 line represents the temperatures below which a change in composition is not required for transformation to occur, i.e. the diffusionless case [19]. As such the bainite transformation stops when the carbon composition of the remaining austenite reaches the T_0(diffusionless) or Ae3(diffusional) lines. The maximum possible phase fractions of austenite from transformations carried out at 225, 250, and 275°C are shown below in Table 25 which predicts notably larger values with the T_0 line than the Ae3 boundary. It also shows an increase in austenite fraction with increasing temperature according to both the T_0 and Ae3 lines. Ms temperatures were calculated based on carbon concentration using empirical equations and for all 6 possible final phase fractions shown in Table 25. Austenite should be stable and therefore there should be no martensite formation if the final equilibrium fractions are reached and carbon is distributed evenly throughout the remaining austenite. It has to be noted that for the examined experimental scenarios (isothermal bainite formation at 225, 250 and 275°C) depending on reaction temperature and time, the fraction of bainitic ferrite might not reach its final equilibrium values. As such, carbon enrichment of the remaining austenite might not be sufficient to completely stabilize and retain the FCC phase at room temperature. Furthermore, geometry effects and shorter diffusion distances promote more carbon enrichment for thin film austenite than blocky austenite islands. This was confirmed by detection of significant amounts of retained austenite thin films in the TEM micrographs.

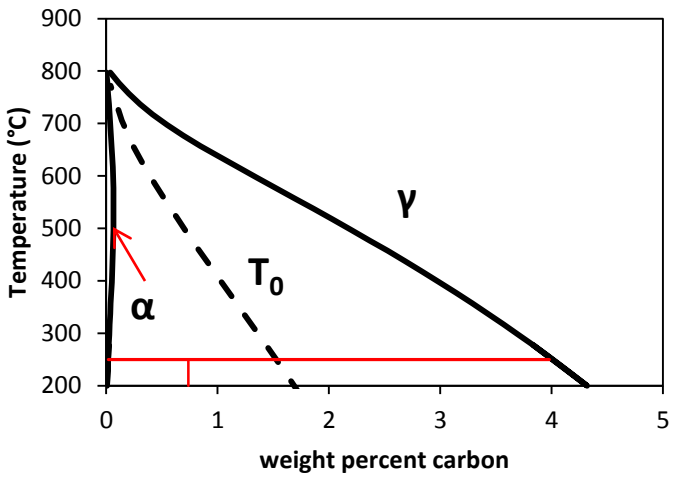

Figure 59-paraequilibrium and T_0 boundaries of CMAT alloy calculated with Thermocalc. The red tie line represents the alloy composition at a transformation temperature of 250°C

Table 25-Maximum possible fractions of retained austenite as calculated in Thermocalc using the T_0(displacive) line and paraequilibrium Ae3 (diffusional) and α-ferrite phase boundaries

Isothermal Transformation Temperature (°C)	T_0 fraction of Austenite	Paraequilibrium fraction of Austenite
225	0.46	0.13
250	0.48	0.14
275	0.50	0.15

Reaction Rate

The majority of experiments were halted before reaching the thermodynamically predicted phase fractions. The amount of bainite formed and final fraction of austenite was ultimately limited by kinetics.

There are currently two theories for the mechanism of bainite formation and kinetics which are diffusion and displacive. For the diffusion theory transformation kinetics are composed of two parts: nucleation and growth. The rate at which both steps occur is dictated by the balance of chemical driving force and carbon diffusion [36]. For high undercoolings driving force will be high, at low undercoolings carbon diffusion will occur faster [36]. The maximum rates of growth and nucleation, and therefore bainite formation, will occur at some intermediate undercooling where there are sufficient contributions from both chemical driving force and carbon diffusion. The results of the present work (Figure 29 and Figure 33) show a decrease in reaction rate as temperature

decreases, but since all bainite formation temperatures are relatively low (below the nose of the C-curve) this does not discount the possibility that at higher transformation temperatures the transformation rate becomes sluggish.

The displacive theory states that the lengthening of bainite sheafs occurs much faster than would be possible with diffusion [19]. Furthermore, it is stated that growth occurs instantaneously and is therefore it is not a factor that needs to be considered, only the nucleation rate is pertinent [19]. The equation for nucleation rate, as proposed by Bhadeshia, is shown in Equation 9, where C_2 is a constant based on the slope of the universal nucleation function (G_N) of bainite, C_3 and C_4 are unknowns that need to be fit to the data, ΔG_m is the maximum possible chemical driving force, T is temperature and R is the gas constant [19].

Equation 9-Displacive Nucleation Rate Function

$$I_v = C_3 exp\left(-\frac{C_4}{RT} - \frac{C_4 \Delta G_m}{C_2 RT}\right) ...[19]$$

As temperature decreases the chemical driving force increases and Equation 9 predicts a decrease in nucleation rate, and therefore a slower total reaction rate. This prediction fits the with the experimental trend observed in this study.

5.1.2. Ausforming Reaction Kinetics

For both the Tata and CMAT alloys it appears that ausforming with a strain of 45% causes transformation to begin immediately upon reaching the isothermal hold temperature of 250°C. That is however the exception to the overall trend observed here. As seen in Figure 31, Figure 34, and Figure 36 increasing amounts of deformation slowed the bainite transformation rate and decreased the final fraction of bainite formed in the time allotted. At the higher transformation temperature of 275°C ausforming with 45% deformation further slowed bainite formation.

Similar trends have been observed in the literature [37], however prior deformation of parent austenite introduces more processing variables and as a result there is a wide range of literature in the subject with small amounts of variation in experimental procedure which can lead to large differences in the results. Extra variables to consider are: alloy composition, deformation temperature, magnitude of deformation, and isothermal bainite formation temperature.

One study carried out by Hase *et al*. examines the effect of deformation to various degrees at the isothermal transformation temperature on an alloy with comparable carbon content to the CMAT and Tata alloys. They found that

ausforming when transforming at 300°C under increased amounts of deformation led to higher final fractions of a bainite forming [33]. They also found that at a higher transformation temperature of 350°C the trend intensified with relatively higher amounts of bainite resulting from larger amounts of deformation [33]. However when the same alloy was ausformed and transformed at 250°C almost no changes were seen [33]. While deforming at high temperature increased the relative final fraction of bainite at the given temperature, treating at lower temperatures still yeilded an overall higher fraction of bainite [33]. While final fraction of bainite was lower at higher temperatures, the reaction rate was higher and it was also further increased with deformation. The sample ausformed and treated at 300°C in particular forms only slightly less bainite, much faster, than the undeformed sample austempered at 250°C [3].

Another study done by Hu *et al.* investigated the effect of the deformation temperature on a 0.4 weight percent carbon alloy. They used two deformation temperatures one of which was the austenitization temperature and the other was the isothermal bainite transformation temperature which was 300°C [38]. The results of the higher temperature deformation tests were similar to those mentioned in this study, higher amounts of deformation led to a lower final fraction of bainite and overall slower reaction kinetics [38]. The authors state that the reduced reaction is due to the mechanical stabalisation of deformed austenite [38]. For the samples deformed at the transformation temperature they found that a medium amount of deformation (25%) actually increased the transformation kinetics and final fraction of bainite [38]. For the specimen deformed 50% at low temperature there was an initial increase in transformation kinetics, but then a dropoff, and an overall lower fraction of bainite compared to its undeformed counterpart [38].

Thermodynamically, deformation increases the driving force of reactions by adding a mechanical component of driving force, ΔG_{Mech} [39]. Ausforming is more effective for bainite at higher temperatures to increase transformation kinetics and final fraction because there is less chemical driving force at low undercoolings [37, 40]. At lower temperature where sufficiently more chemical driving force is available the effect from ausforming is less pronounced. At higher transformation temperatures ausforming also led to higher fractions of bainite when more strain was applied, this is because the T_0 line is shifted to the right [40]. The physical mechanism of ΔG_{Mech} is the introduction of dislocations which also act as nucleation sites for bainite [38], leading to overall accelerated growth rates, at a cost of smaller platelets of bainite forming [19, 37, 41]. However, relatively large amounts of deformation introduce such a high disclocation density that it can slow down, or even stop the transformation interface [38]. As such,

depending on the balance of transformation temperature and amount of strain, the deformation of parent austenite can promote bainite formation due to additional driving force, as well as an increased number of nucleation sites (low strains and at higher transformation temperatures) or slows down the reaction as a result of a high density of dislocations in parent austenite impeding the migration of growing interfaces (high strains and at lower reaction temperatures).

The EBSD images support the theory of higher amounts of deformation causing inhomogeneous nucleation. In the EBSD micrographs of austempered specimens laths can typically be traced back to a prior austenite grain boundary. In the ausformed micrographs however this is not the case. Furthermore bainite packets are smaller and the overall structure is more refined. This is related to increased nucleation and also higher restriction in growth.

Indeed the experimental results of the ausforming experiments, in which bainite was formed at relatively low tempereatures, follow the trends noted in the literature. The 25% deformation experiments only slowed down kinetics and in some cases slightly decreased the incubation time which fits with the theory of more dislocations increasing nucleation rate while decreasing the total volume fraction of bainite, it is just less notable since the transformation temperatures are relatively low and chemical driving force is high. The initial spike in transformation rate and lack of incubation time for 45% deformation specimens was due the transformation starting prior to reaching the isothermal hold (increased nucleation rate), however the introduction of a high density of dislocations ceased the reaction quickly.

5.1.3. Ms of Carbon Enriched Retained Austenite

The Ms temperature in the CMAT alloy decreases as the amounts of applied deformation during ausforming increases, see Figure 38. Similar trends have been seen in the literature, as shown in Figure 60, the difference being that the CMAT alloy did not exhibit the initial increase in Ms. This may be explained by the deformation and subsequent bainite transformation being carried out at higher temperatures, where G_{mech} has a greater contribution, like in [37] which leads to an initial increase bainite formation. However, this was not the case with the CMAT alloy which was treated at lower temperature.

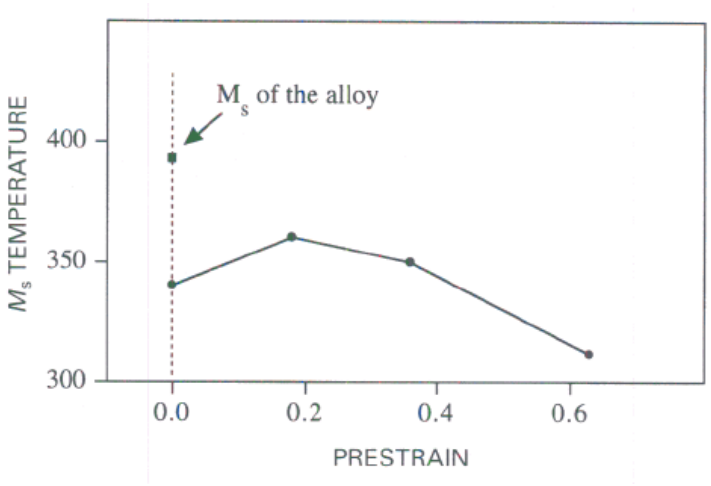

Figure 60-Ms temperature after bainite formation at 475°C for various amounts of prestrain [37]

There are two competing mechanisms affecting the martensite start temperature in this case: the first being mechanical stabilization of austenite and the second is the effect of deformation on bainite fraction and resulting carbon enrichment of the remaining austenite [37]. Increasingly large amounts of deformation mechanically stabilize austenite by introducing dislocations which stop glissile martensite interfaces [19]. The effect of austenite deformation on bainite transformation is explained in more detail in the previous section, but for the current study the final fraction of bainite, and thus carbon enrichment of austenite, decreases with deformation. Bainite formation enriches surrounding austenite with carbon which also stabilizes austenite lowering the Ms temperature. Because deformation led to less bainite formation, there should be less carbon in the retained austenite than there would be in an undeformed sample.

In the case of the CMAT alloy it would seem that the mechanical stabilization of austenite has a greater effect on the Ms than the lack of excess carbon partitioned due to bainite formation.

5.2. Microstructure

5.2.1. Bainitic Ferrite Grain Size

EBSD micrographs clearly show that bainite laths formed at higher temperature were thicker than those formed at lower temperature. This trend is seen throughout the literature [7, 13, 34]. Three concepts to keep in mind when explaining bainite lath thickness are driving force, the effect of austenite strength and the nucleation rate and how these factors vary with undercooling and transformation temperature.

With regards to driving force accounting for thermoelastic equilibrium laths of bainitic ferrite would be coarser at lower temperatures where driving force is greatest [39]. Lath thickness could be related to the diffusion of carbon from laths of bainitic ferrite into adjacent thin films of austenite [19]. The carbon concentration of thin films would limit how close the next parallel lath of ferrite can form, since ferrite can only transform in austenite with a carbon concentration below T_0 or Ae3 depending on which model you are looking at [19]. However, thermoelastic equilibrium does not apply in this case, since as bainite forms it plastically deforms the austenite around it [39].

Austenite is stronger at lower temperatures and there is less dynamic recovery, therefore thinner laths should form at lower temperatures [39]. This theory fits well with the EBSD images. A 100MPa strength increase of the austenite leads to a bainite lath that is 0.2μm thinner [39]. Ausforming also increases the strength of austenite which explains why ausformed microstructures are typically finer than austempered counterparts transformed at the same temperature. Finer ferrite is produced with increased deformation [37, 38, 42].

The impingement of bainite laths is also a factor to consider. At higher nucleation rates more laths are growing, so they must be thinner and shorter due to increased impingement [39]. This is another factor that contributes to the relatively finer structure produced by ausforming. EBSD shows not only thinner but noticeably shorter grains which is supported by the idea that a high nucleation rate produces a smaller microstructure.

5.2.2. Martensite Austenite (MA) Regions

When examining the EBSD maps in Figure 41 there are many spotty regions. In the orientation maps the spots are randomly oriented and in the phase maps they correspond to a mix of austenite and body centered iron. Body centered iron being bainitic ferrite which is body centered cubic, or martensite which is body centered tetragonal. Because of their blocky or round morphology it can be assumed that the body centered iron is martensite, which has transformed from unstable blocky austenite, and not bainite which would have a lath morphology. Examining the phase map of the CMAT specimen transformed at 250°C for 12 hours and comparing the blocky austenite regions to the spotty regions in the map for the specimen transformed at the same temperature for 6 hours provides clear evidence of this.

EBSD work done by Reichert et al. on the heat affected zone of a linepipe steel found MA areas that appear similar in orientation maps [29]. They differentiated martensite by examining crystal orientation, confidence index and image quality [29].

Table 26 was compiled by generating data based on low image quality and morphology. The MA fraction was calculated by adding fractions of low image quality ferrite, low image quality austenite and points that were unidentified due to low confidence index. Data cleaning was comprised of a dilatation step. It filled in areas less than 3 spots in size, most of which were on bainite laths, replacing them with the expected points based on the confidence index of surrounding points. The cleaning step was used to replace data points that were likely misidentified, which would otherwise skew measurements. It is important to note that low confidence index can be from poorly prepared areas as well. Maps were generated to visually confirm that low quality areas only occupy spaces that fit the expected MA morphology, since low confidence index and image quality can also arise from artifacts from poor sample preparation. This discounted the contribution of artifacts to MA fraction.

Table 26-MA fraction from EBSD of CMAT alloy specimens

Heat Treatment	Austenite (%)	Bainite (%)	MA (%)
250°C-6h	4	73.1	23.5
250°C-12h	14.4	85.2	0.4
275°C-6h	14.2	83.9	1.9
275°C-12h	11.7	81.6	3.4
250°C-6h-25%deformation	10.7	47.1	42.2
250°C-12h-25%deformation	1.7	24.4	73.9
250°C-1h-45%deformation	0.3	46.1	53.5
250°C-6h-45%deformation	6.4	64.8	28.8

Comparing the results in Table 26 to the total length change due to bainite formation in Figure 32 and Figure 34 most of the results correlate well. The austempered specimen treated at 250°C for 6 hours has less ferrite and more MA than its 12 hour counterpart. The specimen treated at 250°C for 12 hours has a similar amount of bainite as the sample treated at 275°C for 6 hours. The ausformed specimens also correlate well to dilatometer and mechanical

properties. The specimen deformed 45% and treated at 250°C has roughly half the amount of bainite as the 18 hour counterpart.

Figure 61 shows the percentage of MA regions as determined from EBSD graphed against total elongation during tensile testing. The data suggests that increased fractions of MA have an overall negative effect on ductility. The variability of the results should however be taken into account. Only one EBSD scan per data point was done, and each scan only represents a small area of the sample. Furthermore there is only one tensile test per point as well.

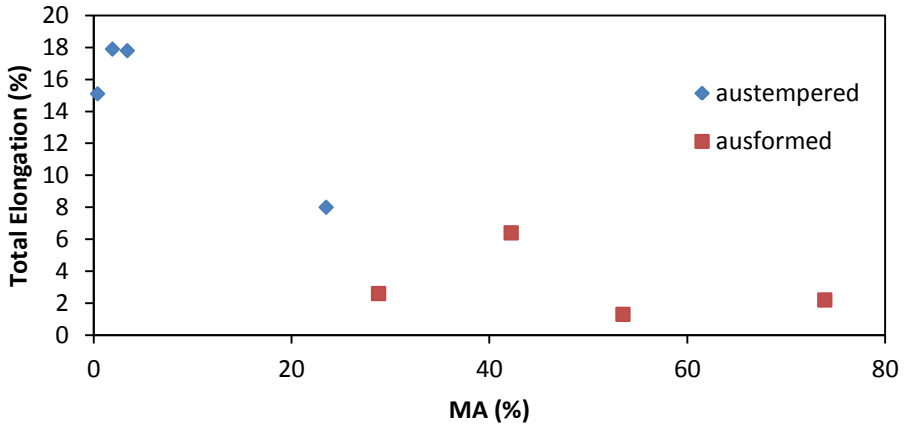

Figure 61-Amount of MA (from EBSD IQ analysis) compared to total elongation during tensile testing for ausformed and austempered CMAT alloy

5.2.3. Banding

Optical Microscopy revealed a banded structure within both the CMAT and Tata steel structures. Macroscopic bands which show segregation of Mn have been observed in similar alloys and are a result of solidification and subsequent forming of parts [43, 44]. Banding is a consequence of Mn segregating as the original ingot casting cools. The segregated areas are then compressed and stretched during the subsequent rolling or forging.

Work done by Goulas *et al*. on the formation of bainite in a 51CrV4 medium carbon, low Si steel compares the transformation of homogensized and banded specimens [45]. They found that the homogenized material transformed to bainite faster and that local substitutional alloying element chemistry had a significant effect on bainite formation kinetics and therefore the final microstructure stating that solute drag played a role [45]. In non-homogeneous

specimens lower bainite transformation rates were observed as well as lower final fractions [45].

Bhadeshia mentions a similar trend stating that homogenous steels transform to bainite faster than segregated ones except in instances were treatment is close to Bs [19]. Furthermore he mentions that an increase in the Mn content of an alloy typically slows bainite formation, and decreases final fraction [19].

Work by Zhang *et al.* on a 0.4% carbon, carbide-free nano bainitic structure found that the banded structure was marginally stronger than the homogenized in some cases [43]. They theorize that this is the result of martensite bands being under compression and bainite bands being in tension, with the compressed martensite leading to an overall increase in UTS [43]. They explain the variation in microstructure in terms of the Mn content. Low Mn areas would have a higher Ae3 temperature therefore they will transform to bainite first whereas higher Mn bands may be too stable to undergo bainite transformation and will instead transform to martensite upon further cooling [43].

In the present work there has been no experimentation on homogenized material for comparison. It can be assumed from the literature that a homogenized version on the alloy would transform to bainite faster and achieve a higher final fraction. However, for future industrial applications the extra time saved on bainite formation would be lost on homogenizing the material at a higher temperature, and the banded structure may even have a higher strength and therefore be better suited for armour applications than its homogenized counterpart.

5.2.4. Local Measurement of Carbon with EELS

The results of the EELS characterization of the CMAT alloy transformed at 250°C and 275°C are shown in Figure 62. There is a notably larger amount of carbon than expected in the bainitic ferrite. Furthermore the concentration of carbon in the austenite was observed to be somewhere in between the Ae3 and T_0 lines. It is also interesting to note that at higher temperature there was more carbon in austenite and less in ferrite which is opposite to the trend predicted by the paraequilibrium and T_0 boundaries. It should be noted that only thin films of austenite were measured, and that unlike XRD, EELS is a very localized test.

The phase fraction of austenite as calculated from the carbon concentrations determined by EELS are 27% for transformation at 250°C and 31% for transformation at 275°C. These fractions reflect the same trend of higher

amounts of retained austenite remaining at higher transformation temperatures, as observed in XRD with 22% austenite formed at 250°C and 25% at 275°C.

Carbon enrichment between the Ae3 and T_0 boundaries have been noted in the literature, typically with carbon concentration closer to T_0 [34, 46]. Atom probe tomography (APT) studies have also found higher than expected levels of carbon in ferrite at lower transformation temperatures [16, 46]. It is believed that excess carbon become trapped in dislocations [16, 47], and that carbon may diffuse to dislocations over time [16].

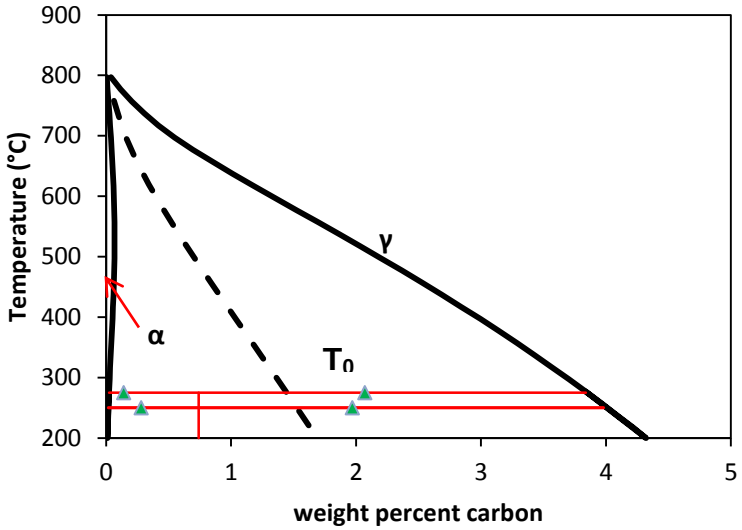

Figure 62-Paraequilibrium and T_0 boundaries with carbon concentrations detected by EELS marked

One APT study also noted that carbon concentration in bainitic ferrite increased with decreasing transformation temperature, which is likely due to the increased dislocation density in bainitic ferrite at lower transformation temperatures [46]. They explained that carbon may be trapped in the dislocations created by bainite formation in the surrounding austenite, and that these carbon holding dislocations are then inherited by bainite as the interface crosses over them [46]. Since austenite is stronger at lower temperatures more dislocations are introduced at lower transformation temperatures leading to more carbon trapped in bainitic ferrite formed at lower temperatures [46]. This also offers an explanation as to why austenite has a higher carbon content at higher transformation temperature. Consider Equation 10 where $\bar{x}$ is the alloy content of carbon, x_γ is the carbon content of austenite, x_α is the carbon content of bainitic ferrite, x_0 is available carbon and V_b is the volume fraction of bainite [18]. It balances the carbon between bainite and austenite. According to the dilatometer curves, Figure 32, after 12h hours there is a significantly larger amount of bainite

formed at 275°C than at 250°C, this leads to higher carbon enrichment of remaining austenite. Combined with the measurement of lower x_α from EELS and then considering Equation 10 a higher x_γ is expected for the specimen transformed at 275°C.

Equation 10-Carbon balance in between bainitic ferrite and austenite

$$x_\gamma = \bar{x} + V_b \frac{(x_0 - x_\alpha)}{(1 - V_b)} \text{... [18]}$$

5.3. Mechanical Properties

5.3.1. Strength

The general trend with regards to strength in both the CMAT and Tata alloys indicated that lower bainite transformation temperatures resulted in higher ultimate tensile strengths. This trend is generally well accepted as mentioned in the literature review section. It mainly related to the strengthening mechanisms of bainite which can be described by Equation 11 which is proposed by Bhadeshia.

Equation 11-Calculation for strength of bainite.

$$\sigma = \sigma_{Fe} + \sum_i \sigma_{ss}^i + \sigma_C + k_\epsilon (L_3)^{-1} + k_p \Delta^{-1} + C_{10} \rho_d^{0.5} \text{...[19]}$$

Where σ_{Fe} is the intrinsic strength of pure annealed iron, σ_{SS} is the strength contribution of substitutional solution atoms, σ_C is the strength from carbon in solid solution, ρ_d is the dislocation density, L_3 is bainite lath thickness, Δ is the average distance between cementite particles which in this case is zero, K_ϵ is approximately 115MPa*m, C_{10} is 0.38μb≈7.34 Pa*m based on dislocation theory for body-centred cubic metals [19].

The intrinsic strength of iron will be the same for all heat treatments, as will the solid solution strength contributions since no substitutional elements partition during bainite transformation [16, 46]. At lower temperatures bainite laths contain higher carbon concentrations [7, 13], as confirmed by the EELS measurements. Bainite laths form much thinner as shown in the EBSD images at lower temperatures. Finer ferrite laths are stronger [7, 9, 16], since the glide distance of dislocations become limited by lath boundaries [48, 39]. Bhadeshia proposes the use of the Langford-Cohen relation, where yield strength is proportional to the inverse of effective grain size, as opposed to the Hall-Petch relation where yield strength is proportional to the inverse square root of effective grain size [19]. Bhadeshia suggests that below an effective grain size of 1μm the Langford-Cohen relation becomes a more accurate representation of yeilding

[19]. The amount of dislocation densities in bainite is also greater at lower transformation temperatures [7, 13].

If the bainite transformations were allowed to proceed to completion a larger fraction of fine-scaled bainite would also be expected for lower transformation temperatures further improving strength. However, as seen in the isothermal dilatometer curves the bainite transformation is not completed and as a result at 250°C and 225°C there are lower fractions of bainite formed compared to 275°C. It is also necessary to mention that as a result of incomplete bainite transformation martensite also forms upon cooling which has a substantial contribution to the increase of strength at the cost of ductility. In the case of the CMAT alloy specimen transformed at 250°C for 6 hours, which from dilatometer measurements had a comparable fraction of both bainite and martensite. Its counterpart treated at 250°C for 12 hours formed a significantly higher fraction of bainite but had a lower UTS, presumably due to its lower fraction of martensite. This was however the exception with regards to a high martensite fraction improving strength since all of the ausformed samples had relatively large fractions of martensite, as detected with EBSD, yet they also all had lower UTS (about 100MPa) values than their austempered counterparts. This could be because the sample treated at 250°C for 6 hours had a balanced enough fraction of bainite to keep the martensite in compression increasing its UTS as described by Zhang *et al*. [43]. In the case of the less bainite being formed, there would be less compression on the martensite yielding a weaker structure.

5.3.2. Ductility (%Elongation, CVN)

Bainite formed at higher transformation temperatures resulted in higher final elongation and CVN values for both the CMAT and Tata alloys. Furthermore, specimens treated at the same temperature for longer times were more ductile than specimens treated for shorter periods of time. The improved CVN [7, 13] and total elongation [7, 18] as a result of higher transformation temperature have been observed in the literature. This is mainly related to the carbon supersaturated retained austenite which contributes to ductility due to its transformation to martensite upon deformation (TRIP mechanism) and its softness relative to bainite [16, 48] and in this case martensite.

The literature discussing the contributions of retained austenite to tensile and toughness properties presents a range of findings. Some studies found that blocky austenite has a negative effect on ductility and that only thin films contribute[48], whereas another states that retained austenite morphology did not have a significant effect on mechanical properties. One study found equal amounts of retained austenite before and after tensile testing which means that

no appreciable amount of retained austenite transformed to martensite transformation occurred [43]. This study was done on a 0.4wt% carbon alloy, where bainite transformation was carried out at 300°C [43]. Another study done on 0.8wt% carbon alloys found that mechanical stability increased with transformation temperature due to retained austenite chemistry [6]. The 300°C was too stable to contribute positively to deformation and the 200°C austenite was so unstable that it transformed to quickly [6]. Furthermore two different alloys where studied one having extra additions of aluminum [6]. Despite having the same fraction of austenite when transformed at 250°C the alloy with extra aluminum underwent 10% less deformation providing further evidence that retained austenite chemistry has a profound effect on its stability and final mechanical properties [6]. This explains why the ausformed samples are so brittle despite having the highest amount of retained austenite. This also explains the trend seen in the CMAT round tensile curves where the lower transformation temperature specimens fractured at lower deformation values. No specimens were tested above 275°C which is likely why over stabilized austenite was not an issue.

Table 27 below shows the amount of carbon calculated based on measured lattice size as well as the martensite start temperatures calculated based on carbon values and maximum elongation values for comparison. It is important to note that the amounts of carbon are an estimate, because of banding the exact amount of Mn is not truly known for the area examined by XRD. Mn also has an effect on lattice size. Still some interesting trends can be seen in the table. In general the blocky regions of austenite are less stable than thin films based on low amounts of carbon and high Ms temperatures. The fraction of unstable blocky austenite correlates well with elongation as shown in Figure 61.

Table 27-Calculated carbon concentrations[22] and martensite start temperatures calculated with Andrew's linear equation[49] alongside maximum elongation values

Heat Treatment	Blocky austenite % Carbon	Blocky austenite Ms(°C)	Thin Film % Carbon	Thin Film Ms(°C)	Maximum Elongation (%)
275°C-6h	1.03	18	1.81	Very stable	17.9
275°C-12h	0.85	98	1.42	-148	17.8
250°C-6h	0.50	249	1.21	-60	8
250°C-12h	0.85	99	1.48	-174	15.1
250°C-6h-25%	0.87	88	1.69	Very Stable	6.4
250°C-12h-25%	0.61	200	1.48	-173	2.2
250°C-6h-45%	0.59	211	1.38	-132	2.6
250°C-1h-45%	0.07	434	0.39	296	1.3

It is also important to consider the final fraction of martensite formed. The untempered martensite that forms under these circumstances is known to be brittle and deleterious final mechanical ductility [19]. This trend is seen with the ausformed CMAT specimens which generally exhibit poor total elongation, since they have low fractions of bainite and high fractions of martensite.

5.3.3. Cracks in Solid Tata Plate

Originally tensile testing was done on a sample with rectangular cross section approximately 8.5mm in height, which was the full thickness of the plate. However these samples were all breaking at much lower stresses than expected and fracture was occurring outside of the gauge section of the tensile bars. Examination of the fracture surfaces suggested that failure was a result of surface cracks in the specimen. Figure 17 shows the first tensile bar tested and highlights the pre-existing crack with a red box. Failure has occurred outside of the gauge section and the highlighted pre-existing crack seems to be the initiation site of the fracture. Figure 64 is an SEM image of the pre-crack area from the fracture surface of the tensile sample. It also seems in this image, that failure began in the pre-cracked area.

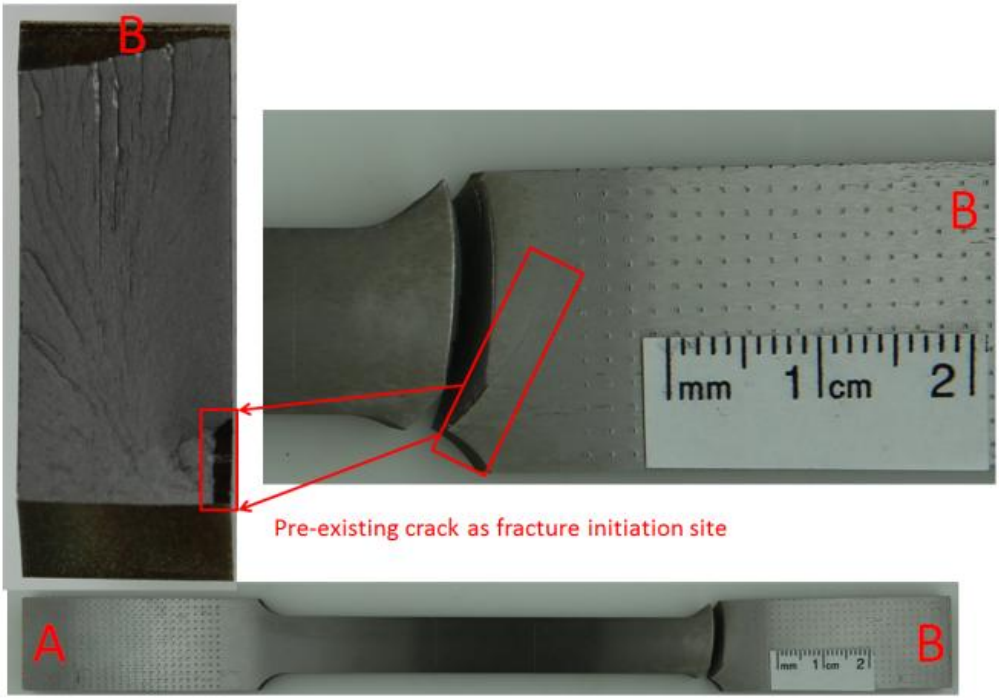

Figure 63-The bottom image shows the 8.5mm thick tensile bar after failure. Above right segment B of the sample is shown with the crack believed to be the failure initiation site. The top left image shows the fracture surface of segment B, again with the pre-existing crack highlighted.

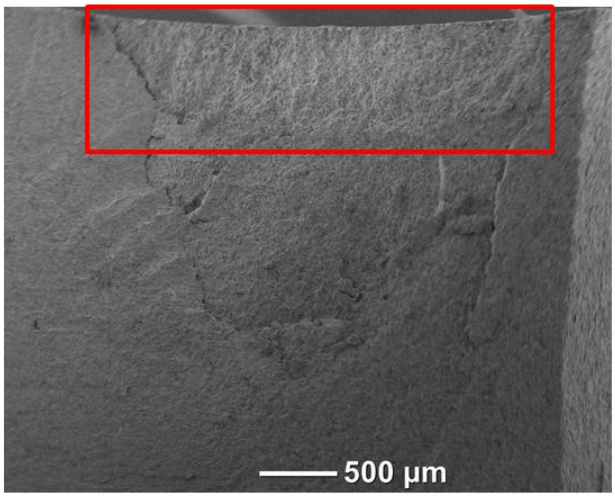

Figure 64-SEM image of the pre-existing crack area on the 8.5 mm thickness tensile bar fracture surface of piece B from the previous figure. The highlighted area corresponds to the pre-existing crack area from the previous figure.

To confirm the presence of pre-existing surface cracks in the plates die penetrant was applied to its surface. The result is shown in Figure 17; multiple cracks traversing the entire width of the plate are present. The position of these

cracks and the location from which the 8.5 mm thick tensile bars were taken from provides further evidence that the samples broke prematurely due to pre-existing cracks.

Subsized samples with a gauge section of 6mm by 6mm, with 1.25mm milled from the top and bottom surfaces in an effort to avoid the effects of surface cracks. However the poor results of those tests suggest that cracks still contributed to premature failure. Examining Figure 17 shows that three surface cracks on the top of the plate pass over the area from which subsized samples were taken.

The large perforated plate was also inspected for cracks but none were found. This suggests that the perforations are beneficial not only for reducing the plate’s mass, but also for heat treatment. The cracks in the unperforated plate may be caused by thermal gradients in the plate due to the quench from the austenitizing temperature to the bainite transformation temperature. The perforations increase surface area and therefore increase heat transfer out of the plate thereby reducing thermal gradients.

6 Conclusion

6.1. Conclusions

A carbide-free, nanoscale bainitic alloy was successfully cast and heat treated at CanmetMATERIALS. EBSD confirmed a fine lath structure of bainitic ferrite with interlath thin films of austenite and TEM analysis failed to reveal any evidence of carbides. The alloy boasts an excellent blend of strength, with a UTS of above 2GPa with ductility, 15% elongation when properly heat transformed to bainite at 250°C for 12 hours.

The best performing heat treatments were successfully carried out on the pilot scale, on plates with dimensions 1'(304.8mm) x 1'(304.8mm) and 4"(101.6mm)x 4"(101.6mm) for ballistic testing.

The kinetics of austempering and ausforming were evaluated with a dilatometer, microstructures were characterized with EBSD, TEM and XRD, and tensile properties were measured. It was determined that higher transformation temperatures led to faster bainite transformation and higher ductility. Better ductility is likely a result of the higher carbon concentration in retained austenite at higher transformation temperatures which increases austenite stability. Lower transformation temperatures yield stronger bainite because of the smaller laths with higher dislocation densities. Laths form like this because parent austenite is stronger at lower temperature.

Martensite forms from unstable austenite due to a lack of adequate carbon enrichment and thus stabilization of remaining austenite. In the case of the specimen transformed at 250°C for 6 hours the high martensite fraction increased the overall strength while decreasing the ductility. In the case of the ausformed specimens martensite content had a negative effect on both strength and ductility.

Ausforming with small deformations of 25% and 35% slightly retarded bainite formation. A large amount deformation, 45%, caused an initial spike in bainite formation but retarded overall bainite transformation even more. Ausforming generally led to an increased fraction of martensite, specifically as MA areas, which led to a decrease in overall mechanical properties.

6.2. Future Work

The next steps will be the ballistic testing and subsequent failure analysis and characterization of the prototype plates produced. The mechanics of a ballistic even are much different than those in a tensile or CVN test and therefore conventional mechanical testing has only provided a screening mechanism for

what heat treatments may perform well. The resultant microstructure will have to be examined and understood in order to further improve the CMAT alloy as armour plate.

Works Cited

[1] CBC News, "Light armoured vehicle rollovers led to more than 50 casualties," CBC, 2 June 2014. [Online]. Available: http://www.cbc.ca/news/politics/light-armoured-vehicle-rollovers-led-to-more-than-50-casualties-1.2662379. [Accessed 2014].

[2] Armour Works International , "Explosion Protection for Military Personnel," ArmourWorks International, [Online]. Available: http://www.armedforces-int.com/gallery/explosion-protection-for-military-personnel/armour-cross-section_01.html. [Accessed November 2014].

[3] H. Bhadeshia and J. Christian, "Bainite in Steels," *Metallurgical Transactions A,* vol. 21, no. A, pp. 767-797, 1990.

[4] F. Caballero, H. Bhadeshia, K. Mawella, D. Jones and P. Brown, "Design of novel high strength bainitic steels: Part 1," *Materials Science and Technology,* vol. 17, pp. 512-516, 2001.

[5] C. Garcia-Matero, F. Caballero and H. Bhadeshia, "Acceleration of Low-temperature Bainite," *ISIJ,* vol. 43, no. 11, pp. 1821-1825, 2003.

[6] C. Garcia-Mateo and F. G. Caballero, "The Role of Retained Austenite on Tensile Properties of Steels with Bainitic Microstructures," *Materials Transactions,* vol. 46, no. 8, pp. 1839-1846, 2005.

[7] C. Garcia-Mateo, F. Caballero and H. Bhadeshia, "Mechanical Properties of Low-Temperature Bainite," in *Microalloying for New Steel Processes and Applications*, Switzerland, 2005.

[8] US Department of the Army, *Armor Plate, Steel, Wrought, Ultra-High-Hardness,* 2009.

[9] C. Garcia-Mateo, F. Caballero and H. Bhadeshia, "Development of Hard Bainite," *ISIJ International,* vol. 43, pp. 1238-1243, 2003.

[10] H. Bhadeshia, "www.msm.cam.ac.uk," 2000. [Online]. Available: http://www.msm.cam.ac.uk/phase-trans/2000/C9/lecture6.pdf. [Accessed 17 May 2014].

[11] F. G. Francisca, M. J. Santofimia, C. Capdevila, C. Garcia-Mateo and C. Garcia de Andres, "Design of Advanced Bainitic Steels by Optimisation of

TTT Diagrams and T0 Curves".

[12] C. Garcia-Mateo and H. Bhadeshia, "Nucleation Theory for High-Carbon Bainite," *Materials Science and Engineering A,* vol. A378, pp. 289-292, 2004.

[13] C. Garcia-Mateo and F. Caballero, "Ultra-high-strength Bainitc Steels," *ISIJ International,* vol. 45, no. 11, pp. 1736-1740, 2005.

[14] C. Garcia-Mateo, M. Peet, F. Caballero and H. Bhadeshia, "Tempering of hard mixture of bainitic ferrite and austenite," *Materials Science and Technology,* vol. 20, pp. 814-818, 2004.

[15] F. Caballero and H. Bhadeshi, "Very Strong Bainite," *Current Opinions in Solid State and Materials Science,* vol. 8, pp. 251-257, 2004.

[16] H. Beladi, I. B. Timokhina and P. D. Hodgson, "Characterization of Nano-structured Bainitic Steel," in *International Journal of Modern Physics: Conference Series*, 2012.

[17] Y. Sakuma, O. Matsumura and H. Tekechi, "Mechanical Properties and Retained Austenite in Intercritically Heat-Treated Bainite-Transformed Steel and Their Variathion with Si and Mn additions," *Metallurgical Transactions,* vol. 22A, pp. 489-498, 1991.

[18] F. Caballero, H. Bhadeshia, K. Mawella, D. Jones and P. Brown, "Very strong low temperature bainite," *Materials Science and Technology,* vol. 18, pp. 279-284, 2002.

[19] H. Bhadeshia, Bainite in Steels - 2nd Edition, Cambridge: Institute of Materials, 2001.

[20] W. Vermeulen, P. Morris, A. de Weijer and S. van der Zwaag, "Prediction of martensite start temperature using artificial neural networks," *Ironmaking and Steelmaking,* vol. 23, no. 5, pp. 433-437, 1996.

[21] Y.-K. Lee, "Empirical formula of isothermal bainite start temperature of steels," *Journal of Materials Science Letters,* vol. 21, pp. 1253-1255, 2002.

[22] D. Dyson and B. Holmes, "Effect of alloying additions on the lattice parameter of austenite," *Journal of the Iron and Steel Institute,* pp. 496-474, 1970.

[23] G. F. V. Vort, Metallography Principles and Practice, New York: McGraw-Hill,

1984.

[24] American Society for Testing and Materials, *Standard Test Methods for Tension Testing of Metallic Materials,* West Conshohocken, 2013.

[25] US Department of the Army, *Armor Plate, Steel, Wrought, Homogeneous (for use in combat-vehicles and for ammunition testing),* 2013.

[26] US Department of the Army, *Armor Plate, Steel, Wrought, High-Hardness,* 2008.

[27] American Society for Testing and Materials, *Standard Test Methods for Notched Bar Impact Testing of Metallic Materials,* West Conshohocken, 2012.

[28] EDAX, *Welcome to OIM Data Collection-OIM Data Collection Manual 7.2,* 1997-2013.

[29] J. M. Reichert, M. Militzer, W. J. Poole and L. Collins, "A new approach using EBSD to quantitatively distinguish complex transformation products along the HAZ in X80 linepipe steel," in *Proceedings of the 2014 10th International Pipeline Conference*, Calgary, 2014.

[30] Tata Steel, *Pavise SBS 600P Ultra High-Hardness Perforated Applique Armour Systems,* 2013.

[31] A. Saha Podder, I. Lonardelli, A. Molinari and H. Bhadeshia, "Thermal stability of retained austenite in bainitic steel: an in situ study," in *Proceedings of the Royal Society*, 2011.

[32] C. Garcia-Mateo, F. Caballero, C. Capdevila and C. Gargia de Andres, "Estimation of dislocation density in bainitic microstructures using high-resolution dilatometry," *Scripta Materialia,* vol. 61, pp. 855-858, 2009.

[33] K. Hase, C. Garcia-Mateo and H.K.D.H. Bhadeshia, "Bainite formation influenced by large stress," *Materials Science and Technology,* vol. 20, pp. 1499-1505, 2004.

[34] F. Hu and K. Wu, "Isothermal transformation of low temperature super bainite," *Advanced materials research ,* Vols. 146-147, pp. 1843-1848, 2011.

[35] H. Bhadeshia, "Thermodynamic analysis of isothermal transformation diagrams," *Metals Science,* vol. 16, pp. 159-162, 1982.

[36] D. Porter and K. Easterling, Phase Transformations in Metals and Alloys, New York: Van Nostrand Reinhold Limited, 1981.

[37] S. Singh and H. Bhadeshia, "Quantitative evidence for mechanical stabilisation of bainite," *Materials Science and Technology,* vol. 12, pp. 610-612, 1996.

[38] H. Hu, H. S. Zurob, G. Xu, D. Embury and G. R. Purdy, "New insights to the effects of ausforming on the bainitic transformation," *Materials Science & Engineering A,* vol. 626, pp. 34-40, 2015.

[39] H. Bhadeshia, "Developments in martensitic and bainitic steels," *Materials Science and Engineering,* no. 378, pp. 34-39, 2004.

[40] C. Chiou, J. Yang and C. Huang, "The effect of prior compressive deformation of austenite on toughness property in an ultra-low carbon bainitic steel," *Materials Chemistry and Physics,* vol. 69, pp. 113-124, 2001.

[41] X. Jin, N. Min, K. Zheng and T. Hsu (Xu Zuyao), "The effect of austenite deformation on bainite formation in an alloyed eutectoid steel," *Materials Science and Engineering,* vol. A, pp. 170-172, 2006.

[42] D. N. Hanlon, J. Sietsma and S. van der Zwaag, "The effect of plastic defromation of austenite on the kinetics of subsequent ferrite formation," *ISIJ International,* vol. 41, no. 9, pp. 1028-1036, 2001.

[43] X. Zhang, G. Xu, X. Wang, D. Embury, O. Bouaziz, G. P. Purdy and H. S. Zurob, "Mechanical Behaviour of Carbide-free Medium Carbon Bainitic Steels," *Metallurgical and Materials Transactions A,* vol. A, no. 45, pp. 1352-1361, 2014.

[44] F. G. Caballero, A. Garcia-Junceda, C. Capdevila and C. Garcia de Andres, "Evolution of microstructural banding during the manufacturing process of dual phase steels," *Materials Transactions,* vol. 47, no. 9, pp. 2269-2276, 2006.

[45] C. Goulas, M. Mecozzi and J. Sietsma, "Investigation of bainite formation in a chemically inhomogeneous medium carbon steel," in *Proceedings of the International Conference on Solid-Solid Phase Transformations in Inorganic Materials 2015*, Whistler, 2015.

[46] F. Caballero, M. Miller, S. Babu and C. Garcia-Mateo, "Atomic scale observations of bainite transformation in a high carbon high silicon steel,"

Acta Materialia, no. 55, pp. 381-390, 2007.

[47] H. Bhadeshia, "The first bulk nanostructured metal," *Science and Technology of Advanced Materials,* no. 14, pp. 1-7, 2013.

[48] F. Caballero, H. Bhadeshia, K. Mawella, D. Jones and P. Brown, "Design of novel high strength bainitic steels: Part 2," *Materials Science and Technology,* vol. 17, pp. 517-522, 2001.

[49] K. Andrews, *J. Iron Steel Inst.,* no. 203, pp. 721-727, 1965.

[50] R. Larn and J. Yang, "The effect of compressive deformation of austenite on the bainitic ferrite transformation in Fe-Mn-C steels," *Materials Science and Engineering,* vol. a, pp. 278-291, 2000.

[51] K. Tsuzaki, T. Ueda, K. Fujiwara and T. Maki, "New Materials and Processes for the Future," in *Proc. 1st Japan International SAMPE Symposium and Exhibition, Society for the Advancement of Materials and Process Engne*, Chiba, Japan, 1989.

Appendix 1. Tables of Experimental Alloys from Literature

Table 28-Mechanical properties for various alloys and processing paths. CENIM 7 were treated by air cooling (AC) or coiling (CT) rather than holding at an isothermal temperature. Items with a * have been read off of diagrams

Alloy [ref.]	**Bainite transformation temperature (°C)**	**YS (GPa)**	**UTS (GPa)**	**ε_T**	**UTS (GPa)*ε_T**	**Impact Energy**	**Hardness**
[18] (comp-ression results)	190	1.959	2.4*	16*	38.4	-	650 (HV 30)
1 [6]	200	1.41	2.18	4.6	10.03	43*(K_{IC} MPa $m^{1/2}$) [7]	660 (HV20) [5]
1 [6]	250	1.48	2.06	19	39.14	35*(K_{IC} MPa $m^{1/2}$) [7]	589 (HV20) [5]
1[6]	300	1.24	1.77	29	51.33	36*(K_{IC} MPa $m^{1/2}$) [7]	500 (HV20) [5]
2[6]	200	1.41	2.26	7.63	17.24	-	650 (HV20) [5]
2[6]	250	1.40	1.93	9.4	18.14	-	565 (HV20) [5]
2[6]	300	1.25	1.7	27.5	46.75	-	500 (HV20) [5]
CENIM 1[11] (AC 450°C)	-	1.084	1.808	11	19.89	36 J(20C)	530 (HV30)
CENIM 1 [11] (AC 600°C)	-	1.021	1.696	11	18.66	22 J(20C)	522 (HV30)
CENIM 2 [11] (AC 500°C)	-	1.020	1.627	11.6	18.87	36 J(20C)	519 (HV30)
CENIM 2 [11] (AC	-	1.132	1.627	10.3	16.76	47 J(20C)	460 (HV30)

550°C)							
CENIM 3 [11] (AC 500°C)	-	1.068	1.671	12.2	20.39	44 J(20C)	495 (HV30)
CENIM 3 [11] (AC 550°C)	-	1.077	1.698	10.8	18.33	46 J(20C)	505 (HV30)
CENIM 4 [11] (AC 500°C)	-	1.097	1.710	13.9	23.79	38 J(20C)	531 (HV30)
CENIM 5 [11] (AC 500°C)	-	1.059	1.696	11.6	19.67	40 J(20C)	521 (HV30)
CENIM 5 [11] (AC 550°C)	-	1.105	1.801	11	19.81	31 J(20C)	555 (HV30)
CENIM 6 [11] (CT 500°C)	-	0.834	1.495	13.6	20.33	24 J(20C)	503 (HV30)
CENIM 6 [11] (AC 500°C)	-	1.074	1.799	10.7	19.24	25 J(20C)	555 (HV30)
CENIM 7 [11] (CT 350°C)	-	0.851	1.531	13.6	20.82	31 J(20C)	412 (HV30)
CENIM 7 [11] (AC 500°C)	-	1.125	1.929	9.7	18.71	25 J(20C)	559 (HV30)
CENIM 7 [11] (AC 600°C)	-	1.203	1.945	7	13.62	26 J(20C)	563 (HV30)
Mn [48]	-	1.167	1.790	13	23.27	34 J(20C)	597 (HV30)
Ni1 [48]	-	1.150	1.725	14	24.15	58 J(20C)	493 (HV30)
Ni2 [48]	-	1.100	1.625	14	22.75	50 J(20C)	536 (HV30)

Table 29-List of alloys found in the literature

Alloy [ref.]	C	Si	Mn	Mo	Cr	V	Ni	Co	Al	P	S
TATA	0.85	0.75	1.4	0.3	1.0	-	-	-	-	0.015	0.0
[18]	nm	1.59	1.94	0.30	1.33	0.11	0.02	-	-	-	-
[7]	0.80	1.59	2.01	0.24	1	-	-	1.51	-	0.002	0.002
1 [5]	0.98	1.46	1.89	0.26	1.26	0.09	-	-	-	-	-
2 [5] [6]	0.83	1.57	1.98	0.24	1.02	-	-	1.54	-	0.002	0.002
3 [5] [6]	0.78	1.49	1.95	0.24	0.97	-	-	1.60	0.99	0.002	0.002
[16]	0.8	1.5	1.98	0.24	0.98	-	-	1.58	1.06	-	-
A [15]	0.79	1.59	1.94	0.30	1.33	0.11	-	-	-	-	-
B [15]	0.98	1.46	1.89	0.26	1.26	0.09	-	-	-	-	-
C [15]	0.83	1.57	1.98	0.24	1.02	-	-	1.54	-	-	-
D [15]	0.78	1.49	1.95	0.24	0.97	-	-	1.60	0.99	-	-
CENIM 1 [11]	0.290	1.5	2.25	0.26	-	-	-	-	-	-	-
CENIM 2 [11]	0.29	1.46	1.97	0.25	0.46	-	-	-	-	-	-
CENIM 3 [11]	0.290	1.49	1.56	0.25	1.47	-	-	-	-	-	-
CENIM 4 [11]	0.27	1.71	1.53	0.245	0.17	-	1.47	-	-	-	-
CENIM 5 [11]	0.29	1.47	1.97	0.25	1.20	-	-	0.97	-	-	-
CENIM 6 [11]	0.285	1.50	2.04	0.245	1.50	-	-	1.48	-	-	-
CENIM 7 [11]	0.30	1.44	2.06	0.24	1.6	-	1.7	1.43	1.01	-	-
Mn [48]	0.32	1.45	1.97	0.26	1.26	0.10	<0.02	-	-	-	-
Ni1 [48]	0.31	1.51	<0.01	0.25	1.44	0.10	3.52	-	-	-	-
Ni2 [48]	0.30	1.51	<0.01	0.25	1.42	<0.005	3.53	-	-	-	-
A[17]*	0.201	1.240	0.950	-	-	-	-	-	-	0.0040	0.0063

B [17]*	0.200	1.560	0.951	-	-	-	-	-	-	0.0030	0.0057
C [17]*	0.199	2.100	0.940	-	-	-	-	-	-	0.0030	0.0058
D [17]*	0.202	1.210	1.550	-	-	-	-	-	-	0.0050	0.0062
E [17]*	0.195	1.210	1.550	-	-	-	-	-	-	0.0050	0.0058
F [17]*	0.202	0.810	1.870	-	-	-	-	-	-	0.0080	0.0065
G [17]*	0.201	1.240	1.800	-	-	-	-	-	-	0.0030	0.0062
H [17]*	0.202	1.640	1.834	-	-	-	-	-	-	0.0030	0.0062